Precise Hypofractionated Radiotherapy of Moving Tumors.

Dissertation

zur

Erlangung der naturwissenschaftlichen Doktorwürde
(Dr. sc. nat.)

vorgelegt der

Mathematisch-naturwissenschaftlichen Fakultät

der

Universität Zürich

von

Stephanie Lang

aus

Deutschland

Promotionskomitee

Prof. Dr. Martin Pruschy (Vorsitz)
Prof. Dr. Michael Hengartner
PD Dr. Dr. Andreas Mack
Dr. Stephan Klöck (Leitung der Dissertation)

Zürich, 2014

Contents

Abstract

Hypofractionated radiotherapy is currently a clinical area of research. Clinical trials are looking into giving larger doses of ionizing radiation per fraction, by using fewer fractions. The goal is to prove that the tumor can be better controlled in this way or that the treatment time can be shortened with the same or better clinical outcome. However for moving tumors large safety margins need to be applied to cover the tumor with the full dose. This leads to a large amount of healthy tissue irradiated with high doses and eventually increases side effects. To savely apply hypofractionated treatments to moving structures, motion management techniques are needed. Two approaches to reduce intrafractional motion of moving tumors to be able to increase the dose per fraction are implemented and evaluated within the frame of this thesis. On the one hand with the introduction of the flattening filter free (FFF) technique, a reduction in treatment time was achieved which led to excellent stability of the patients during treatment. On the other hand a prototype system was developed to compensate respiratory motion.

In a first step two FFF beams with nominal energy 6 MV (X6FFF) and 10 MV (X10FFF) were commissioned. These beams allow a maximum dose rate of up to 24 Gy per minute (X10FFF in depth of maximum dose, a source-surface distance of 100 cm and a field size of 10x10 cm^2), leading to shortened treatment times and eventually reduced target movement. A prerequisite for the characterisation of FFF radiation beams is the knowledge of the behaviour of detectors in the high dose per pulse FFF beams. Therefore a study was performed evaluating seven widely used ionization chambers. For flattened beams, the ion collection efficiency of all air-vented ionization chambers (except for the pinpoint chamber) was above 0.995. By removing the flattening filter a reduction in collection efficiency was found of approximately 0.5-0.9% for a 10 MV beam (X10). Using the liquid ionization chamber the ion collection efficiency for flattened beams was above 0.990 for all dose rates. However, this chamber showed a low collection efficiency of 0.940 for the X10FFF beam at a dose rate of 31.9 Gy/min. All investigated air-vented ionization chambers can be reliably used for relative dosimetry of FFF beams. Due to their increased saturation in high dose rate FFF beams, liquid ionization chambers appear to be unsuitable for dosimetry within this context.

In the next step a planning study was performed, evaluating FFF beams for hypofractionated prostate cancer. FFF beams have a larger dose rate on the central axis than flattened beams, an increased surface dose and a reduced beam quality

factor. Therefore the planning study evaluated the use of FFF beams for patient treatments and the capability of the planning system to optimize the FFF beams. Dose distributions, out-of field doses and treatment times were evaluated. Volumetric modulated arc therapy (VMAT) treatment planning was performed for seven patients with prostate cancer using TrueBeam linear accelerator and photon beams with (X6, X10) and without (X6FFF, X10FFF) flattening filter. No difference was detected in PTV coverage, conformity and homogeneity among the four beams. Mean body dose and body volume receiving 50% of the prescribed dose decreased with increasing mean energy ($R2 = 0.8275$, $p < 0.01$). There was a significant increase in the mean dose to the rectum for the X10 compared to X6 (2.6%, $p < 0.01$). Mean dose to the bladder increased by 1.3% for X6FFF and decreased by 2.3% for X10FFF. Therefore it was concluded, that X10FFF beam provided the best solution, sparing rectum and bladder and minimizing whole body dose. Using a single arc and FFF, treatment time was reduced by 35% (2SD = 10%) compared to a flattened beam (Dose per fraction 3 Gy).

After verifying the planning system, the capability of the linear accelerator to deliver the high dose rate beams was investigated. There are concerns regarding the safe delivery of FFF beams, especially regarding the monitor chamber, which is used to steer the beam. Additionally the increased output of TrueBeam places higher demands on the reaction time of the servo system as well as the control system of the linear accelerator. Pre-treatment quality assurance (QA) data from 4 centers were analysed with different verification devices to assess reliability and dosimetric accuracy of FFF beam delivery for intensity modulated radiotherapy (IMRT) and VMAT techniques. Gamma evaluation was performed with a dose difference of 3% and a distance to agreement of 3 mm scoring the gamma agreement index (GAI, % of field area passing the test). 224 patients with 1–6 lesions in various anatomical regions and dose per fraction ranging from 1.8 Gy to 25 Gy were included in the study; 88 were treated with X6FFF beam and 136 with X10FFF beam. Gafchromic films in solid water, air-vented chambers, DELTA4 phantom, ARCCHECK phantom or MATRIXX phantom were used to verify the dose distributions. Dose calculation as well as dose delivery was equally accurate for IMRT and VMAT delivery (IMRT: GAI = 99.3% (1SD = 1.1%); VMAT: GAI=98.8% (1SD = 1.1%)) as well as for the two beams evaluated (X6FFF: GAI = 99.1% (1SD = 1.0%); X10FFF: GAI=98.8% (1SD = 1.2%)). Based on the high GAI scores of all verified plans, it was concluded that the TrueBeam FFF modality, analyzed with a variety of verification devices and planned with Eclipse planning system is dosimetrically accurate (within the specified limits 3mm/3%) for both X6FFF and X10FFF beam energies.

Due to the high available dose rate FFF beams are often considered for hypofractionated treatments of breast, lung and prostate cancer. The clinical efficiency and accuracy benefit of FFF beams for extra-cranial lesions was evaluated. The internal target volume (ITV) concept was used to treat 16 patients with lung tumors and 10 patients with abdominal tumors. ITV to planning target volume (PTV) margins were calculated according to the Van Herk Formula and tumor stability

was determined for the short treatment times of FFF beams. Beam-on time was on average 1.6 min (1SD = 0.6 min), with the recorded total treatment times of 18.5 min (1SD = 3.5 min). The time advantage of using FFF beams was dose-dependent and started at 4 Gy for X6FFF and at 10 Gy for X10FFF beams. The average of the tumor displacements during treatment was 2.0 mm (1SD = 1.0 mm). This showed that stereotactic body radiotherapy (SBRT) using FFF beams is time efficient and associated with excellent patient stability. According to Van Herk's formula, ITV to PTV margins of 6 mm are sufficient in our patient cohort. Further studies are necessary to assess clinical outcome and toxicity.

It was shown by several authors that prostate as well as patient motion increases with increased treatment time. The use of flattening filter free beams has the potential to reduce motion of the patient as well as prostate motion, however for periodic respiratory motion there is no benefit expected. In the second part of the thesis the reduction of safety margins for respiratory motion was addressed. A treatment couch tracking system to counter steer respiratory tumor motion was developed and implemented. Three different motion detection sensors with different lag times were evaluated: the topometrical system Topos, the respiratory gating system RPM and a laser sensor. The control system was implemented in the block diagram environment Simulink. To achieve real time performance the Simulink models were executed on a real time engine, provided by Real-Time Windows Target. To achieve high control performance with good reference tracking and good disturbance rejection, a proportional-integral control system was implemented. The geometrical accuracy of the system was evaluated by measuring the mean deviation to the reference position (static position) during motion tracking. A hexapod system was moving according to seven respiration patterns previously acquired with the RPM system as well as according to a $\sin^6$ function with two different frequencies (0.33 Hz and 0.17 Hz). The treatment table Protura compensated the motion. It was found that short delay times are needed to be able to track all the respiration frequencies. The laser based tracking system with the small lag time of 60 ms could track all the respiration patterns. An increase in delay time from 60 ms (Laser based system) to 130 ms (RPM based system) resulted in a non-sufficient tracking performance for the $\sin^6$ pattern (frequency 0.33 Hz). The system with the largest lag time of 300 ms was only able to track four of the respiration patterns. For the four patient respiration patterns, which could be tracked by all three systems, a mean absolute deviation of 0.19 mm was achieved using the laser sensor, 0.45 mm using the RPM system and 0.52 mm using the TOPOS system. More scientific work is necessary to extend our prototype to tracking of internal motion

With the development of the couch tracking system, a second approach to reduce intra-fractional motion was implemented and evaluated. In the future we want to combine the fast treatments with FFF beams and the active motion compensation with the tracking system in order to optimally treat the patients.

Zusammenfassung

Die hypofraktionierte Strahlentherapie, dh die Therapie wird in wenige Fraktionen mit hohen Einzeldosen durchgeführt, hat sowohl in vor-klinischen als auch in ersten klinischen Studien gute Resultate gezeigt. Deshalb gibt es im Moment eine grosse Anzahl klinischer Studien die zeigen sollen, dass eine hypofraktionierte Bestrahlung zu einer besseren Tumorkontrolle führt. Jedoch sind die Bestrahlungen mit hohen Einzeldosen problematisch für bewegliche Tumore. Damit der Tumor genügend Dosis bekommt, muss der ganze Bewegungsbereich des Tumors bestrahlt werden. Dadurch wird auch viel gesundes Gewebe mit einer therapeutischen Dosis bestrahlt, was zu stärkeren Nebenwirkungen führen kann. Dieser Umstand verhindert, dass die therapeutischen Dosen für eine verbesserte Tumorkontrolle erhöht werden können. Deshalb sind Techniken gefordert, die die Bewegung des Tumors kontrollieren, um den Anteil gesunden Gewebes, der bewegungsbedingt mitbestrahlt wird, zu minimieren.
Im Rahmen dieser Doktorarbeit wurden zwei Techniken entwickelt, die die intrafraktionelle Bewegung reduzieren können und es damit erlauben, beweglichen Tumore mit höheren Einzeldosen zu bestrahlen. Zum Einen wurde eine neuartige Technik zur Verkürzung der Behandlungszeit und somit auch der intra-fraktionellen Bewegung eingeführt und zum Anderen eine Methode entwickelt die es erlaubt Atembewegungen auszugleichen. Zunächst wurden zwei ausgleichsfilterfreie (FFF) Strahlmodalitäten mit nomineller Energie 6 MV (X6FFF) und 10 MV (X10FFF) kommissioniert. Diese Strahlmodalitäten erreichen Dosisleistungen von bis zu 24 Gy/min. Das führt zu kürzeren Bestrahlungszeiten und eventuell zu weniger intrafraktioneller Bewegung. Vor der Kommissionierung dieser Strahlmodalitäten, ist es wichtig, das Verhalten der Messkammern in diesen neu-artigen Strahlmodalitäten zu kennen. Deshalb wurde eine Studie durchgeführt, welche sieben verschiedene Ionisationskammern untersucht. Alle belüfteten Ionisationskammern zeigten in den Strahlmodalitäten mit Ausgleichsfilter eine Ionensammeleffizienz von über 0.995. In den FFF Strahlen reduzierte sich die Ionensammeleffizienz um ungefähr 0.005-0.009 (10 MV Strahl). Anders verhält es sich mit der flüssigkeitsgefüllten Ionisationskammer. Die Ionensammelausbeute für die Strahlmodalitäten mit Ausgleichsfilter betrügt mehr als 0.99, für die FFF Strahlmodalitäten beträgt die Ausbeute nur 0.94 (10 MV mit einer Dosisleistung von 31.9 Gy/min). Zusammenfassend kann man sagen, dass die luftgefüllten Ionisationskammern in den FFF Strahlmodalitäten für Relativdosimeterie benutzt werden können, die flüssigkeitsgefüllten Ionisationskam-

mer jedoch nicht geeignet sind.
Im nächsten Schritt wurde eine Planungsstudie durchgeführt, die die FFF Strahlen für die hypofraktionierte Bestrahlung von Prostata Tumore evaluiert. FFF Strahlen unterscheiden sich im Profil von Strahlen mit Ausgleichsfilter, sie haben eine erhöhte Oberflächendosis und einen niedrigeren Strahlqualitätsfaktor. Das Ziel der Planungsstudie war es herauszufinden, ob die FFF Strahlen für die Bestrahlung von Patienten benutzt werden können und ob das Planungssystem die Pläne mit diesen Strahlmodalitäten optimieren kann. Die Bestrahlungsplanung wurde für sieben Patienten mit volumenmodulierter Bogenbestrahlungs Technik (VMAT) und vier verschiedenen Strahlmodalitäten (X6 , X6FFF, X10, X10FFF) am TrueBeam Beschleuniger durchgeführt. Es gab keine signifikanten Unterschiede in der Zielvolumenabdeckung (PTV Abdeckung) und bezüglich der Konformität und der Homogenität zwischen den vier Modalitäten. Die mittlere Körperdosis wurde mit zunehmender mittlerer Energie kleiner ($R2 = 0.8275$, $p < 0.01$). Die X10 Strahlmodalität erhöhte die mittlere Dosis im Rektum signifikant um 2.6% ($p < 0.01$) im Vergleich zur X6 Modalität. Die mittlere Dosis in der Blase erhöhte sich um 1.3%, wenn der X6FFF Strahl benutzt wurde und nahm um 2.3% ab, wenn mit X10FFF geplant wurde. Zusammenfassend kann man sagen, dass der X10FFF Strahl den besten Kompromiss bildet zwischen einer niedrigen Ganzkörperdosis und der Schonung der Risikoorgane (Blase, Rektum). Patienten, die nur mit einem Bogen und dem X10FFF Strahl bestrahlt wurden, hatten eine um 35% (2SD = 10%) verkürzte Bestrahlungszeit (3 Gy pro Fraktion) im Vergleich zur Bestrahlung mit den Strahlmodalitäten mit Ausgleichsfiter.
Nachdem mit der Planungsstudie gezeigt werden konnte, dass die FFF Strahlen zur Planung von hypofraktionierten Schemata geeignet sind, wurde getestet, ob der Beschleuniger die FFF Strahlmodalitäten dosimetrisch genau applizieren kann. Im Vorfeld hierzu gab es mehrere Publikationen, die sich bezüglich der Genauigkeit herkömmlicher Monitorkammern in FFF Strahlen kritisch geäussert hatten. Das Kontrollsystem der Monitorkammer muss aufgrund des erhöhten Dosisoutputs im FFF Modus schneller reagieren können. Um die dosimetrische Genauigkeit zu verifizieren, wurde die patientenspezifische Qualitätssicherung von 4 Radiotherapiezentren analysiert. Sowohl die VMAT als auch die intensitätsmodulierte Technik (IMRT) wurden untersucht. Die Pläne wurden anhand des Gamma Übereinstimmungs Indexes (GAI) beurteilt, der eine Dosisdifferenz von maximal 3% und eine räumlich Diskrepanz von maximal 3 mm tolerierte. Die Patienten spezifische QA von 224 Patienten mit 1-6 Zielvolumina an verschiedenen anatomischen Orten und mit Fraktionsdosen von 1.8 Gy - 25 Gy wurde ausgewertet: 88 dieser Patienten wurden mit der X6FFF Strahlqualität bestrahlt und 136 mit der X10FFF Strahlqualität. Verifiziert wurden die Dosisverteilungen mit gafchromischen Filmen im wasseräquivalenten Plattenphantom oder mit Ionisationskammern, oder mit dem DELTA^4, oder dem ARCCHECK oder dem MATRIXX Phantom. Es hat sich gezeigt dass es zwischen IMRT und VMAT Bestrahlung in Bezug auf die Genauigkeit der Dosisberechnung und der Dosisapplikation am Beschleuniger keinen signifikanten Unterschied

gab (IMRT: GAI = 99.3% (1SD = 1.1%); VMAT: GAI=98.8% (1SD = 1.1%)). Ebenso gab es keinen signifikanten Unterschied in der Genauigkeit zwischen den zwei Strahlmodalitäten (X6FFF: GAI = 99.1% (1SD = 1.0%); X10FFF: GAI=98.8% (1SD = 1.2%)). Zusammenfassend haben unsere Ergebnisse gezeigt, dass die FFF Strahlmodalitäten des TrueBeam Beschleunigers in Verbindung mit dem Eclipse Planungssystems sicher und dosimetrisch genau sind.
FFF Strahlmodalitäten werden aufgrund ihrer hohen Dosisleistung vorallem für hypo-fraktionierte Bestrahlungen verwendet. Im Rahmen dieser Doktorarbeit wurde die klinische Awendung der FFF Strahlen für extra-kranielle Läsionen ausgewertet, insbesondere sollte die erhöhte Stabilität aufgrund der kürzeren Behandlungszeiten belegt werden. Sechzehn Patienten mit Lungenkarzinomen und 10 Patienten mit Tumoren im Abdomen wurden mit dem internen Zielvolumen Konzept (ITV) bestrahlt. Die Sicherheitssäume zwischen dem ITV und dem PTV wurden mit Hilfe der Van Herk Formel berechnet. Zusätzlich wurde untersucht, wie stabil der Tumor, während der aufgrund der FFF Strahlen kurzen Behandlungzeit ist. Die mittlere Strahlzeit war 1.6 min (1SD = 0.6 min) und die mittlere Gesamtzeit einer Behandlungssitzung 18.5 min (1SD = 3.5 min). Der Zeitvorteil für die FFF Strahlen im Vergleich zu denen ohne Ausgleichsfilter war für hohe Fraktionsdosen (>4 Gy) statistisch signifikant. Der Zeitgewinn wurde mit zunehmender Fraktionsdosis grösser. Im Mittel bewegte sich der Tumor während der Bestrahlung um 2mm, daraus wurde ein Sicherheitssaum von 6 mm berechnet. Die Verwendung von FFF Strahlmodalitäten führt zu einer zeiteffizienten Durchführung von SBRT Behandlungen und einer stabilen Tumorposition. Weitere Studien sind nötig um die Wirkung der FFF Strahlen sowie die Nebenwirkungen zu quantifizieren.
Durch die Anwendung von Ausgleichsfilter-freien Strahlen kann die intra-fraktionelle Bewegung des Patienten sowie die Bewegung der Prostata reduziert werden. Für periodische Atembewegungen kann jedoch durch die Anwendung der FFF Strahlen keine Reduktion erwartet werden.
Im letzten Teil dieser Arbeit wurde ein Tracking System entwickelt und evaluiert, das es ermöglicht Atembewegungen mit dem Behandlungstisch auszugleichen. Drei verschiedene Sensoren zur Detektion der Bewegung wurden getestet: Das topometrische System Topos (Cyber Technology), das Respiratory Patient Monitoring System (RPM) (Varian Medical Systems) und ein Laser Triangulations System (Micro Epsilon). Ein Proportional-Integral Kontrollsystem wurde implementiert, um der Atembewegung gegenzusteuern. Die geometrische Unsicherheit des Systems wurde quantifiziert indem die mittlere absolute Abweichung zur Null-Bewegungslinie mit und ohne Tracking verglichen wurde. Ein hexapod system (Physics Instruments, Germany) hat sieben physiologische Atembewegungskurven und zwei $\sin^6$ Funktionen (0.33 Hz und 0.17 Hz) nachgefahren. Diese Bewegung wurde mit dem Behandlungstisch Protura (Civco Medical Systems) ausgeglichen. Es hat sich gezeigt, dass kurze Totzeiten nötig sind, um allen Atemfrequenzen folgen zu können. Mit dem Lasersystem, welches die kürzeste Todzeit hatte, konnten alle Atemkurven ausgeglichen werden. Ein Anstieg von 60 ms (Laser System) auf 130 ms (RPM System)

führte dazu, dass die $\sin^6$ Funktion (0.33 Hz) nicht mehr ausgeglichen werden konnte. Das TOPOS System mit der grössten Totzeit von 300 ms konnte nur vier Atembewegungsmuster ausgleichen. Mehr wissenschaftliche Arbeiten sind nötig, um diesen Prototypen so zu erweitern, dass er auch interne Bewegungen ausgleichen kann.
Durch die Entwicklung des Tracking Systems wurde ein zweiter Ansatz zur Reduktion von intra-fraktioneller Bewegung aufgezeigt und evaluiert. Das Ziel für die Zukunft ist, die FFF Strahlen mit der aktiven Kompensation der intra-fraktionellen Bewegung zu kombinieren, um eine optimale Bestrahlung zu erzielen.

Chapter 1

Motivation and Outline of the thesis

1.1 Motivation

Currently, standard external beam radiotherapy consists of 50 to 78 Gy of radiation separated into 1.8 to 2 Gy fractions given daily for 7 to 9 weeks. The clinical experience on these fractionation schedules is large and the normal tissue tolerances are well known [8]. Studies of the response of cancer cell cultures to radiation, however, suggest that fractions with a dose larger than 2 Gy may be more effective. Hypofractionated treatment schedules are proposed for several types of cancers, including breast cancer [13, 7, 132], prostate cancer [37, 82, 73], lung cancer [59, 90] and liver cancer [62, 75]. However, concerns about normal tissue toxicity require a more effective normal tissue sparing than for conventional fractionations. A reduction of safety margins between the actual gross tumor volume (GTV) and the treated volume (PTV) is needed to better spare organs at risk. For tumors of the lung, liver, breast and prostate a large part of the safety margin is to account for motion of the tumor during the treatment session [115, 116]. Two approaches to reduce intrafractional motion of moving tumors, to be able to increase the dose per fraction, are implemented and evaluated within the frame of this thesis. First, flattening filter free beams were implemented for clinical use. Flattening filter free beams have an increased dose rate compared to conventional beams, which leads to reduced treatment times and potentially to reduced intrafractional motion. At the University Hospital we were the first clinic in the world to have these flattening filter free beams available for clinical use. Within the frame of this thesis the FFF beams were characterized, suitable tools for beam characterisation were found and patient specific quality assurance was addressed. Additionally the dosimetric and time benefit for hypofractionated treatments of lung and prostate tumors were evaluated.
The use of flattening filter free beams can reduce motion of the patient as well as prostate motion due to the shorter treatment times, however for periodic respiratory motion there is no benefit expected. In the second part of the thesis the reduction

of safety margins for respiratory motion was addressed. A couch tracking approach to compensate respiratory motion was implemented and evaluated. Not addressed within this thesis are further methods for treatment margin reduction such as image guided radiotherapy, positioning devices for patients, gated treatments and four dimensional planning.

1.2 Outline and Contribution to the Chapters

In Chapter 2 the fundamentals of the research performed within the frame of this thesis are explained. The basic function of a linear accelerator, the accuracy of linear accelerators and the properties of flattening filter free beams are described in Chapter 2.2-2.4. Additionally motion management techniques, hypofractionation and margin concepts are discussed (Chapter 2.5-2.7). The Chapter was written by myself, part of it will be published in a review article in the SPG Mitteilungen.
Within the frame of this thesis two flattening filter free (FFF) beams with nominal energy 6 MV (X6FFF) and 10 MV (X10FFF) were commissioned. As described in Chapter 2.4, these beams allow a maximum dose rate of up to 24 Gy per minute ((X10FFF in depth of maximum dose, a source-surface distance of 100 cm and a field size of 10x10 cm^2), leading to shortened treatment times and eventually less target movement during a treatment session. A prerequisite for commissioning is the knowledge of the behaviour of detectors in the high dose per pulse FFF beams. In Chapter 3 a study, which evaluates seven widely used ionization chambers, is described. The study was designed by myself and all the measurements were performed with the support of Jan Hrbacek. Additionally the manuscript was drafted by myself.
FFF beams have a higher dose rate on the central axis than flattened beams, an increased surface dose and a reduced beam quality factor. To show that the FFF beams can be used for treatment planning, a planning study for hypo-fractionated prostate treatments was performed in Chapter 4. In this planning study the use of FFF beams for patient treatments and the capability of the planning system to optimize the FFF beams were evaluated. Dose distributions, out-of field doses and treatment times were evaluated and compared to conventional flattened beams. Daniel Zwahlen and myself are equally contributing authors to this manuscript. The execution of the treatment planning study and the corresponding statistical analysis were performed by myself. Together with Daniel Zwahlen the results were interpreted. Daniel Zwahlen put the results into a clinical context and drafted introduction and conclusion. Materials and methods and results were drafted by myself.
After the verification of the planning system, the capability of the linear accelerator to deliver the high dose rate beams was investigated and is described in Chapter 5. The study was motivated by early concerns regarding the safe delivery of FFF beams [39], especially regarding the monitor chamber, which is used to steer the beam. The monitor chamber is described more in detail in Chapter 2.2. Pre-treatment quality

assurance (QA) data from 4 clinics were analysed with different verification devices to assess reliability and dosimetric accuracy of FFF beam delivery for intensity modulated radiotherapy (IMRT) and volumetric modulated radiotherapy (VMAT) techniques. The multi-center study was initiated by myself, the data was collected and the manuscript drafted by myself.
FFF beams are, due to the high available dose rate, often considered for hypo-fractionated treatments of breast, lung and prostate cancer. In Chapter 6 the clinical application of FFF beams for extra-cranial lesions is discussed. The internal target volume (ITV) concept as described in Chapter 2.7.1 was used to treat 16 patients with lung tumors and 10 patients with abdominal tumors. ITV to planning target volume (PTV) margins were calculated according to the Van Herk Formula (Chapter 2.6) and tumor stability was determined for the short treatment times of FFF beams. The clinical study was designed by Oliver Riesterer and myself. The data evaluation and parts of the treatment planning were done by myself.
As a last part of the thesis the possibility of couch tracking (Chapter 2.7.3) to compensate for respiratory tumor motion was evaluated (Chapter 7). Since this is a technique which is not yet clinically used and there are no commercial solutions available, the control system of the couch was implemented. Three different motion detection sensors with different lag times were evaluated: the topometrical system Topos, the respiratorygating system (RPM) or the laser triangulation system (Micro Epsilon). In a pre-clinical study the compensation of the patient breathing was geometrically and dosimetrically analysed. My contribution to this project was the development of the first prototype systems, which was further improved in close collaboration with the control system group of the ETH Zürich. The system was evaluated by myself and the manuschrift was drafted by myself.
In the last Chapter a conclusion on the work done in this thesis is given and an outlook on further possible investigations and applications of the research described in Chapter 3 to 7 is drawn.

Chapter 2

Introduction *

2.1 Radiation Therapy

Cancer is the second most common cause of death in Switzerland (Todesursachenstatistik, BFS, [10]). In 2011, 9054 men and 7223 women died of cancer. For men the leading cause of cancer death is lung cancer, followed by prostate cancer. For women the leading cause of cancer death is breast cancer, followed by lung cancer [131].
Different treatment approaches, such as surgery, radiation therapy and chemotherapy are used to treat cancer. Todays cancer patient typically receives a multimodal treatment that include at least two, or all three treatment modalities. Depending on the tumor location, cell type tumor grade and the general condition of the patient, the clinician decides together with the patient on an adequate treatment option. During the course of their disease 50-60% of all cancer patients will be treated with radiotherapy at least once, which underlines the importance of the discipline. [101].
In radiation therapy ionising radiation is used to kill or control malignant cancer cells. High energy photons and electrons are most frequently used. Recently, some cancer treatment centers have been built, that treat with protons, neutrons and heavy ions.
The physical effects of high energy photons as well as charged particles in matter (e.g. human tissue) are indirect and direct ionizations of atoms. Photons are mainly indirectly ionizing. They produce high energy electrons, once they interact with matter. The three main interaction processes of photons in matter are: Photoelectric effect, Compton Effect and Pair Production. In the megavoltage (1-20 MeV) range, the most commonly photon energy range used in radiation-oncology the Compton Effect is predominant. The high energy electrons have enough energy to produce a large number of ionizations by collisions. Charged particles are directly ionizing. They have enough energy to produce ionizations by collisions as they penetrate into matter. The major biological effect of ionizing radiation is DNA damage,

*Parts of this chapter will be published in SPS Mitteilungen, No 40, Nov 2013 [71].

e.g. when a secondary electron or a charged particle ionizes DNA molecules directly or indirectly by hydroxyl radicals that interact with the DNA. Hydroxyl radicals are produced as a result of the ionization and chemical reaction of water molecules. By radiating a tumor to 1-2 Gy to a tumor more than 1000 single strand breaks and approximatly 40 double strand breaks of the DNA double helix are induced per cancer cell. This damage could theoretically be repaired by the cellular DNA damage repair system. Cancer cells however, are much more sensitive to radiation than normal cells. Cancer cells divide more often and are therefore more vulnerable to radiation and they often have defective repair systems due to DNA mutations.
Two principle techniques exist in radiation therapy, brachytherapy and external beam radiotherapy. In brachytherapy, the radiation source is placed inside the body of the patient in close proximity to the tumor, or even within the tumor. In external beam radiotherapy (EBRT) the radiation targets on a specific part of the body from outside. The dose in EBRT can be delivered to the target using different techniques. Three dimensional conformal radiotherapy (3DCT) uses static multi leaf collimators (MLC) at different gantry and collimator angles to block critical organs. More recently, dynamic MLC techniques were introduced into clinical practise. Modulated techniques such as IMRT and VMAT modulate the energy fluence using the MLC, the dose rate and or the gantry speed.

2.2 Linear accelerators in Radiation Therapy

High energy photons or electrons (4-20 MeV) produced by a linear accelerator are most commonly used in radiation therapy to treat tumors. A typical linear accelerator consists of 5 main parts [63]:

- The modulator; serving as a power supply for the linear accelerator.
- The stand; the non-rotating part, that contains the water supply and the high frequency amplifier (klystron or magnetron).
- The gantry; the rotating part of the linear accelerator. All beam generating and shaping parts are located in the gantry.
- The imaging system: Planar megavoltage (MV) or kilovoltage (kV) imaging is available on all commonly used linear accelerators to compare the internal anatomy of the patient to the anatomy at the planning computer tomography (CT). More advanced imaging such as kV or MV cone beam CT (CBCT) is used for more accurate tumor targeting.
- The treatment couch; used for positioning of the patient. Most commonly four dimensional corrections (longitudinal, lateral, vertical and rotation) are applied, however, six degree of freedom (additionally pitch and roll) couches were recently introduced in radiation therapy. There is a potential to use the

treatment couch for dynamic couch tracking, which is discussed in more detail in Chapter 7.

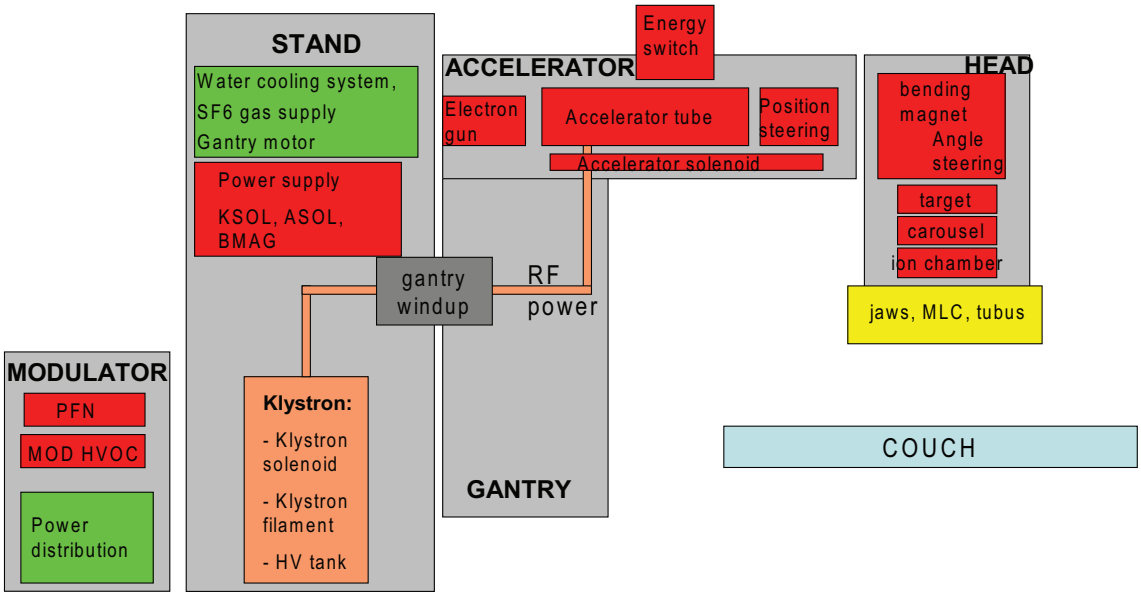

Figure 2.1: Shematic drawing of a linear accelerator

Figure 2.1 is a schematic drawing of a high energy linear accelerator, as the one installed at the University Hospital in Zürich. The first part of the beam generation is the electron gun, which consists of an anode and a cathode. The cathode is heated and a negative potential is applied to it. This causes the electrons to exit the anode material (glow emission). They are focused and accelerated by the anode and injected into the accelerator tube. In the tube a high frequency wave (3 GHz) further accelerates the electrons to a maximum energy between 4 MeV and 20 MeV. The energy switch determines the length of the accelerating wave within the accelerator tube. The longer the wave the higher the residual energy of the electrons. The klystron inside the stand produces the high frequency wave. The modulator supplies the power for the klystron and the electron gun.
After leaving the waveguide, the electrons are bent by 270° by a magnet. If electrons are used for treatment, the electron pencil beam is scattered multiple times on scatteing foils, to broaden the beam. The dose, as well as the symmetry and the flatness of the beam are checked in two monitor chambers. The beam is collimated by a tubus and, depending on the size and shape of the tumor an adequate insert defines the shape of the beam before irradiating the patient.
If photons are used for treatment, a tungsten target is placed in the electron beam's path to produce high intensity Bremsstrahlung. The primary collimator selects the middle part of the beam by cutting off the beam's field edges. Due to the higher probability of forward scattering, there is more dose in the center part of the beam than on the sides. This can be corrected for by using a flattening filter. The

flattening filter is a metal cone that absorbs dose more in the center part of the beam than on the sides to flatten the dose profile. The flatness, as well as the symmetry and the output of the beam are checked by the two monitor chambers. For photon beams, several beam shaping devices are available. The collimator jaws have a very low transmission of 0.1% and used for the basic collimation of the beam. The MLCs are used to achieve more complex shapes. However, the transmission through the MLCs and therefore the dose outside the field is higher (1.2%, [53]) than that of the jaws. Additionally wedges or blocks can be used to further modify the beam to optimized dose to the target [63].

2.3 Accuracy of linear accelerators

The dosimteric as well as geometric accuracy of linear accelerators is essential for the treatment outcome. Modern linear accelerator can achieve sub-millimeter accuracy in all axes as Depuydt et al [25] discussed in their study for various linear accelerators. They have performed starshots of the rotational axes of the gantry, the couch and the collimator of a Varian TrueBeam linear accelerator, a Brainlab Vero system, an Accuray Tomotherapy system, as well as an Elekta Synergy linear accelerator. Figure 2.2 shows the setup used to perform the gantry starshot as well as the digitized image of the film. Similarly, Kim et al [64] published an accuracy of

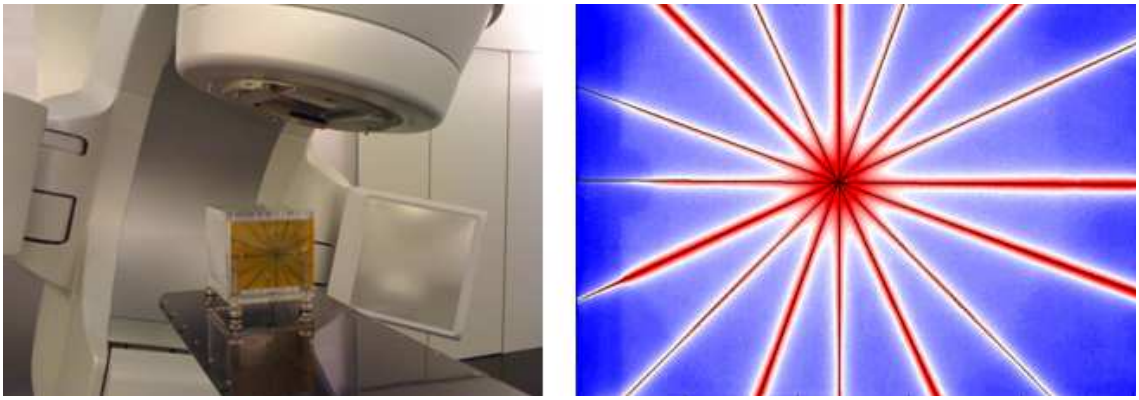

Figure 2.2: Left: Setup used to perform the gantry starshot; Right: digitized image of the film. The film is irradiated from various angles with a a field size of 20 x 0.5 cm^2. The Intersection of the lines defines the position and the size of the isocenter circle

below 1 mm of the rotational axes of the Novalis Tx linear accelerator. Their study was performed using a test similar to the classical Winston Lutz test [81].
Beside the geometric accuracy the dosimteric accuracy of the is important for the treatment outcome. Dutreix [29] concluded that an overall precision of +/-5% on the absorbed dose, at any point in the patient, is required to achieve the predicted treatment outcome. According to the ICRU report 24, the available evidence for

certain types of tumors, points to the need for a dosimetric accuracy of +/-5% at 95% confidence level in the delivery of an absorbed dose to a target volume [54]. Fogliata et al [35] recently showed an agreement of 3% (gamma agreement score 100% for 3%/3mm) between measured and calculated dose distributions in water, bone and normal lung tissue, if an advanced type B dose calculation algorithm is used. Type B algorithm take the scatter in different materials better into account compared to traditional type A algorithms. Similar Aarup et al [1] showed for lung tissue an accuracy within 3% for the Analytical Anisotropic Algorithm and the Collapsed Cone Convolution algorithms (both type B algorithms).
To investigate the overall accuracy of the treatment process end to end testing is being conducted [130]. The phantom undergoes the whole treatment chain as a patient would do, a magnetic resonance image (MRI) and a CT are performed on the phantom. The two imaging modalities are then fused. The organs at risk as well as the tumor gross target volume (GTV) are contoured on the MRI, whereas the treatment plan is created and the dose distribution is calculated on the CT. The treatment plan is irradiated on the phantom at the treatment machine. High resolution detector systems (radiosensitve film or gel) record the dose distribution, which is evaluated afterwards. An overall accuracy of 3%/2mm can be achieved on a static phantom [130]. However patient motion and change in anatomy of the patient can lead to additional inaccuracy. Within the frame of this thesis different investigations were done to reduce patient motion using a faster treatment technique with FFF beams (Chapter 4 and 6) and a couch tracking motion compensation method (Chapter 7). The goal was to reduce the geometrical inaccuracy of the treatment to be similar to the inaccuracy of the linear accelerator.

2.4 Flattening filter free beams

Historically, a relatively flat beam profile over the entire treatment field was desired to calculate dose distributions in a simplified way. This was achieved using the flattening filter. With beam intensity modulated techniques, including IMRT and VMAT, the MLC is used to modify the fluence distribution producing optimal fluence maps for FFF beams similar to those with flattening filter [123, 124]. An increasing interest in FFF technology results from the expectation that it will allow faster treatment delivery with dose rates up to 24 Gy/min [38] (X10FFF in depth of maximum dose, a source-surface distance of 100 cm and a field size of 10x10 cm^2). The high dose rate can be achieved with FFF beams, because the photons are not absorbed in the flattening filter as for conventional beams. It was shown by several investigators that treatment efficiency is increased by a factor of 2-4 for stereotactic body radiotherapy (SBRT) [111, 95].
The beam generation for the FFF beams is similar to the generation for flattened beams. The initial electron pulse, the accelerating wave as well as the magnetic strength of the the bending magnet and most of the time the target are the same

(figure 2.3) as for flattened beams. For higher energies a thicker target can be used,

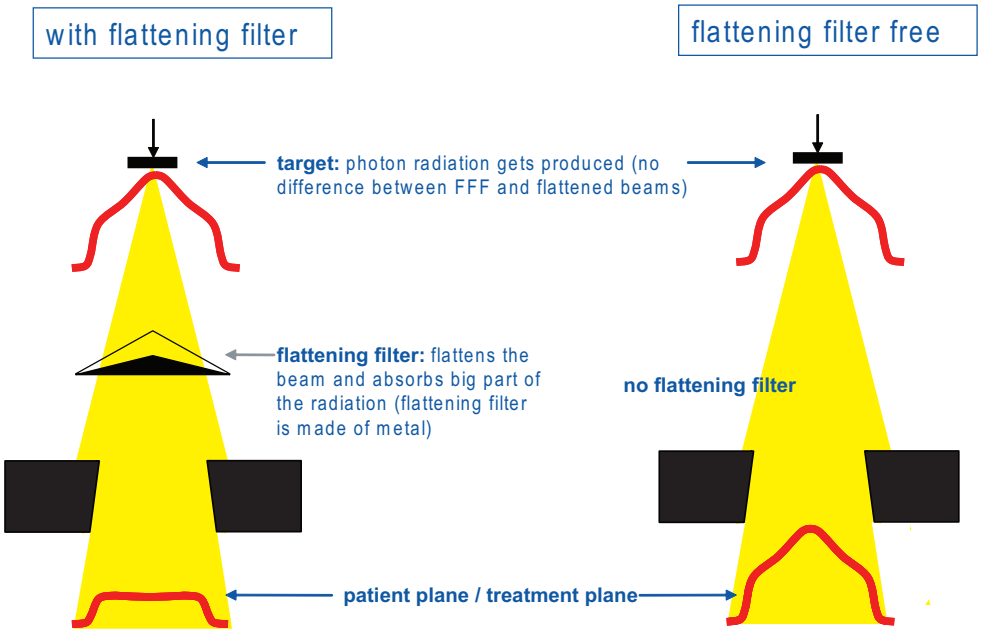

Figure 2.3: The only difference in beam generation between flattened and FFF is the missing flattening filter for FFF beams

to reduce contaminating electrons. The missing flattening filter leads to the differences in beam characteristics. The most obvious difference is the beam profile (figure 2.4). The FFF profile has a higer dose rate on the central axes compared to the field edges. Hrbacek et al [53] showed that the energy fluence ratio can be up to a factor of four for a beam with nominal energy of 10 MeV.
Flattened photon beams are partially absorbed in the flattening filter. Mainly the low energy part of the spectrum is absorbed, which leads to beam hardening. FFF beams don't experience beam hardening and therefore have a lower mean energy compared to flattened beams (figure 2.4). Additionally the flattening filter is the main source of photon scatter in the beam path. This leads to higher out of field dose for conventional beams compared to FFF beams. Another effect, which leads to a reduced out of field dose, is less transmission through the head shielding as the beam production efficiency is higher. Several investigations showed the reduction of out of field dose in a water phantom as well as in an anthropomorphic phantom [53, 66, 20].

2.5 Hypofractionation

The optimal fractionation scheme strongly depends on the type of tumor. A certain amount of radiation causes non-repairable and repairable damage to tissue depend-

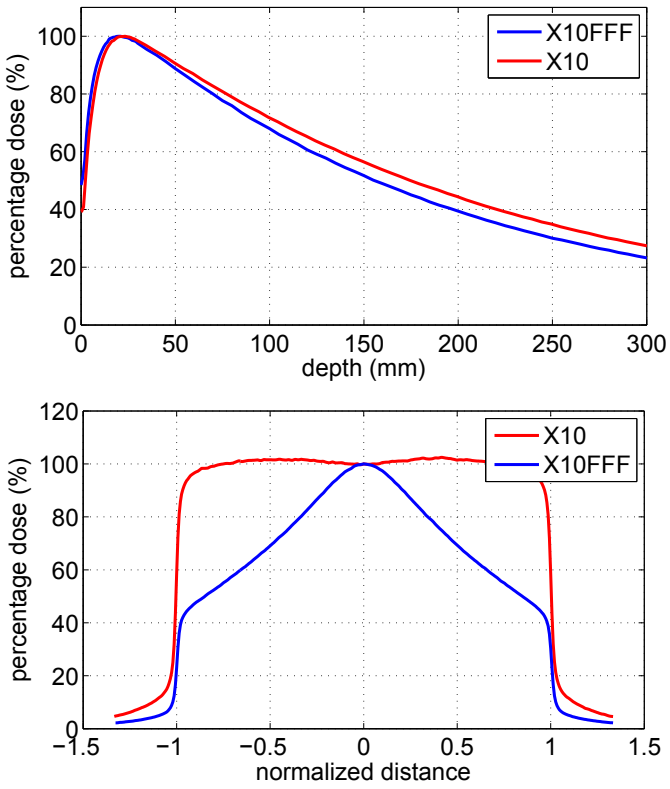

Figure 2.4: Top: Depth dose curve of a X10FFF beam compared to a flattened beam. The FFF beam has a lower mean energy (measured at a source surface distance of 90 cm). Bottom: Profile of a X10FFF beam compared to a flattened beam (measured at a source surface distance of 90 cm and a depth of 10 cm).

ing on the tissue type. Many fractions with a lower dose per fraction most effectively balance tumor control and damage to healthy tissue, if the ratio of non-repairable to repairable damage (therapeutic ratio) for the tumour is greater than the ratio for the surrounding healthy tissue. If these ratios are comparable or the ratio for the surrounding tissue is larger, then a larger dose per fraction (hypofractionation) with a lower total dose is most effective. The clinical experience on the use of conventional fractionation schedules of 2 Gy per fraction is large and normal tissue tolerances are well known. Studies of the response of cancer cell cultures to radiation, however, suggest that fractions with a dose larger than 2 Gy may be more effective. Hypofractionated treatment schedules are proposed for several types of cancers, including breast cancer [13, 7, 132], prostate cancer [37, 82, 73], lung cancer [59, 90] and liver cancer [62, 75]. Concerns about normal tissue toxicity require a more effective normal tissue sparing than for conventional fractionations. Multiple advancements have been made in the past ten years to achieve less dose deposition to

the surrounding tissue. Image guided radiotherapy (IGRT) using MV portal images, kV- image pairs and kV CBCTs have led to better localisation and therefore allow a reduction of treatment margins [44, 100]. Advanced treatment techniques such as IMRT sliding window, VMAT and tomotherapy result in an improved conformity of dose distributions with the option of simultaneous integrated volumes of higher doses [68, 96, 31]. However hypofractionation, reduced margins and micro structure adapted dose distributions with sharp gradients require a stable tumour position. Comparing pre and post treatment CBCT, Reggiori et al showed that the mean movement of the prostate is 0.16 cm (+/- 0.06) during a time period of 4-5 min and increases to 0.29 cm (+/- 0.16) during a time interval of 8 min [107]. Therefore tumor motion management is needed cope with intra-fractional motion.

2.6 Margins in Radiation Therapy

One of the first steps in treatment planning in radiation therapy is the definition of the target volume. According to the ICRU guidelines 50 and 62 [55], different target volumes are defined. The gross tumor volume (GTV) is the gross demonstrable extent and location of the tumor [56]. It includes the primary tumor, metastatic regional node(s) and or distant metastasis. The clinical target volume (CTV) is defined as the GTV and or subclinical malignant disease with a certain probability of occurrence considered relevant for therapy [56]. The planning target volume (PTV) was first introduced in ICRU report 50 [55]. The dose in radiation therapy is prescribed to the PTV. The PTV extends the CTV by the uncertainty of the dose delivery (figure 2.5). This ensures the coverage of the CTV by the prescribed dose. Geometrical uncertainties in RT include both treatment preparation variations (systematic errors such as equipment tolerances, planning setup error, organ motion and target volume delineation) and execution variations (random errors such as treatment setup error, inter- and intra-fraction organ motion). The different types of errors need to be added or combined. If the errors are added linearly, the resulting PTV is often too large. This leads to unnecessary irradiation of healthy tissue and might increase the probability of unwanted side effects. A more advanced approach for margin calculation based on the probability distribution was introduced van Herk et al [122]. The margin M ensures that the minimum dose to the CTV is 95% of the prescribed dose for 90% of the patients:

$$M = 2.5\Sigma + 1.64(\sigma - \sigma_P) \tag{2.1}$$

σ_P describes width of beam penumbra fitted to a Gauss function, Σ represents the systematic and σ the random error [122, 108]. Systematic errors can be calculated for intra-fractional motion, contouring as well as setup; Random errors for intra-fractional motion and patient setup. The total systematic error Σ is then calculated as:

$$\Sigma = (\Sigma^2_{contour} + \Sigma^2_{setup} + \Sigma^2_{IFM})^{1/2} \tag{2.2}$$

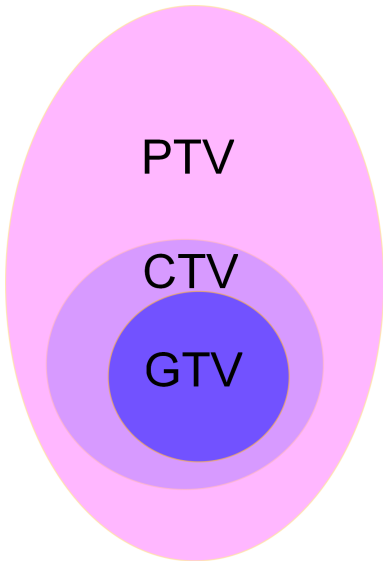

Figure 2.5: The GTV is the tumor volume defined by imaging, the CTV extends the GTV by the subclinical malignant disease and the PTV extends the CTV to account for uncertainties in dose delivery.

The total random error σ is calculated as:

$$\sigma = (\sigma_{setup}^2 + \sigma_{IFM}^2)^{1/2} \tag{2.3}$$

2.6.1 Internal target volume

In the ICRU report 62 [56] it is recommended to add an internal margin (IM) around the CTV to compensate for physiological tumor motion and deformation. The ITV includes the CTV and the IM (figure 2.6). ITVs are commonly used for tumors that move due to breathing. The difference between GTV and ITV can be quite large. In the case of figure 2.6 the GTV is 1.76 ccm, whereas the ITV is 9.82 ccm.

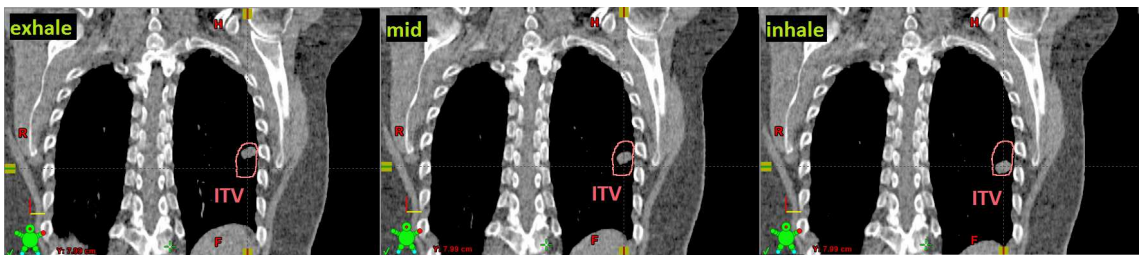

Figure 2.6: The ITV is outlined in red in three breathing phases (inhale, exhale and mid phase. The tumor remains inside the ITV for all three phases

2.7 Motion management

As shown in Chapter 2.3 modern accelerators achieve sub-millimeter accuracy. However not all tumors are stable during the treatment session. Tumors in the lung can move up to 16 mm [114], in the liver up to 34 mm [110] and the thoracic wall moves up to 14 mm [105] due to respiratory motion. Prostate tumors move up to 9 mm mainly due to bowel motion and bladder filling [88]. Tumor motion management is needed to irradiate the tumor while sparing the healthy tissue. This becomes more important for hypo-fractionation, where high doses are applied in a small number of treatment fractions. Several methods for tumor motion management are described below.

2.7.1 ITV concept

As described in section 1.4.1, the ITV accounts for changes in position of the GTV as well as deformation of the GTV due to organ motion. The ITV concept is commonly used for lung and liver tumors [58, 138]. The amount of motion is determined using a four dimensional CT (4DCT). During a 4DCT many CT datasets are acquired, each of them corresponds to a particular respiration phase. In each respiration phase the GTV is contoured and the ITV is defined as the sum of all phases (figure 2.6). This ensures sufficient target coverage however leads to unnecessary dose to healthy tissue. Additionally for modulated techniques such as IMRT and VMAT, there is evidence of an interplay effect between the moving tumor and the moving MLC, which leads to under- and overdosage of the PTV [127, 112].

2.7.2 Gating

The goal of gated treatement delivery is to ensure accurate targeting of the moving tumor, while sparing the healthy tissue. The breathing motion of the patient is monitored and the beam is triggered by this signal. Only during a certain phase range (phase gating) or a certain amplitude range (amplitude gating) the beam is switched on. The higher the desired accuracy is, the tighter becomes the window between upper and lower limit. This results in shorter duty cycles and longer treatment times. Figure 2.7 shows an example of amplitude based gating. The planning CT is recorded in the same phase or amplitude range. Additional to free breathing gating, a triggered radiation can be realized during patient's breath-hold. For breath-hold gating the patient is encouraged to hold his breath for as long as possible.
Several methods exist to track the breathing signal of the patient. Most of them rely on optical detection methods of the surface of the patient or at least of a point on the surface of the patient. The respiratory position monitoring (RPM) gating system (Varian Medical System) uses an infrared camera, which detects the reflected light from a marker block that is placed on the chest wall of the patient. Several investigations have described the application of the RPM system for breast, lung

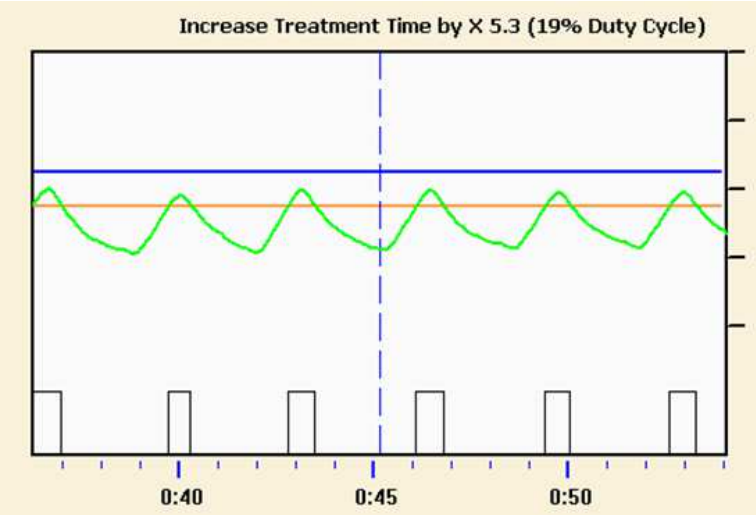

Figure 2.7: Amplitude based gating. The beam is switched on, if the respiration (green line) is within a certain amplitude range (in this case between the orange and blue line).

and liver treatments [128, 57, 43]. Surface detection systems [76, 9] have the advantage that gating can be performed at more than one point. A certain area of the body surface can be selected for gating. This might improve the correlation between external surface motion and internal tumor motion. Wong et al [137] published the idea to use a spirometer for gating. Gating based on spirometry as well as surface detection relies on a stable correlation model between the internal tumor motion and the external motion or air flow. Several publications have shown that this is not necessarly true and the correlation from the planning CT might not be valid on the treatment machine for some patients [41, 50].
Butler et al [16] conducted a study to compare the dose to the healthy lung with and without gated irradiation of lung tumors. They analysed the masses of lung tissue receiving at least 20 Gy (M20). A clear benefit of gated treatments (reduction of M20 between 3% and 57%) over non-gated treatments was found. The main disadvantage of gated treatment delivery is the extended treatment time. Depending on the duty cycle (time in which the beam is switched on), the treatment time can be prolonged up to a factor of four (compare figure 2.7)

2.7.3 Tracking

Tumor tracking is another way to cope with intra-fractional motion. It can be realized by dynamically following the target volume with the radiation beam. This was first implemented in a robotic radiosurgery system, the CyberKnife system [2], and has been further realized by the use of a dynamic MLC [89] and the gimbaled head of the VERO system [25]. Another possibility is to leave the treatment beam

undisturbed but to move the treatment couch in order to achieve a stable tumor position. Several visibility studies have been performed showing the capability of different couch systems to perform tracking. Already in 2005 D'Souza et al [27] presented a couch tracking system based on a hexapod, which could perform tracking for slow breathing periods of 16s. More recently Buzurovic et al [18], Haas et al [46] and Wilbert et al [135] have developed more advanced couch control systems using proportional integral feedback systems. However, none of these couch tracking systems is clinically available.
Menten et al [85] compared a dynamic couch tracking system with a MLC tracking approach for periodic organ motion as well as prostate motion. MLC tracking reduced the respiratory induced motion to 2.0 mm (from 4.1 mm). The treatment couch tracking reduced the amplitude to 2.1 mm. Although this suggests a higher accuracy of the MLC tracking system, dosimetric evaluation of the system showed that the gamma agreement index (GAI) scores between tracked and static dose distributions were higher for treatments performed with couch tracking. GAI scores for tracking of prostate motion were 85% for MLC tracking and 95.3% for treatment couch tracking.
Besides the active tracking component, such as the treatment couch or the MLC, fast motion detection is essential for real-time tumor tracking. Several systems are suggested in the literature, ranging from surface detections systems [76, 9], kV- or MV- marker detection [78, 77] to the detection of three implanted resonant circuits (beacons) in a magnet array [136, 5]. The advantage of a surface detection system is that the patient does not receive any additional dose, however the correlation between the target volume and the surface of the patient might not be stable [41, 50]. MV and kV imaging as well as beacon detection has the advantage of imaging the internal anatomy of the patient. However kV imaging adds a large additional dose to a large volume of the patient. Beacon detection seems to be a good alternative however it leads to some limitation in treatment planning because certain angles can no longer be used for irradiation due to additional equipment requirements. Additionally the necessary extra equipment is expensive and not standardly supplied with linear accelerators. Chapter 7 describes the development and evaluation of a tracking system with clinical available equipment. Three different motion detection sensors are evaluated within the tracking system.

Chapter 3

Ion recombination correction for different ionization chambers in high dose rate flattening filter free photon beams *

3.1 Abstract

Recently there has been an increased interest in flattening filter free linear accelerators. Removal of the filter results in available dose rates up to 24 Gy/min (for nominal energy 10 MV in depth of maximum dose, a source-surface distance of 100 cm and a field size of 10x10 cm^2). To guarantee accurate relative and reference dosimetry for the flattening filter free beams we investigated the charge collection efficiency of multiple air-vented and one liquid ionization chamber for dose rates up to 31.9 Gy/min. For flattened beams, the ion collection efficiency of all air-vented ionization chambers (except for the pinpoint chamber) was above 0.995. By removing the flattening filter we found a reduction in collection efficiency of approximately 0.5-0.9 % for a 10 MV beam. For flattening filter free beams, the Markus chamber showed the largest collection efficiency of 0.994. The observed collection efficiencies were dependent on dose per pulse, but independent of pulse repetition frequency. Using the liquid ionization chamber the ion collection efficiency for flattened beams was above 0.990 for all dose rates. However, this chamber showed a low collection efficiency of 0.940 for the flattening filter free 10 MV beam at a dose rate of 31.9 Gy/min. All investigated air-vented ionization chambers can be reliably used for relative dosimetry of flattening filter free beams. The order of correction for reference dosimetry is given in the manuscript. Due to their increased saturation in high dose rate flattening filter free beams, liquid ionization chambers appear to be

*This chapter has been published in Physics in Medicine and Biology, Vol. 59, No. 9, April 2012 (Lang et al [69]).

unsuitable for dosimetry within these contexts.

3.2 Introduction

Recently there has been an increased interest in flattening filter free (FFF) linear accelerators [125, 20, 65, 53]. Removal of the filter results in available dose rates up to 14 Gy/min and 24 Gy/min for nominal energies of 6 and 10 MV (in depth of maximum dose (dmax), a source-surface distance (SSD) of 100 cm and a field size of 10x10 cm^2), respectively. To guarantee accurate relative and reference dosimetry for such flattening filter free beams we investigated the charge collection efficiency of multiple air-vented and one liquid ionization chamber for dose rates up to 31.9 Gy/min. The two main processes leading to ion recombination are 'initial recombination' and 'general recombination'. Initial recombination is caused by the recombination of two particles originating from the same particle track. It has been previously shown by several authors that within air-vented ionization chambers this contribution is minimal and independent of dose rate [15, 26]. General recombination occurs when particles originating from different particle tracks recombine. Boag [11] developed a theoretical method to account for the general recombination in both pulsed and continuous beams. He proposed the two voltage method [12] to determine the correction for incomplete collection of ions at sufficiently high applied voltages. Since then, numerous investigations regarding the ion collection efficiency of different chambers used for reference dosimetry under a range of conditions have been published [15, 26, 48, 24, 14]. Recently, Bruggmoser et al [14] determined saturation coefficients for a selection of plane parallel and cylindrical chambers in pulsed photon and electron beams up to 42 mGy/pulse. For liquid ionization chambers the two voltage method cannot be applied because the effect of initial recombination cannot be neglected due to the high ionization density in the particle track and the short mean free path of ions in liquid [86, 97, 121]. Moreover, initial recombination is affected by applied voltage and thus leads to a dependency of the general recombination efficiency upon the applied voltage. Pardo-Montero and Gomez [98] developed and verified a three voltage method as well as a modified two voltage method to determine charge collection efficiency in parallel plate liquid ionization chambers. We contribute to these investigations a detailed analysis of recombination effects in several air-vented ionization chambers as well as one liquid ionization chamber using pulsed high dose rate photon beams without flattening filter. This paper is the first systematic study of the performance of ionization chambers with an FFF accelerator commissioned for clinical use. Earlier investigations have been limited to high dose per pulse electron beams [14]. While the clinical use of the FFF is rapidly increasing [111] detailed studies regarding the behaviour of commonly used detectors in conjunction with these beams are lacking. The beam pulse pattern of both FFF and flattened beams were analyzed to show the influence of dose rate, dose per pulse and pulse repetition frequency on collection efficiency. Detectors used for reference

as well as relative dosimetry were investigated to ensure that depth dose curves and profiles were not distorted due to insufficient charge collection within high dose rate regions.

3.3 Materials and Methods

3.3.1 Linear accelerator and beam characteristics

Experimental data was collected using a Varian TrueBeam® linear accelerator (Varian Medical Systems, Paulo Alto) at nominal energies of 6 MV and 10 MV with and without flattening filter in the beam path (X6, X10 and X6FFF, X10FFF, respectively). Characteristics of the four beams have been previously described in detail by Hrbacek et al [53]. For X6 and X10 beams, dose rates between 1 Gy/min and 6 Gy/min (dmax, SSD= 100 cm, 10x10 cm^2) are clinically available. By comparison X6FFF allows dose rates between 4 Gy/min and 14 Gy/min, while X10FFF allows dose rates between 4 Gy/min and 24 Gy/min (dmax, SSD= 100 cm, 10x10 cm^2).
Table 3.1 summarizes the parameters regarding the beam pulse pattern of the four

Table 3.1: Basic characteristics of the beam pulse pattern for the four beams available on TrueBeam® linear accelerator (Varian). Dose rate (DR) (measured at the depth of maximum dose (dmax), SSD = 100 cm and for field size of 10x10 cm^2), Dose rate (measured for a 40x40 cm^2 field at SSD = 90 cm and dmax), time between two pulses (Δt) and DPP (40x40 cm^2, SSD = 90 cm, dmax) were measured using delta4® phantom (ScandiDos, Sweden). For X6 and X10 the pulses come regularly (every 2.78 ms @maximum dose rate), however for X6FFF and X10FFF every forth to fifth pulse is dropped

Energy	**DR (Gy/min)**	**DR (40x40) (Gy/min)**	**Δt (ms)**	**DPP in dmax (mGy)**
X10FFF	4.0-24.0	5.3-31.9	16.7 - 2.8	1.7
X6FFF	4.0-14.0	5.6-21.6	9.7 - 2.8	1.1
X6	1.0-6.0	1.4-8.6	16.7 - 2.8	0.4
X10	1.0-6.0	1.4-8.4	16.7 – 2.8	0.4

energies at respective minimum and maximum dose rates. Dose per pulse (DPP) and pulse repetition frequency (PRF) were measured with the delta4® phantom (ScandiDos, Uppsala). At maximum dose rate PRF was equal for all beams. The increased dose rate of FFF beams is due to the increased DPP relative to flattened beams. Reduction of the dose rate is achieved within the TrueBeam system by changing the PRF, whilst maintaining the same DPP. For X6 and X10, pulses are generated at regular intervals (every 2.8 ms at maximum dose rate). For X6FFF

and X10FFF however, every forth to fifth pulse is omitted. Therefore for X6 and X10 DR, DPP and PRF can be related but not for the FFF beams.

3.3.2 Detectors under investigation

The general ion collection efficiency at different DPP and PRF was determined for six ionization chambers in total:

- PTW 34001 Roos chamber
- PTW 34045 Advanced Markus Chamber
- PTW 31010 Semiflex chamber
- PTW 31016 PinPoint chamber
- PTW 30013 Farmer chamber
- PTW 31018 microLion chamber, liquid ionisation chamber

. Details on the chambers, provided in the manuals of the vendor (PTW, Freiburg), are summarized in table 3.2.

Table 3.2: Basic specifications of the chambers (PTW, Freiburg) investigated: 4 different thimble (t) chambers and 2 plane-parallel (pp) chambers. Chambers differed in terms of active volume, applied voltage and geometry. The microLion chamber is filled with liquid isooctane. All other chambers are vented and respectively filled with air.

chamber	**type**	**active volume (cm^3)**	**operating voltage (V)**	**charge collection time (ms)**
31010 Semiflex	t	0.125	400	0.1
31016 PinPoint	t	0.016	400	0.06
34001 Roos	pp	0.35	200	0.125
34045 AdvMarkus	pp	0.02	300	0.022
30013 Farmer	t	0.6	400	0.14
31018 MicroLion	t/liquid	0.002	800	5.3

3.3.3 Ion collection efficiency for gas filled chambers

According to Boag [11] the ion collection efficiency of an air vented ionization chamber in pulsed beams can be expressed as:

$$f = u^{-1}\ \ln(1-u) \tag{3.1}$$

$$u = \mu\rho\frac{d^2}{V}. \tag{3.2}$$

(μ is a constant involving the ion recombination coefficient and mobilities, ρ is the pulse charge density, d the equivalent electrode spacing and V the polarizing voltage). For small charge densities this formula can be expanded up to the first order term, which leads to a description of the saturation correction:

$$k_S = \frac{1}{f} = 1 + \frac{\mu}{2}\rho\frac{d^2}{V} \tag{3.3}$$

For chambers that follow this relation the saturation coefficient k_S can be determined using Boag's two voltage method [12]:

$$k_S = \frac{\frac{V_1}{V2} - 1}{\frac{V_1}{V2} - \frac{Q_1}{Q_2}} \tag{3.4}$$

V_1 is the operating voltage and V_2 an arbitrary voltage (smaller than the operating voltage), Q_1 and Q_2 are the collected charges at these voltages. We determined the correction factors for all air vented filled ionization chambers according to this formula. The operating voltages V_2 for the chambers can be found in table 2. V_2 was chosen to be half of V_1, as recommended by Almond et al [4]. All measurements were performed for a geometry, which maximizes dose rate, i.e. shortest SSD (90 cm) (within commissioning relevant limits), largest field size 40 x 40 cm^2), and at the depth of maximum dose. The dose corresponding to 100 MU was:

- 1.40 Gy @ depth of 1.21cm for X6FF
- 1.33 Gy @ depth of 2.10 cm for X10FFF
- 1.46 Gy @ depth of 1.43 cm for X6
- 1.40 Gy @ depth of 2.23 cm for X10.

This resulted in a DPP of 1.1 mGy for X6FFF, 1.7 mGy for X10FFF, 0.4 mGy for X6 and 0.4 mGy for X10. The dependency of ion collection efficiency upon PRF, DPP and beam energy was studied.

3.3.4 Ion collection efficiency for liquid ionization chambers

In liquid ionization chambers the influence of initial recombination cannot be neglected. The charge released within the chamber is dependent upon the applied voltage. If DPP is low and the time between pulses is longer than the ion collection time of the chamber, the collected charge Q, will relate linearly to the applied voltage V [98]:

$$Q = Q_0(1 + c \cdot V) \tag{3.5}$$

We determined the coefficients c and Q0 at PRF less than 100 Hz and a DPP of 0.03 mGy (SSD = 120 cm, depth = 25 cm, X6 and X10). According to the modified 2-voltage method of Pardo-Montero and Gomez [98], which is valid so long as the ion collection time is small relative to the time between two consecutive pulses, the ion collection efficiency can be determined as follows:

$$f = \frac{(1+cV_2)^2 V_1 Q_1 - (1+cV_1)(1+cV_2)V_2 Q_1}{(1+cV_2)^2 V_1 Q_1 - (1+cV_1)^2 V_2 Q_2} \tag{3.6}$$

According to this method we determined the collection efficiency of the liquid ionization chamber for all four beams at the lowest available PRF (time between two pulses > ion collection time of 5.3 ms). For higher PRF the relative collection efficiency compared to the Markus chamber was determined. The ratio of reading between the liquid filled chamber and the Markus chamber was compared for different doses per pulse. Dose per pulse was changed by varying the measurement depth (2 cm to 30 cm) as well as the SSD (SSD=90 cm and SSD=120 cm). The collection efficiency of the Markus chamber was above 0.994 (shown in the first part of the results) and therefore neglected for the relative comparison to the liquid ionization chamber. For the lowest dose per pulse (SSD = 120 cm, depth = 30 cm) the ratio was set to 1, as it is known that the collection efficiency is high (above 0.995) for a dose per pulse below 0.3 mGy [119].

3.3.5 Propagation of uncertainty

Q_1 and Q_2 were measured multiple times and mean values and standard deviations of the mean u_{Q1} and u_{Q2} were calculated. Using uncertainty propagation the standard deviation for the ion collection efficiency u_f was calculated according to:

$$u_f = \sqrt{\frac{df}{dQ_1}^2 u_{Q1} + \frac{df}{dQ_2}^2 u_{Q2}} \tag{3.7}$$

3.4 Results

3.4.1 Ion collection efficiency for air-vented chambers

Table 3.3 summarizes ion collection efficiency factors of all investigated air-vented chambers for all four beams. The collection efficiency was above 0.985 ($2u_f = 0.002$) in all cases. The Markus chamber demonstrated the largest collection efficiency 0.994 ($2u_f = 0.002$) for X10FFF; 0.997 ($2u_f = 0.001$) for X6 and X10). The collection efficiency was independent of pulse repetition frequency (figure 3.1), implying that for a given beam with specific DPP the collection efficiency does not change with dose rate. The collection efficiency corrections for 6 MV and 10 MV beams did not significantly differ. Figure 3.2 shows the relationship between ion collection efficiency

Table 3.3: Ion collection efficiencies of the five air-vented ionization chambers (PTW, Freiburg) at depth of maximum dose, field size 40 x 40 cm^2 and SSD = 90 cm. Two standard deviations are given in brackets.

Chamber	**X6** (DPP=0.4mGy)	**X10** (DPP=0.4mGy)	**X6FFF** (DPP=1.1mGy)	**X10FFF** (DPP=1.7mGy)
Semiflex	0.995 (0.003)	0.995 (0.001)	0.991 (0.001)	0.988 (0.001)
PinPoint	0.991 (0.001)	0.992 (0.001)	0.990 (0.002)	0.990 (0.003)
Farmer	0.997 (0.001)	0.997 (0.002)	0.992 (0.001)	0.989 (0.002)
AdvMarkus	0.999 (0.001)	0.999 (0.001)	0.998 (0.001)	0.994 (0.002)
Roos	0.997 (0.001)	0.996 (0.001)	0.992 (0.001)	0.986 (0.002)

and DPP; the collection of charge became less efficient with increasing DPP (table 1 shows DPP for the four beams). Extrapolating the linear fit of the data to zero shows the initial recombination of all chambers below 0.2 % ($2u_f = 0.1\%$), except for the pinpoint chamber which generated an initial recombination of 0.87 % ($2u_f = 0.2\%$).

3.4.2 Ion collection efficiency for liquid filled chambers

The coefficient c which describes the relationship between produced charge and applied voltage (equation 4) was determined to be $0.001123V^{-1}$ ($u = 3.30 \cdot 10^{-5}V^{-1}$). Figure 3.3 shows the relationship between DPP and collection efficiency for both methods. The collection efficiency was seen to decrease with increasing DPP and PRF. Both methods show comparable results. Collection efficiency for flattened beams was above 0.99. With increasing DPP, the collection efficiency decreases to approximately 0.96 for the X10FFF at low PRF and 0.94 at high PRF (both DPP = 1.7 mGy).

3.5 Discussion

3.5.1 Ion collection efficiency for air vented chambers

Our results confirm that air vented chambers can be used for relative dosimetry of FFF beams without correction for collection efficiency. When applied for the reference dosimetry, a collection efficiency of 0.991 (for X10FFF) and 0.998 (for X6) was found for the Farmer chamber at the reference geometry (SSD=100 cm, depth=10 cm, field size 10x10 cm^2). For the pinpoint chamber, a low ion collection coefficient for all four beams was found as well as a very high initial recombination factor. Agostinelli et al [3] reported for the PinPoint chamber (PTW 31014), that the saturation curve was not linear above 150 V. Therefore, the two-voltage method leads to an underestimation of the collection efficiency by approximately 0.5 % (for an applied voltage of 400 V). The design of the two PinPoint chambers PTW 31014

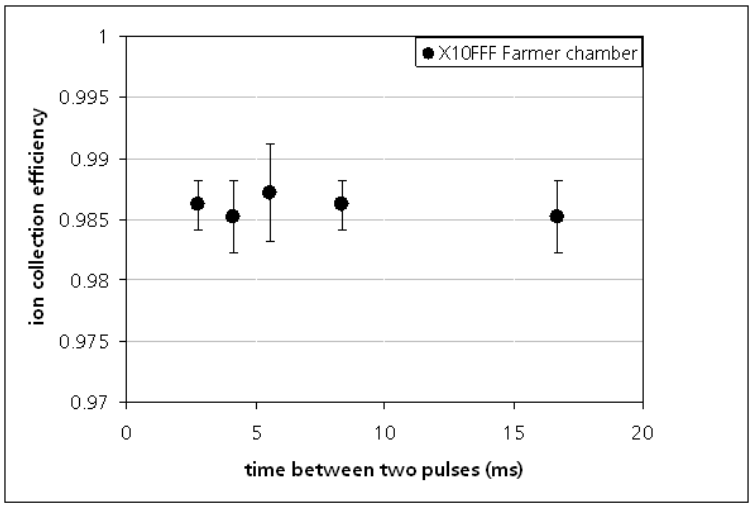

Figure 3.1: Dependency of collection efficiency on pulse repetition frequency when using the Farmer chamber (PTW, Freiburg). The time between pulses (dt) was altered by varying the dose rate of the X10FFF beam between 2400 MU/min (dt = 2.78 ms) and 400 MU/min (dt = 16.67 ms).

and PTW 31016 is very similar. It is therefore likely that the PTW 31016 chamber operated at 400 V was also within the non-linear region and collection efficiency using the two-voltage method was underestimated.
Results obtained for the collection efficiency of the Roos and Farmer chamber are in a good agreement with those published by Bruggmoser et al [14]. Their calculated collection efficiency of 0.985 in pulsed electron beams (for a DPP of 1.7 mGy) corresponds with our measurement of the X10FFF beam. The collection efficiency for doses per pulse of 1.1 mGy, 0.41 mGy and 0.39 mGy were determined to be 0.990, 0.996 and 0.9965, respectively, by Bruggmoser et al [14]. Similarly, we found 0.992 (X6FFF, DPP = 1.1 mGy), 0.996 (X6, DPP = 0.4 mGy) and 0.9965 (X10, DPP = 0.4 mGy)). Using the Farmer chamber, Bruggmoser et al [14] published slightly lower collection efficiencies (0.981 @ DPP = 1.7 mGy, 0.989 @ DPP = 1.1 mGy and 0.9955 @ 0.41 mGy). However, a different polarizing voltage was applied (300 V rather than 400 V).

3.5.2 Ion collection efficiency for liquid filled chambers

The microLion chamber had an ion collection efficiency of 0.94 when exposed to the X10FFF beam at maximum dose rate. Ion collection efficiency correction should therefore be applied for both reference and relative dosimetry. Lowering of the dose rate increased the ion collection efficiency because the time between pulses became long enough for the pulses to be fully collected. Measuring depth dose curves of a 10 x 10 cm^2 field (X10FFF, DR 24 Gy/min), the collection efficiency varied from 0.941

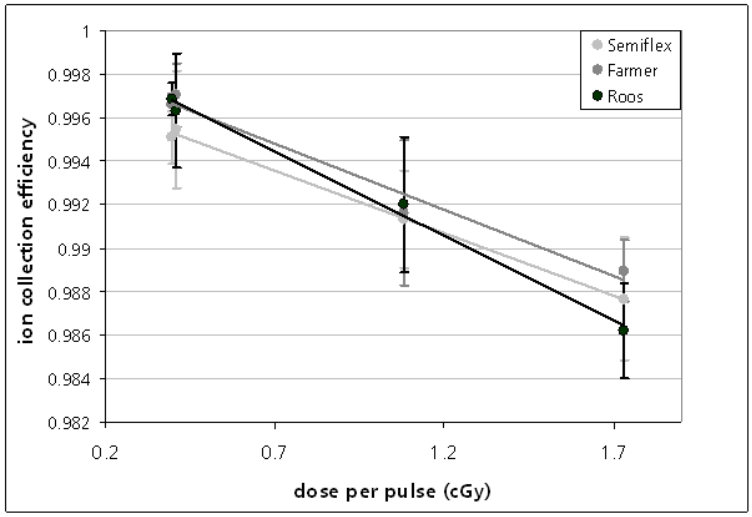

Figure 3.2: Ion collection efficiency decreases linearly with increasing dose per pulse for the Farmer chamber, SemiFlex chamber and Roos chamber (all PTW, Freiburg). (X10FFF : DPP = 1.73 mGy, X6FFF: 1.08 mGy, X6: 0.4 mGy and X10: 0.39 mGy).

at the depth of maximum dose to 0.977 at 30 cm depth. Normalising the beam to the dose maximum, as is common practise, leads to an overestimation of dose in the tail region of the depth dose curve. This discrepancy increased with depth. Most liquid filled ionization chambers described in the literature have a larger active volume [60, 61] or use a different liquid [22] than the MicroLion chamber. A similar chamber design was evaluated by Steward et al [119]. For a 6 MV beam with dose rate of 1 Gy/min and DPP of 0.36 mGy, a collection efficiency of 0.995 was determined. This is in agreement with our result (0.996 (u = 0.005)). Wickman and Nyström [133] reported a collection efficiency of 0.9945 for pulsed radiation at a PRF of 100 Hz, which reduced to 0.992 when the PRF was increased to 200 Hz. In our study, a similar reduction was observed when the PRF was increased to 330 Hz.

3.6 Conclusion

Five commonly used air vented ionisation chambers were investigated to determine their collection efficiency in high dose rate and high dose per pulse flattening filter free photon beams. For all chambers collection efficiency was above 0.986 and can therefore be used reliably for relative dosimetry. The Markus chamber demonstrated the largest ion collection efficiency (0.994 @ DPP = 1.7 mGy, X10FFF beam). The order of correction for reference dosimetry is given within the manuscript. Additionally, the performance of the iso-octane filled MicroLion chamber was tested. Ion collection efficiency for flattened beams was above 0.99 for both investigated beams at all dose rates. However, we observed a relatively low collection efficiency of 0.960

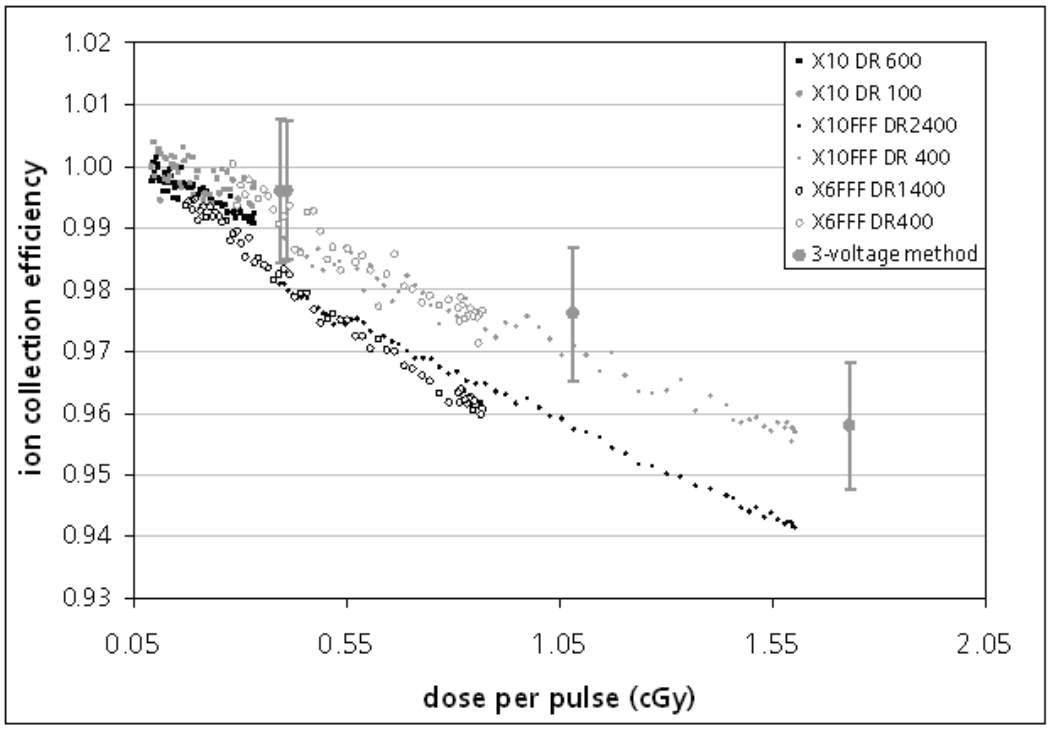

Figure 3.3: Relative ion collection efficiency of the microLion chamber (PTW, Freiburg) for the four beams at different dose rates (DR) decreases with increasing dose per pulse. The results obtained using the modified two voltage method agree well with the relative measurements (compared with advanced Markus chamber, PTW).

for the X10FFF beam at a dose rate of 5.32 Gy/min. Increasing the dose rate to 31.9 Gy/min further decreased the collection efficiency to 0.940. It is therefore not advisable to use this chamber for flattening filter free depth dose curve measurements.

Chapter 4

The use of photon beams of a flattening filter-free linear accelerator for hypofractionated volumetric modulated arc therapy in localized prostate cancer*

4.1 Abstract

Purpose: To evaluate the potential usage of flattening filter-free (FFF) photon beams in the treatment of prostate cancer.
Methods and Materials: Volumetric modulated arc therapy (VMAT) treatment planning was performed for seven patients using TrueBeam® linear accelerator and photon beams with (X6, X10) and without (X6FFF, X10FFF) flattening filter. Prescribed dose was 19 x 3 Gy = 57 Gy. One or two 360° arcs with dose rate of 600 MU/min for flattened beams, and 1200 MU/min for FFF beams were used.
Results: No difference was detected between the four beams in PTV coverage, conformity and homogeneity. Mean body dose and body volume receiving 50% of the prescribed dose decreased with increasing mean energy ($R2 = 0.8275$, $p < 0.01$). X6FFF delivered 3.6% more dose compared to the X6 ($p < 0.01$). X10FFF delivered 3.0% ($p < 0.01$), and the X10 5.8% ($p < 0.01$) less mean body dose compared to X6. There was a significant increase in the mean dose to the rectum for the X10 compared to X6 (2.6%, $p < 0.01$). Mean dose to the bladder increased by 1.3% for X6FFF and decreased by 2.3% for X10FFF. Using a single arc and FFF, treatment time was reduced by 35% (2SD = 10%).
Conclusion: FFF beams resulted in dose distributions similar to flattened beams.

This chapter has been published in International Journal of Radiation Oncology Biology* Physics, Vol. 83, No. 5, August 2012 (Zwahlen et al [139]).

X10FFF beam provided the best solution, sparing rectum and bladder and minimizing whole body dose. FFF beams lead to a time efficient treatment delivery, particularly when combined with hypofractionated VMAT.

4.2 Introduction

The possibility of a low $\alpha\backslash\beta$ -ratio for prostate cancer provides a radiobiological advantage for hypofractionated radiation therapy (RT) with excellent local control and low toxicity [109]. Intensity modulated RT (IMRT) and volumetric modulated arc therapy (VMAT) are used to reduce doses to bladder and rectum while maintaining optimised dose coverage and conformity of the planning target volume (PTV) [113]. Compared to 3D conformal RT (3DCRT) these highly conformal treatments require more monitor units (MU) and increased treatment time. There is also increased leakage and scatter dose from the linear accelerator (LINAC) multileaf collimator (MLC) outside the treatment volume resulting in a higher whole body dose [47]. Increasing head shielding and removing the flattening filter reduces head leakage and scatter. Removal of the flattening filter reduces number of photon interactions within the gantry and increases dose delivery efficiency [125].
TrueBeam® STx (Varian Medical Systems, Paolo Alto, CA, USA) is a new platform of LINAC designed to deliver flattened, as well as flattening filter-free (FFF), beams [53]. Historically, the flattening filter provided a relatively flat beam profile over the entire treatment field and dose distributions was calculated in a simplified way. With beam intensity modulated techniques, including IMRT and VMAT, the MLC is used to modify the fluence distribution producing optimal fluence maps for FFF beams similar to those with flattening filter [125, 126]. Interest in FFF technology is resulting from the expectation that it will allow faster treatment delivery with dose rates up to 24 Gy/min [38].
Several studies summarised the properties of FFF beams of various LINACs based on Monte Carlo simulations or dosimetric measurements [53, 126, 20, 40, 65, 118]. Few studies investigated the feasibility of using FFF beams for IMRT treatment planning [20, 118, 123, 124]. The studies were performed for prototype LINAC and treatment planning systems with pre-clinical release and showed comparable IMRT dosimetric plan quality for FFF compared to flattened beams.
This is the first treatment planning study investigating hypofractionated VMAT with 6 MV and 10 MV FFF photon beams in a clinically released setting for patients with localised prostate cancer.

4.3 Materials and Methods

4.3.1 Patient selection and contouring

Planning study included the computed tomographies of seven patients with localized prostate cancer. After ethics approval, men were treated in the CHHiP trial (Conventional or Hypofractionated High Dose Intensity Modulated Radiotherapy for Prostate Cancer, The Institute of Cancer Research, Sutton, Surrey, UK) at the University Hospital Zurich. Patients were randomized between conventional radiation therapy (74 Gy in 37 fractions) and the experimental groups of 60 Gy in 20 fractions and 57 Gy in 19 fractions (treating 5 days per week) [23]. Patients were treated with RapidArc®plans and 6 MV flattened beams in 2010.
Contouring of target volumes and organs at risk (OAR) was performed using the CHHiP protocol, version 8 [23]. Gross tumour volume (GTV) included the prostate only. Clinical target volume (CTV) 1 included prostate and base of seminal vesicles (proximal 2 cm) with 5 mm margin or prostate and seminal vesicles with 5 mm margin for patients with risk of seminal vesicle involvement. CTV 2 encompassed prostate only with 5 mm margin. CTV 3 included prostate only. PTV 1 to 3 added a 5 mm margin to the relevant CTV, except that for PTV 2 and 3 there was 0 mm margin posteriorly or posterior inferiorly. OARs outlined included bladder, rectum, bowel, femoral heads, urethral bulb and skin. Generated PTV and OAR volumes are summarized in Table 4.1.

Table 4.1: Volumes for planning target volumes, organs at risk, and dose constraints

Volume	Mean (+/- 1 SD) (ccm)	Range (ccm)	Dose constraints
PTV 1	202.5 (+/- 29.0)	149.0 - 238.2	V99% $\geq$ 76% of PD, mean (PTV1-PTV2) $\geq$ 80% of PD
PTV 2	136.1 (+/- 31.5)	101.3 - 198.3	V99% $\geq$ 91% of PD, mean (PTV1-PTV2) $\geq$ 96% of PD
PTV 3	75.3 (+/- 16.1)	56.3-104.1	V99% $\geq$ 95% of PD, V99% $<$ 105% of PD
Rectum	129.9 (+/- 31.3)	134.7 - 334.0	V68% $\leq$ 60%, V81% $\leq$ 50%, V95% $\leq$ 15%, V100% $\leq$ 3%
Bladder	253.6 (+/- 68.8)	107.9 - 198.9	V68% $\leq$ 50%, V81% $\leq$ 25%, V100% $\leq$ 5%,
Urethral bulb			V68% $\leq$ 50%, V81% $\leq$ 10%
Femoral heads			V68% $\leq$ 50%
Bowel			V68% $\leq$ 17 mL

4.3.2 Photon beams

Treatment planning was performed using four photon beams of TrueBeam® STx LINAC. Beams with nominal energies of 6 MV and 10 MV with flattening filter in the beam path (X6 and X10) and FFF beams (X6FFF, X10FFF) were investigated. Detailed description of these beam characteristics is reported elsewhere [53]. Removal of the flattening filter had several implications on the beam properties including a non-flat beam profile, an increase in maximal dose rate of up to 14 Gy/min for X6FFF and 24 Gy/min for X10FFF as well as a decrease in mean radial energy (TPR20/10: X6 0.667, X6FFF 0.631, X10 0.738, X10FFF 0.692) as there was no beam hardening. As a measure of beam energy, the beam quality index TPR20/10 (ratio of the tissue phantom ratio at 20 cm and 10 cm) was used.

4.3.3 Treatment planning

Prescribed dose was 19 x 3 Gy = 57 Gy. Four VMAT plans (RapidArc®) were calculated for each patient using the Eclipse® External Beam Planning System (PRO 8.9, AAA 8.9, Varian Medical Systems). The plans were normalized that PTV3 received a mean dose of 100% of the prescribed dose. Dose constraints were specified in the CHHiP trial protocol [23] and are reported in Table 4.1. One 360° arc (n = 3) was used to fulfil the constraints with maximum dose rate of 600 MU/min for flattened beams and 1200 MU/min for unflattened beams. A second arc (n = 4) was added in case constraints could not be met. For plans using one arc, collimator angle was 45°. Using two arcs separation in collimator angle was 90°. Objectives for OAR were interactively lowered during optimisation for X6 beams without compromising target coverage. After achieving a satisfactory set of constraints, plans for all four energies were optimized using these constraints. Final dose calculation was performed with Eclipse® AAA 8.9 algorithm and a calculation grid size of 2.5mm.

4.3.4 Plan evaluation and statistical methods

Plan evaluation was performed according to the CHHiP trial protocol [23]. MU, mean body dose, surface dose (cumulative dose in the first 2 mm of the body), mean doses to rectum and bladder, conformity index (volume enclosed by the prescription isodose / target volume) of PTV 1, ratio of volume receiving 50% of dose to PTV 1 and treatment time were recorded.
Plans using X6FFF, X10FFF and X10 beams were compared to the X6 base plan and ratios of acquired dosimetric parameters recorded.
Statistical analysis was performed with MATLAB®, version 7.6, software (MathWorks, Natick, MA, U.S.A.). Mean values and standard deviation of the mean (SD) were collected. Relative dosimetric changes were compared applying the non-parametric Wilcoxon signed-rank test. A two-sided p value of 0.05 was considered statistically significant. Confidence intervals (CI) included 95% of the measured data. Box-Whisker-Plots were created for selected data, showing ratios of X6FFF, X10FFF and X10 beams to X6 beam.

4.4 Results

4.4.1 Dose distribution and PTV coverage

For all treatment plans, there were only minor differences in dose distributions using X6FFF, X10FFF, X10 and X6 beams. No difference was detected between the four beam qualities with respect to PTV coverage and conformity. Target inhomogeneity was increased by 1% for X6FFF and X10FFF beams compared to flattened beams (Fig. 4.1), and below the expected specification of 10% (Table 4.2).

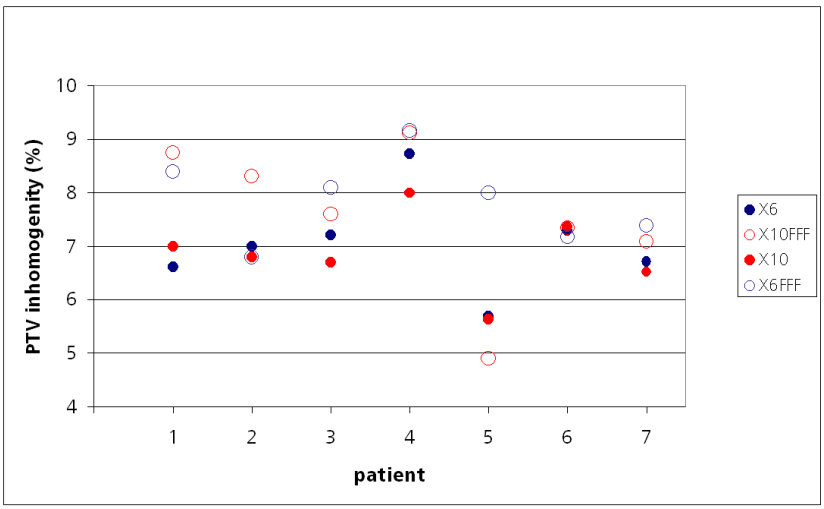

Figure 4.1: PTV inhomogeneity (defined as Dmax-Dmin in PTV3) for the four different energies. Inhomogeneity is increased for FFF beams.

Table 4.2: Dosimetric parameters for the plans using the four different beam modalities: MU, dose parameters, and beam-on time (mean +/- 1 SD). The beam-on time included patients treated with one and two arcs.

	X6	**X6FFF**	**X10**	**X10FFF**
Number of Mus	897 (+/- 202)	951 (+/- 141)	718 (+/- 88)	896 (+/- 133)
Mean body dose (Gy)	8.52 (+/- 2.40)	8.83 (+/- 2.46)	8.06 (+/- 2.36)	8.27 (+/- 2.32)
Mean dose to rectum (Gy)	55.6 (+/- 3.6)	55.7 (+/- 3.2)	57.0 (+/- 3.8)	55.6 (+/- 4.11)
Mean dose to bladder (Gy)	36.2 (+/- 7.7)	36.7 (+/- 8.0)	36.0 (+/- 8.3)	35.5 (+/- 8.0)
Conformity PTV 1	1.38 (+/- 0.11)	1.39 (+/- 0.12)	1.38 (+/- 0.12)	1.38 (+/- 0.13)
Inhomogeneity PTV 3	7.1 (+/-0.99)	7.9 (+/-0.85)	6.9 (+/-0.78)	7.6 (+/-1.51)
Beam-on time (min)	1 min, 47 sec	1 min, 34 sec	1 min, 43 sec	1 min, 34 sec

4.4.2 Monitor units and mean body dose

The mean body dose decreased significantly with increasing mean energy of the beam (R2 = 0.8275, $p < 0.01$) (Fig. 4.2). X6FFF beam delivered 3.6% more dose compared to the X6 beam ($p < 0.01$, CI = 2.2% - 4.9%). X10FFF beam delivered 3.0% less dose ($p < 0.01$, CI = -2.3% - -4.7%) and the X10 beam 5.8% less dose ($p < 0.01$, CI = -3.8% - -7.8%). The volume receiving 50% of the prescribed dose to PTV 1 decreased significantly with increasing mean energy (Fig. 4.3).

MU significantly increased for X6FFF by 7.7% ($p < 0.02$, CI = 0.8% - 16.5%), and for X10FFF by 1.2% ($p = 0.7$, CI = - 8.2% - 9.8%), however increase was not significant. A significant decrease of 18.8% ($p < 0.02$, CI = -4.7% - -30.9%) in MU for X10 was detected due to the higher mean energy (Table 4.2).

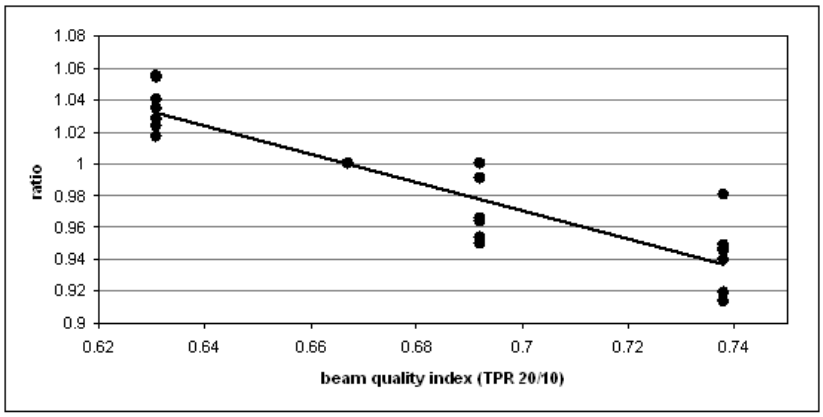

Figure 4.2: Mean body dose dependence on the beam quality. Body dose was normalized to mean body dose of X6 beam.

4.4.3 Dose to skin and organs at risk

Compared to X6 beam, the mean skin dose significantly increased by 8.2% ($p < 0.01$, CI = 5.9% - 11.3%) for X6FFF beam and decreased significantly by 9.1 % ($p < 0.01$, CI = -7.8% - -11.7%) and 12.9% ($p < 0.01$, CI = -9.9% - 14.1%) for X10FFF and X10 beams. There was no difference in mean dose to the rectum and dose parameters V68%, V81%, V95%, V100% were not statistically different for X6, X6FFF and X10FFF beams (Table 4.2). A significant increase in mean dose of 2.6% ($p < 0.01$, CI = 0.6% - 4.2%) to the rectum was measured for X10 compared to X6 beam energy. The mean dose to the bladder was increased significantly by 1.3% for X6FFF ($p < 0.02$, CI = -0.1% - 2.2%) and decreased significantly by 2.3% ($p < 0.02$, CI = -0.2% - 3.7%) for X10FFF; no significant changes were detected for X10 (Table 4.2).
For the urethral bulb there was no difference for V68% and V81% with respect to the four beams, and V68% for bowel and femoral heads were within the required constraints for all patients and beam energies.

4.4.4 Treatment time

For plans using a single arc, treatment time was significantly reduced to one minute when using X6FFF and 10XFFF beams. The mean treatment time for single arc X6 and X10 plans were 1 minute 30 seconds and 1 minute 25 seconds (Table 4.2). The higher maximum dose rates for FFF beams allowed the gantry to run at maximum speed during the full arc. For flattened beams the gantry had to slow down in order to deliver the necessary MU. There was no difference in treatment time if two arcs were used.

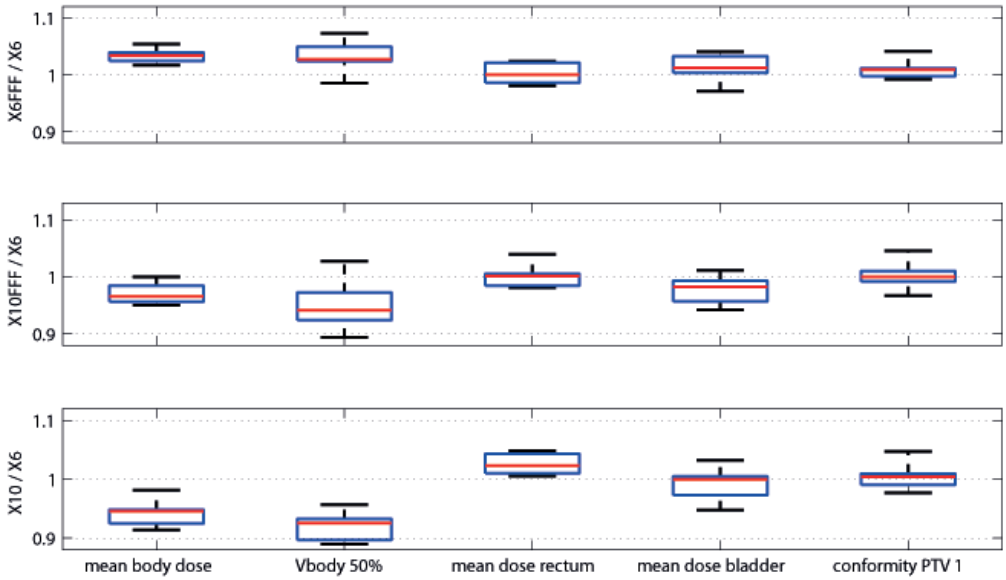

Figure 4.3: Box-Whisker-Plots for different dose parameters. Ratio of X6FFF (top), X10FFF (middle), X10 (bottom) with X6. The red line represents the median value, the blue box the interquartile range and the whiskers minimum and maximum.

4.5 Discussion

The results of this planning study demonstrated that with hypofractionated VMAT dose distribution, conformity and homogeneity within the PTVs were similar using either flattened or unflattened 6 and 10 MV photon beams. We showed that the mean body dose was a function of beam energy and decreased with increasing mean energy. Absence of the flattening filter resulted in a 3.6% higher mean body dose for X6FFF compared to X6 beams. X10FFF decreased the mean body dose by 3% compared to the X6 beam; however, it increased the mean body dose by 2.8% compared to X10. For the rectum, mean organ dose increased for the 10 MV-unflattened photon beam compared to the 6 MV beams. Interestingly, usage of X10FFF decreased mean bladder dose compared to the other three beam qualities. Finally, with FFF technology treatment time for a single arc was significantly reduced due to increased dose rate and faster delivery time.

Ensuring high quality 3DCRT, homogeneous photon fluence across the treatment field is of high priority to achieve optimal PTV coverage. A flattening filter was needed to ensure homogeneous target coverage. With the introduction of MLC changing leaf positions across the field modulate photon fluence to achieve optimal fluence maps [126, 118]. A uniform beam is no longer necessary as comparable treatment planning results for either flattened or unflattened beams have been reported

[38], in particular for smaller treatment fields used in extracranial stereotactic RT for lung cancer [123]. Vassiliev et al. [123] reported in their planning study using 6 and 18 MV IMRT, with and without flattening filter, similar treatment plans regarding PTV coverage for prostate cancer. Depending on the beam energy, X6FFF produced superior IMRT plans than X6. X18FFF resulted in inferior plans compared to X18 due to larger differences between optimal and deliverable fluence maps when compared to 6 MV [124]. However, plans and treatment delivery parameters were not fully optimized for FFF beams and the authors state that improvement of PTV coverage for either plan might have been possible with different user-specific cost functions for either the PTV or organs at risk. Similarly, Stathakis et al. observed negligible differences in PTV coverage between flattened and FFF 6 and 18 MV IMRT prostate plans. As expected, our data confirmed the authors finding that superficial dose was decreasing with increasing mean energy [118]. Compared to our study both groups [118, 124] implemented IMRT techniques with FFF beams on a non-clinical prototype LINAC. Using VMAT technique, we found similar results: PTV coverage was unchanged using flattened or unflattened beam. However, we could detect a small difference of 1% in PTV inhomogeneity for FFF beams (Fig. 4.1). At this stage, it is unknown if the measured target inhomogeneity has any clinical relevance for treatment outcome of future patients with localized prostate cancer. Applying tighter objectives in the planning optimization process may reduce target inhomogeneities. However we designed our study keeping all treatment planning objectives constant for all four beam energies.

For flattened beam intensity modulation treatments, including IMRT and VMAT, the number of MU needed is an indicator for the mean body dose [36]. We found that a higher number of MU for FFF beams compared to flattened beams did not necessarily lead to an increased mean body dose. Due to the non-flat profile of the FFF beam, the integral dose of open fields in a water phantom is smaller than for a flattened beam in relation to 100 MU (Fig. 4.4). This finding was more pronounced with increasing field size. Therefore, compared to X6 an increase in MU for FFF beams was expected. Indeed, the planning study showed that the number of MU increased for X6FFF and X10FFF by 7.7% and 1.2%. In contrary, Vassiliev et al. [124] as well as Stathakis et al. [118] found a significant decrease in the number of MU for their FFF treatment plans. The reason was that our FFF beams were calibrated in order that 100 MU corresponded to 1 Gy at the depth of maximum dose, as this was common for flattened beams [4]. However, for all prototype LINACs with FFF capabilities used by other groups, only the flattened beams were calibrated. This resulted in a higher dose per 100 MU for the unflattened beams. Therefore they report a decrease in number of MU that we could not confirm in our study. Our data demonstrated that the mean body dose slightly decreased with the mean energy of the beam, despite the increase in number of MU that did not impact on the mean body dose.

Use of beam modulating techniques exposes the whole body to a larger amount of scattered low dose radiation as significant parts of treatment fields are being blocked

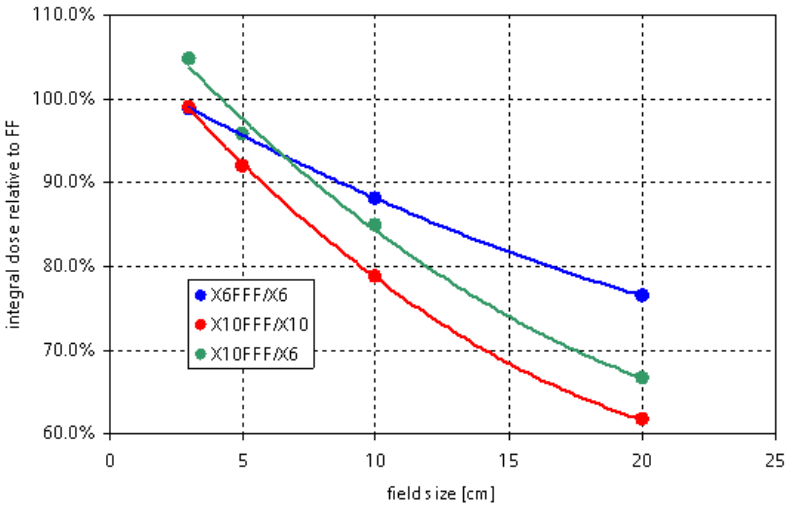

Figure 4.4: Integral dose of open fields in a water phantom relative to X6 beam corresponding to 100 MU for different field sizes.

by the MLC increasing MU and scatter dose [113]. Prostate cancer patients treated with IMRT might be exposed to a 2-fold increased risk of developing secondary malignancies compared to 3DCRT [113]. It is expected that FFF beams compared to flattened beams deposit less dose outside the target volume due to the missing scatter from the flattening filter and the reduced head scatter [20, 124, 66, 67]. Kragl et al. demonstrated that using FFF beams for IMRT prostate treatments resulted in a reduction of treatment head leakage by 52% and 65% for 6 and 10 MV, respectively [66]. Similarly, Cashmore et al. found in their study that IMRT using FFF beams removed unwanted and unnecessary scatter dose from the treatment head and lowered peripheral dose by up to 70% [20]. Applying hypofractionated treatment regimens for localized prostate cancer, treatment delivery time is important. With flattened beams and a limited output of MU/min higher dose per fraction leads to longer beam-on time and organ motion becomes relevant [52]. We found a time advantage for both FFF beams compared to X6 beam if one arc was used for planning. If the gantry was running at maximum speed, the time needed for one arc was one minute. Flattened beams can deliver in one minute 600 MU, X6FFF 1400 MU and X10FFF 2400 MU. Therefore, whenever more than 600 MU per arc are needed, FFF beams reduce treatment time compared to flattened beams. The number of MU needed for the seven patients ranged between 564 MU to 803 MU (for X10) and 803 MU to 1283 MU (for X6). For FFF beams the number of MU was slightly increased. Therefore there is a time advantage for both FFF beams compared to X6 beam if one arc is used for planning. Fu et al. found a time advantage for FFF IMRT treatments of 46% depending on the dose per fraction. The time advantage increased when using higher dose per fraction, however was insignificant for standard fractionation

of 2 Gy [38]. For sliding window IMRT the potential benefit of high dose rate is limited by the speed of the MLC. For treatments with RapidArc® gantry speed is the limiting factor. This study has several limitations. Our findings were based on a planning, rather than a clinical study. It is known that treatment planning systems do not correctly model the low dose region [49]. Therefore the expected advantage of FFF beams to reduce the dose outside the target volume is not shown in our planning study. At the present time, our results may be interpreted as having theoretical value rather than showing a clinical benefit for patients. However, this study revealed that non-inferior VMAT plans could be generated to deliver fast and high quality hypofractionated RT. We acknowledge the relevance and importance of image-guidance for modern prostate cancer radiotherapy when combining hypofractionated VMAT, high dose rate and fast delivery time due to organ motion; however, this was beyond the scope of this paper. Finally, as we carefully analysed the differences and their impact on treatment planning and delivery, we believe our study contributes to a better understanding of the differences between flattened and unflattened beams in future clinical use.

Chapter 5

Pretreatment quality assurance of flattening filter free beams on 224 patients for intensity modulated plans: A multicentric study *

5.1 Abstract

Purpose: Pretreatment quality assurance data from four centers, members of the European TrueBeam council were analyzed with different verification devices to assess reliability of flattening filter free beam delivery for intensity modulated radiotherapy (IMRT) and RapidArc (RA) techniques.
Methods: TrueBeam®(Varian Medical System) is a new linear accelerator designed for delivering flattened, as well as flattening filter free beams. Pretreatment dosimetric validation of plan delivery was performed with different verification devices and responses to high dose rates were tested. Treatment planning was done in Eclipse planning system (PRO 8.9, AAA 8.9). Gamma evaluation was performed with (dose difference) = 3 % and (distance to agreement) = 3 mm scoring the gamma agreement index (GAI, % of field area passing the test). Two hundred and twenty-four patients with 1–6 lesions in various anatomical regions and dose per fraction ranging from 1.8 Gy to 25 Gy were included in the study; 88 were treated with 6 MV flattening filter free (X6FFF) beam energy and 136 with 10 MV flattening filter free (X10FFF) beam. Gafchromic films in solid water, DELTA4, ARCCHECK, and MATRIXX phantom were used to verify the dose distributions. Additionally, point measurements were performed using a PinPoint chamber and a Farmer chamber.
Results: Dose calculation as well as dose delivery was equally accurate for IMRT and RA delivery (IMRT: GAI = 99.3% (+/-1.1); RA: GAI=98.8% (+/-1.1) as well as

*This chapter has been published in Medical Physics, Vol. 39, No. 3, March 2012 (Lang et al [70]).

for the two beams evaluated (X6FFF: GAI = 99.1% (+/-1.0); X10FFF: GAI=98.8% (+/-1.2). Only small differences were found for the four verification devices. A point dose verification was performed on 52 cases, obtaining a dose deviation of 0.34%. The GAI variations with number of monitor units were statistically significant.
Conclusions: The TrueBeam FFF modality, analyzed with a variety of verification devices and planned with Eclipse planning system is dosimetrically accurate (within the specified limits 3mm/3%) for both X6FFF and X10FFF beam energy.

5.2 Introduction

In the past, the flattening filter (FF) was introduced into the linear accelerator to achieve a uniform profile over the entire field size. More recently, the introduction of intensity modulated radiotherapy (IMRT) techniques makes a flat profile in many cases redundant as the multileaf collimator (MLC) is used to reach the best possible dose distribution. TrueBeam®(Varian Medical System, Palo Alto, USA) is a new accelerator designed for delivering both in FF and flattering filter free (FFF) modality whose beam's characteristics have recently been published in literature [53]. Removal of the filter leads to an increased dose rate [53], which is expected to reduce treatment time, and consequently intrafractional motion. Fu et al [38] showed for intensity modulated prostate and nasopharynx cases a reduction of beam on time of 43%. Additionally FFF beams are expected to reduce secondary malignancies due to reduced MLC transmission, head scatter, and leakage radiation [53, 67, 66, 20]. Kragl et al [66] showed a 31% dose reduction 20 cm outside the treatment volume for SBRT cases, 16% for prostate cases and 18% for head and neck cases for a 10 MV FFF (X10FFF) beam compared to the FF beam. Cashmore et al. [20] investigated out-of-field dose for paediatric IMRT showing a reduction of up to 70% for distant organs. However, there are concerns regarding the safe delivery of FFF beams [39], especially regarding the monitor chamber, which is used to steer the beam. The signal produced in the monitor chamber is mainly due to the electrons generated in the FF. In order to have enough signal for FFF beams a thin foil is introduced into the beam path which was shown for prototype FFF accelerators in literature to give sufficient electron signal for monitoring the beam [39, 118, 20].
Additionally the increased output of TrueBeam makes higher demands on the reaction time of the servo system of the linear accelerator. Several studies demonstrated the verification of dose calculation algorithm for FFF beams under physical conditions (in a water phantom) [53, 118, 34] ; however, only little data are published on the dose calculation of FFF IMRT and RapidArc (RA) fields [118, 20].
This manuscript describes an evaluation of multi-institute pretreatment quality assurance (QA) data to assess reliability of FFF beam delivery for IMRT and RA techniques. Data from 4 centers [Instituto Clinico Humanitas (ICH), UniversityHospital Zurich (USZ), KantonsSpital Winterthur (KSW), and Institut Catala‘ d'Oncologia (IOC)] acquired with different verification devices were analyzed. The study demon-

strates clinical reliability of FFF beam delivery and dose calculation offered by the Varian TrueBeam system. Additionally the multicenter study allowed the use of a variety of QA devices, giving the reader an overview of devices suitable for the use in high dose rate flattening filter free photon beams.

5.3 Materials and Methods

Two hundred and twenty-four patients with 1–6 lesions in various anatomical regions and dose per fraction ranging from 1.8 to 25 Gy were included in the study; 88 were treated with 6 MV FFF beam energy (X6FFF) and 136 with X10FFF beams. Measurements were performed for plans of variable complexity: lung stage I and lung metastases (76 cases), brain metastases and vestibular schwannoma (32), spinal tumors (10), liver metastases (28), pancreatic lesions (15), mediastinal tumors (12), prostatic cancer (12), and others (39). Gafchromic®films in solid water, DELTA^4®, ARCCHECK®, and MATRIXX®phantom were used to verify the dose distributions (Table 5.1). Furthermore, for 27 patients, a PinPoint (PinPoint chamber, PTW) dose verification was performed in solid water. A detailed summary of type and number of plans verified by each institution can be found in Table 5.1.

Table 5.1: Number of plans verified by the different institutions; devices used: m: Matrixx, gf: gafchromic film in solid water, d: delta4, a: ArcCheck.

	ICH	**USZ**	**KSW**	**ICO**	**total**
Total	100	27*+ 52#	27	18	224
RA	100	19*+ 50#	27	18	214
IMRT	0	5*+ 5#	0	0	10
X6FFF	19	19*+ 36#	10	4	88
X10FFF	81	8*+ 16#	17	14	136
device	m	*gf + #d	a	a	—

5.3.1 Linear accelerator and flattening filter free beams

All measurements were performed on TrueBeamVR linear accelerators using X6FFF and X10FFF energy modes. FFF beams (on TrueBeam) have a lower mean energy, an increased dose per pulse and an increased maximum dose rate compared to FF beams [53]. Maximum dose rates of 2400 and 1400 MU/min can be achieved with the X10FFF and the X6FFF beams, respectively. The supervisor system of TrueBeam linear accelerator communicates with all subnodes of the machine with a frequency of 100 Hz. Therefore, corrections of the beam can be applied every 10ms. All four linacs are calibrated that 100 MU correspond to 1Gy in the depth of maximum dose, a field size of 10x10 cm^2 and a source surface distance of 100 cm. Tissue phantom

ratios (TPR20/10) for the two beams in the different institutions can be found in Table II. Three linacs (ICO, ICH, KSW) were equipped with a Millennium MLC and one linac (USZ) with high definition MLC (HDMLC). Both MLCs have in total 60 leaf pairs. For the Millenium MLC, the inner 40 leaf pairs have a width of 0.5 cm and the outer leaf pairs have a width of 1 cm, total length of the MLC is 40 cm. For HDMLC, the total length is 22 cm, the inner 8 cm are covered by 32 leaf pairs with a width of 0.25 cm, the outer leaf pairs have a width of 0.5 cm. Data on the transmission and dynamic leaf gap in the differentinstitutes can be found in Table 5.2.

Table 5.2: Characteristics of the MLCs of the five institutes and tissue phantom ratio (TPR20/10) for the two beams. At USZ, a HDMLC is installed, which differs in transmission (T) and dynamic leaf gap (DLG) from the Millenium MLC.

	ICH	**USZ**	**KSW**	**ICO**
T X6FFF (%)	1.6	1.0	1.6	1.6
T X10FFF (%)	1.8	1.2	1.7	1.8
DLG X6FFF (mm)	2.0	0.9	1.3	1.1
DLG X10FFF (mm)	2.0	1.0	1.5	1.4
TPR 20/10 X6FFF	0.623	0.631	0.630	0.631
TPR 20/10 X10FFF	0.706	0.702	0.705	0.707

5.3.2 Treatment planning

Treatment planning was always performed with Eclipse®treatment planning system (Varian, Palo Alto, Medical Systems). RA plans were optimized using progressive resolution optimizer (PRO) 8.9, for IMRT plans dose volume optimizer (DVO) 8.9 was used. Dose distributions were calculated using anisotropic analytical algorithm (AAA) 8.9 algorithm with a calculation grid size of 2.5 mm; for targets with a diameter below 2 cm a calculation grid size of 1.2 mm was used. All treatments were planned with X10FFF or X6FFF beam. For RA the 1–4 arcs were used for treatment planning (average 2.12), for IMRT 4–7 field were used (average 5.40). The maximum dose rate was chosen according to the clinical needs. For small doses per fraction it is sometimes beneficial to restrict the maximum dose rate to reduce the dose to healthy tissue. Additionally, since the effect of the high dose rate on healthy tissue is not yet known, the maximum dose rate was restricted for some cases.

5.3.3 Quality assurance systems

The multicenter study allowed the inclusion of different QA devices for verification (5.1).

Gafchromic EBT2 film

Gafchromic®EBT2 (ISP, Ashland) film (20.3 x 25.4 cm^2) was used in a solid water phantom (30x30x20 cm3). One to three transversal planes were verified. For each sheet of film an individual five step calibration was done, by irradiating 5x2.5 cm pieces of film (using 6 Mv flattened beam) with doses between 0Gy and 1.2 times the maximum dose. Additionally it was corrected for the light source inhomogeneity of the flatbed scanner (Epson 10000XL) and the film thickness using B-component of RGB readout. The films were evaluated using the R readout (up to a dose of 6 Gy) and above that dose the G readout in a home-made gamma analysis software (MATLAB, MathWorks, USA). Films were scanned with a resolution of 150 dpi, resulting in a distance between two measurement points of 0.17mm.

DELTA4 phantom

DELTA4®(ScandiDos, Uppsala, Sweden) is a cylindrical phantom for pretreatment patient QA. Absolute dose is measured in 1069 p-Si diode detectors arranged in two orthogonal detector arrays. The spacing between detectors is 5mm in the central part (8x8 cm^2) and 10mm outside (20x20 cm^2). The diameter of the detectors is 1mm. Properties of the phantom have been described in detail by Bedford et al [6].

ARCCHECK

ARCCHECK®(Sun Nuclear Corporation, Melbourne, USA) is a cylindrically shaped QA device with 1386 diode detectors of a size of 0.8 x 0.8 mm^2 helically arranged in a physical depth of 29 mm and a detector spacing of 10 mm. Both the array diameter and length are 21.0 cm. The inner cavity has a diameter of 15.0 cm. Central axis dose was simultaneously measured by a Farmer-type chamber (PTW, Freiburg, Germany) positioned at the center of the cavity by a dedicated insert. The dose measured by the phantom was the absolute dose, no correction was applied.

MATRIXX

MATRIXX®(IBA, Schwarzenbruck, Germany) is a two dimensional ionization chamber array, consisting of 1024 (32x32) independent parallel plate cylindrical ionization chambers (diameter 4mm, height: 5.5 mm, sensitive volume: 70 mm^3) arranged in a square of 24x24 cm^2. The distance between each ionization chamber is 7.5mm from center to center of adjacent chambers. This system was calibrated in absolute dose for each beam energy and used in the same way as for RapidArc with FF fields [129]. The treatment plans were projected on a phantom made up of a CT scan of the MATRIXX with 5 cm of plexiglas above and underneath the active measuring area to account for build up and backscatter. The GAI was then evaluated comparing the irradiated and calculated verification plans with the gamma evaluation method implemented in the measuring software OMNIPRO (version 1.5, IBA, Schwarzenbruck,

Germany).

5.3.4 Gamma analysis and statistics

All plans were evaluated using a global gamma agreement index (GAI). As gamma criteria 3% dose difference (DD) (from isocenter dose) and up to 3 mm distance to agreement (DTA) was used, pixels with less than 10% of max dose were not taken into account. The calculated dose was taken as the reference. Each arc was evaluated separately and the average was taken. For MATRIXX and gafchromic film dosimetry, the measured dose was manually adjusted during evaluation. Differences of mean values were tested on significance using an unpaired Mann-Whitney U-test. p-values below 0.05 were considered to be significant. A one-way ANOVA was used to evaluate if any of the variables [beam energy, verification device, max dose rate, PTV size, number of monitor units (MU)] had a statistically significant effect on the gamma index.

5.4 Results

Patient specific plan verification was performed for a total of 224 volumes in four different institutes. Average gamma score was 98.9% (+/−1.1) (3 mm, 3%). All four institutes showed equally good gamma scores (table 5.3). The histogram of GAIs (Fig.

Table 5.3: GAI (in %) of the different institutions. 1 SD is given in brackets.

	ICH	**USZ**	**KSW**	**ICO**	**total**
Total	98.7 (1.0)	99.4 (0.8)	99.4 (0.7)	98.0 (1.8)	98.9 (1.1)
RA	98.7 (1.0)	99.4 (0.9)	99.4 (1.1)	98.0 (1.1)	98.8 (1.1)
IMRT	—	99.3 (0.9)	—	—	99.3 (0.9)
X6FFF	98.6 (1.0)	99.3 (0.7)	99.5 (0.5)	98.3 (1.8)	99.1 (1.0)
X10FFF	98.7 (1.0)	99.7 (0.8)	99.3 (0.9)	97.7 (1.8)	98.8 (1.2)

5.1) shows that only three plans had a GAI below 95%. In all the four clinics, a GAI below 95% means that the plan failed preclinical QA and needs further investigation. Dose calculation, as well as dose delivery, was equally accurate for IMRT and RA delivery (IMRT: GAI=99.3% (61.1); RA: GAI=98.8% (61.1)) as well as for the two beams evaluated (X6FFF: GAI=99.1% (+/−1.0); X10FFF: GAI=98.8% (+/−1.2)). Four different devices were used for verification. The average GAI for the plans verified with the high resolution gafchromic films was 99.4% (+/−1.01), which is higher than for plans verified with the ARCCHECK (GAI=98.8% (+/−1.4%), $p<10^5$) and the MATRIXX (GAI=98.7% (+/−1.4%), $p<10^5$) devices. Plans verified with the DELTA4 phantom showed a GAI=99.4% (+/−0.86) similar to the gafchromic ones. Figure 5.2 shows that there is no dependency of the GAI on the maximum dose rate

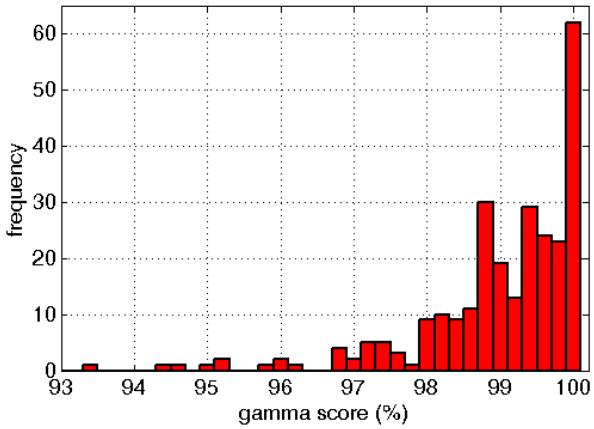

Figure 5.1: Histogram of GAI for both energies and all four institutions.

used during irradiation of the arc. Similarly no dependence on the mean dose rate was found. GAI decreased with increasing ratio of MU to dose per fraction (Fig. 5.2) ($p<10^5$), which is an indicator for the modulation of the plan. GAI slightly decreased with decreasing target volume ($p<0.02$) (Fig. 5.2). For ARCCHECK and DELTA4 phantom (no manual adjustment of dose distributions) small volumes were more sensitive to setup errors due to the discrete character of the detectors.

Two institutions (USZ and KSW) additionally performed point dose measurements in the isocenter using a PinPoint chamber (USZ) and a Farmer chamber (KSW). Dose differences for a total of 52 patients are shown in Fig. 5.3. Mean dose difference is 0.34% (significantly different from 0,$p<0.01$). Both institutions showed a mean dose difference slightly above 0% (KSW: 0.30%, USZ: 0.38%). In 88% of cases, the verified isocenter dose was within $+/-2\%$ (Fig. 5.3). Larger dose deviations were mostly due to sharp gradients in the measurement point. Therefore, small setup errors can have a large impact on the result.

5.5 Discussion

An increasing interest in flattening filter free beams is evident in recent years [53, 38, 67, 65, 66, 39, 39, 20, 126, 124, 123, 99, 118]. An extensive retrospective investigation on technical and quality assurance data from the treatment of 224 patients from four radiotherapy departments were performed to provide evidence about intensity modulated fields using the FFF modality included in the new TrueBeam accelerator. The analysis of the technical and delivery features of the new linac accelerator TrueBeam was performed in different institutes, with a variety of clinical indications, and dose prescriptions.Furthermore, the early clinical data of a subsection of these patients have recently been published [111].

The FFF characteristic to increase the dose rate up to 2400 MU/min (i.e. 24 Gy/min

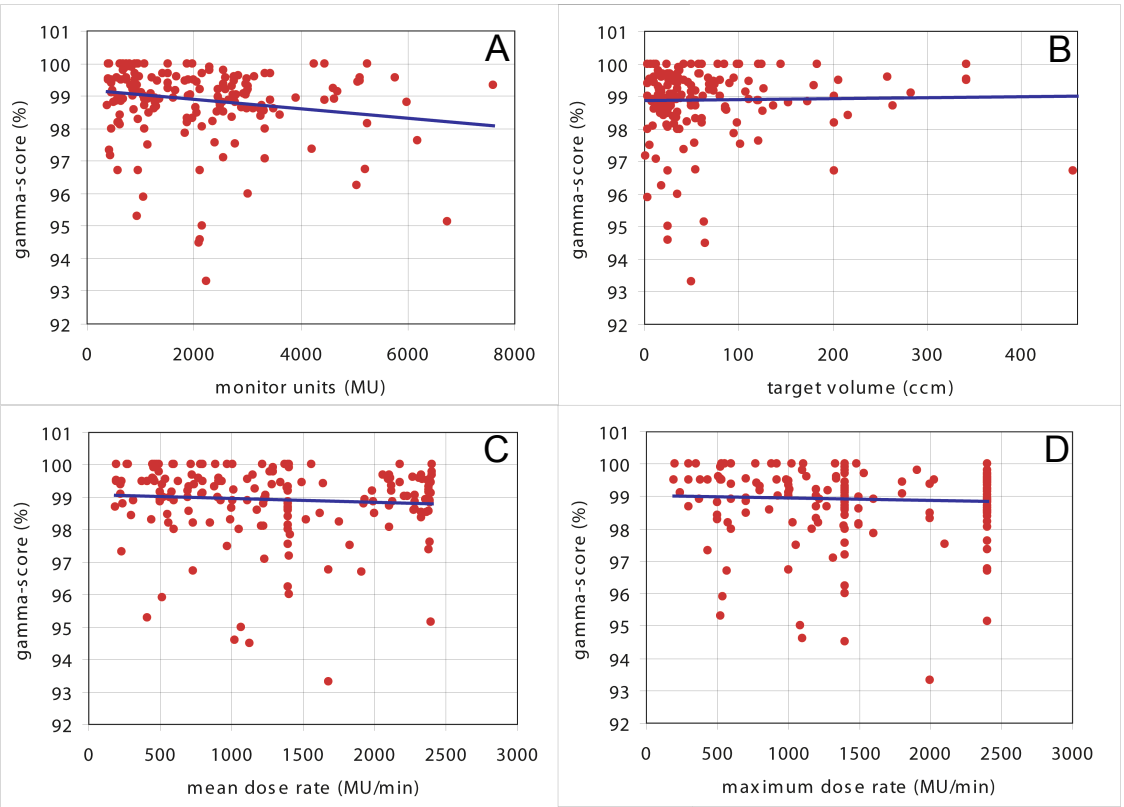

Figure 5.2: Dependency of the GAI on A) monitor units, B) target volume. C) mean dose rate and D) maximum dose rate.

in standard condition) enables a reduction in beam on time, in particular for hypofractionated treatments where the treatment beam on time can be lower than 2 min (if FFF is associated with VMAT technique).
The introduction of a new accelerator with a new method of operating has to be supported by an extensive dosimetric verification which must include both machine general performance and verification of treatment plans by measurements of delivered dose distributions. Hrbacek et al. [53] reported the data of the clinical commissioning of the flattening filter free linear accelerator TrueBeam, showing the capability of delivering RT treatments safely. In this work we have focused on dosimetric verifications of modulated plans, performed both as part of commissioning and as patient specific QA of clinical treatments. To our knowledge, very little data have been reported on the pretreatment quality assurance in delivering FFF treatments using modulated treatments [118]. The authors believe that a wide patient specific QA analysis using prior experience and tools is required when implementing a new technology before reaching the patient. In particular, a comprehensive patient specific QA protocol based on results from a large number of patients, from multiple sites, and using different and independent devices should be considered to verify the

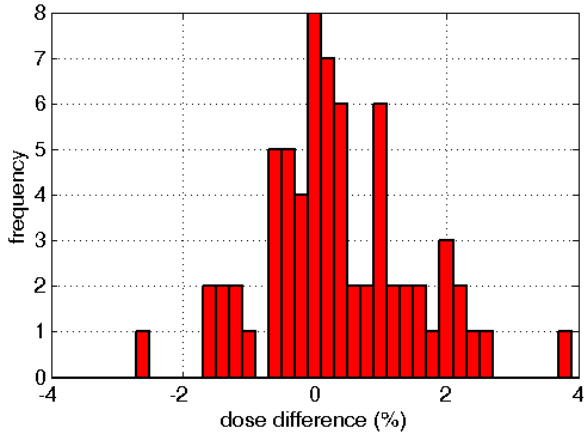

Figure 5.3: Dose differences (%) measured in the isocenter for in total 52 patient. Mean dose difference is 0.34 % (significant different from 0, $p < 0.01$).

treatment accuracy. For this reason, one of the first aims of the European TrueBeam council was the interverification of a cohort of patients for cross-validation. The objective of this study was to verify whether machines in different institutes and with different instruments and procedures could give a common results about the quality of the delivery in basic conditions, that is the reason why no further variables were added in the analysis (such as inhomogeneous phantoms, etc.).
In this study, different instrumentations were used checking a point, a plan (2D detectors, and film), or the volumetric shape (DELTA4 and ARCCHECK), for some of these devices, the evaluation of VMAT plans has already been published in literature [30, 84] but never for FFF beams. Gafchromic, ionization chamber, and diodes were used. Spatial resolution ranged from 0.2mm for the Gafchromic to 7.5mm for MATRIXX. This different spatial resolution has to be taken in account when deciding which device to use for QA, in some cases (e.g., very small lesions, or highly modulated dose distributions), a higher resolution is required and a low resolution device as MATRIXX could not be the optimal choice; the subset of plans considered with these characteristic is the reason of the lower mean value obtained with MATRIXX compared with Gafchromic. Nevertheless, the great fraction of low modulated plans (e.g., SBRT) made the GAI values not so affected by the different resolutions of the devices used.
The evaluation of calculated dose on Eclipse and delivered dose at TrueBeam measured by four different devices indicated an excellent agreement for both IMRT and VMAT. Three plans resulted with a GAI<95%, in one case, it was a two-lesions single-isocenter plan optimized with four arcs and verified with MATRIXX. The highly modulated dose distribution achieved, in combination with the discrete spacing of detectors may lead to a low GAI. In case transmission or dynamic leaf gap were entered slightly incorrect into the TPS, a high modulation could increase leakage through the MLC leading to a decrease in GAI, some evidence of this correlation is

present in literature [30, 42]; this can partly be the reason of the difference in uncertainty between two centers using the same device as shown in Table III. The result can be caused by the sum of dosimetric and mechanical differences (e.g. DLG) that can exist between both Linacs and MLCs, though of the same model. The other two plans with a GAI<95% covered very small target volumes (5–6 cm^2) that are sometimes prone to dose calculation inaccuracies as shown in Refs. [32, 92, 33]. Better results could have been obtained with a 1mm calculation grid (and a 1mm DTA) but the 3mm DTA choice was taken in order to have more homogeneous results with reference to the resolution range of the QA devices used (up to 7.5 mm for MATRIXX). Point measurements performed with PinPoint and Farmer chambers showed mean difference of 0.34% between the ion chamber measurements and the Eclipse computed doses, results very similar to those found by O'Daniel et al [91]. Measurements were performed for plans of variable complexity: lung stage I and lung metastases, metahepatic diseases, spinal tumors, pancreatic lesions. Therefore, considering the large variety and large number of plans (224) verified by means of systems with different characteristics in terms of geometry and detectors, the high dose rates achievable (up to 2400 MU/min), and the different dose prescriptions (from 1.8 Gy/day to 25.0 Gy/day), the obtained results assess the reliability of FFF delivered doses. Additionally the study presents a set of QA devices suitable for the use in high dose rate flattening filter free beams; clearly, the device-specific considerations in relation to the different plan characteristics (e.g., high resolution required for SBRT or very modulated plans) already present in literature, remain valid also for FFF beams.

5.6 Conclusion

The TrueBeam FFF modality, analyzed with a variety of verification devices and planned with Eclipse planning system is dosimetrically accurate (within the specified limits 3 mm/3%) for both X6FFF and X10FFF beam energy.

Chapter 6

Clinical application of flattening filter free beams for extracranial stereotactic radiotherapy*

6.1 Abstract

Purpose: To investigate the clinical application of flattening filter free (FFF) beams at maximum dose rate for stereotactic body radiotherapy (SBRT).
Methods and Materials: Patients with tumors in the lung or abdomen were subjected to SBRT using 6 MV FFF or 10 MV FFF beams. For each patient, three plans were calculated using 6 MV flattened, 6 MV FFF and 10 MV FFF beams. Treatment times were recorded and analysed, and tumor displacements were assessed by pre- and post-treatment cone beam computed tomography (CBCT).
Results: Altogether, 26 patients (16 lung, 10 abdominal tumors) were treated. The average dose rate per patient ranged from 442 to 1860 MU/min. Beam-on time was on average 1.6 min (1SD = 0.6 min), with the total treatment times recorded at 18.5 min (1SD = 3.5 min). The time advantage of using FFF beams was dose-dependent and started at 4 Gy for 6 MV FFF and at 10 Gy for 10 MV FFF beams. The average of the tumor displacements during treatment was 2.0 mm (1SD = 1.0 mm).
Conclusions: SBRT using FFF beams is time efficient and associated with excellent patient stability. According to Van Herk's formula, ITV to PTV margins of 6 mm are sufficient in our patient cohort. Further studies are necessary to assess clinical outcome and toxicity.

*This chapter has been published in Radiotherapy and Oncology, Vol. 106, No. 2, February 2013 (Lang et al [72]).

6.2 Introduction

Photon beams produced by conventional C-arm linear accelerators are directed through a flattening filter, resulting in uniform photon fluence. Novel linear accelerator technology allows compensation of nonuniform photon fluence by the use of modulated treatment techniques. Several recent planning studies demonstrated that dose distributions achieved with flattening filter free (FFF) beams are at least similar to those with flattened beams [139, 95, 106, 118, 124, 123]. When the filter is removed from the photon beam, the dose rate can be multiplied, thereby substantially shortening beam-on time, which makes FFF beams especially attractive for stereotactic radiotherapy with high dose per fraction. This appears important because it has beenestablished that a reduction in treatment time translates into improved patient stability and treatment accuracy [103, 51]. The use of volumetric modulated arc radiotherapy (VMAT) for stereotactic body radiotherapy (SBRT) has recently been shown to shorten beam on times by a factor of 3.1 if compared to static field IMRT (VMAT: 3.9 min, IMRT: 12 min) [94]. Further reductions in beam on time may be achieved by using FFF beams in conjunction with VMAT. However, a potential time advantage depends on dose per fraction and is co-determined by modulation complexity, tumor location and mechanical aspects of treatment delivery, such as gantry speed and MLC speed. We present our experience with the clinical application of FFF beams for (SBRT). We analysed our first 26 patients treated with this technique, focusing on the time advantage using FFF beams versus flattened beams, and patient stability.

6.3 Materials and Methods

Patients with primary or metastatic tumors of the lung or upper abdomen were subjected to SBRT using the TrueBeam® linear accelerator (Varian Medical Systems, Palo Alto, CA). Treatment planning was performed on the average projection of 4-dimensional computed tomographies (4DCTs) in the Eclipse® treatment planning system (Varian Medical system, PRO 8.9, AAA 8.9) using 6MV (X6FFF) or 10MV (X10FFF) FFF beams. Hrbacek et al. have previously reported a detailed description of the beam characteristics [53]. All patients were planned using VMAT (RapidArc®, Varian Medical Systems) technique with 1-3 arcs allowing the optimizer to use the maximum dose rate of 1400 monitor units/min (MU/min) for X6FFF and 2400 MU/min for X10FFF beams. Tumors of the lung were planned with X6FFF beams and tumors of the upper abdomen with X6FFF or X10FFF beams (depending on tumour depth within the patient). In the case of lung tumors, avoidance sectors or partial arcs were used to spare the contra-lateral lung. Planning objectives were chosen according to current RTOG protocols (see RTOG 0915 protocol). Treatment plans were normalized to the maximum dose and the dose was prescribed to the 60%-90% isodose line that covered 95% of the volume. The conformity index (CI, volume enclosed by the prescription isodose / PTV volume),

as well as the number of MU and mean dose rate, were recorded. Each plan was verified prior to patient treatment on the Delta4®-phantom (ScandiDos, Uppsala, Sweden). The passing criteria for the verification measurement was a gamma agreement index (GAI) of 95% (DD = 3%, DTA =2 mm) To ensure positional stability, reproducibility of the set-up and patient comfort, patients were placed supine in a customized vacuum bag (CIVCO, Kalona, IA). An abdominal compression device was used in selected patients for tumors close to the diaphragm. For management of tumor motion, an internal target volume (ITV) was contoured on the 4DCT images including all tumor positions within the breathing cycle. Image guidance was performed by pre treatment cone beam computed tomography (CBCT). In the case of lung tumors, an automated ITV match was performed. For abdominal lesions, an automated match to surgical clips (1 patient) or a manual match to anatomical structures (all other patients) was performed. Every match was checked by the responsible clinician. Patient stability during treatment was observed by monitoring the patients' breathing amplitude using an RPM gating system (Varian Medical Systems, Palo Alto, CA). Treatment was only delivered if the breathing amplitude and frequency agreed within +/- 20% of the values acquired on the 4DCT. If amplitude or frequency were out of tolerance, an individualized training was undertaken with the patient. Beam-on time, as well as total treatment time, was measured each day for all the patients and for each patient the mean values and standard deviation (SD) was calculated. In order to evaluate the time efficiency benefit using FFF beams, three plans were calculated using 6 MV flattened (X6), X6FFF and X10FFF beams for each patient. Beam-on times for the three plans were measured using a stopwatch and subsequently compared.Shortened beam-on time should translate into minimal intra-fraction patient and target shifts. Therefore patient shifts were determined by comparing the bony match of pre- and post-treatment CBCTs and baseline shifts were assessed by comparing the position of the tumor in pre- and post-treatment CBCTs in relation to the bony anatomy. Total tumor displacement includes patient shift as well as baseline shift. For estimation of ITV to PTV margins, Van Herk's formula was used [122]: Systematic Σ and random σ errors were calculated for intra-fractional motion. A systematic contouring error of 2 mm was assumed [116]. Setup error was neglected. ITV to PTV margins M were calculated using Van Herks formula adapted for lung tissue [14]:

$$M = 2.5\Sigma + \beta\sqrt{\sigma^2 + \sigma_P^2} - \beta\sigma_p \tag{6.1}$$

where $\beta = 0.84$ and $\sigma_P = 6.4$mm

6.4 Results

6.4.1 Tumors and volumes treated

Between July 2010 and November 2011, 26 patients were treated - 16 patients with tumors in the lung and 10 patients with tumors in the abdomen (4 liver, 4 pancreas, 2 adrenal gland tumors). The median age of the patients was 64.5 (46-89) years. In 2 patients, 2 PTVs were treated, respectively. Of the 28 lesions treated, 16 lesions were treated with curative intention (11 lung, 4 pancreas, 1 liver), and 12 lesions were metastases (6 lung, 2 adrenal gland, 4 liver). In 2 patients, lung metastases were treated in the remaining lung after previous pneumonectomy (P1 and P14, see Table 6.1). The mean PTV size was 49.7 cm^3 (9.8 - 283.5 cm^3).

6.4.2 Treatment planning and treatment delivery

Mean dose rates of the treatments varied between 442 MU/min and 1394 MU/min for X6FFF and between 1076 MU/min and 1860 MU/min for X10FFF beams, mainly depending on the dose per fraction and the number of arcs used. Individualized radiation doses and fractionation schedules were used (Table 6.1). The mean GAI for pre-treatment QA was 98.97% (1SD = 0.82%), showing that the FFF beams were delivered correctly (Table 6.1). All plans fulfilled the planning objectives, and most plans achieved a CI close to 1. Only one plan with the tumor close to the chest wall showed a larger CI of 1.47.

6.4.3 Treatment and beam-on time

Treatment times for all patients were recorded to investigate time efficiency of using FFF beams. Patient setup in the room required on average 6.5 min (1SD = 4.6

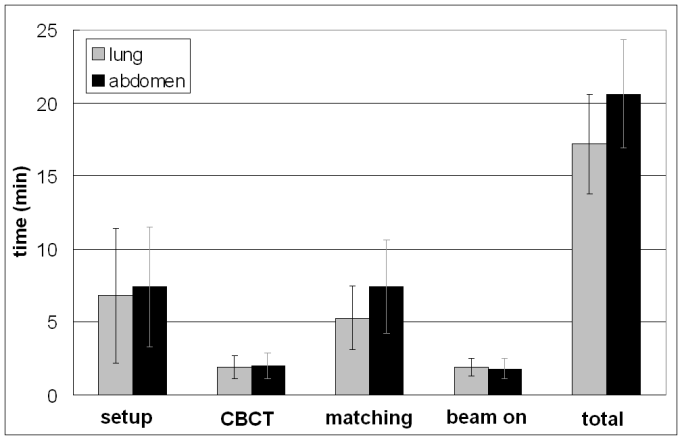

Figure 6.1: Total treatment time, separated into patient setup inside the room, CBCT acquisition, matching of the CBCT and actual beam on time.

Table 6.1: Patient and Treatment Details: Conformity index (CI) is defined as the volume enclosed by the prescription isodose divided by the PTV volume. Delta4 phantom was used to measure gamma agreement index (GAI, 2mm/ 3%).

patients	site	PTV (ccm)	schedule	energy MeV	# arcs	# MU	mean DR (MU/min)	max DR (MU/min)	mean T (treatment) (min)	mean T (total) (min)	GAI (%)	CI
P1	lung	15.6	8 x 4.5 Gy @70%	X6FFF	2	1074	851	1200	1.26	18.2 (+/- 4.4)	99.3	1.06
P2	lung	37.7	10 x 5 Gy @80%	X6FFF	1	1563	1351	1400	1.16	26.8 (+/- 7.1)	97.3	1.21
P3	lung	14.7	5 x 8.5 Gy @85%	X6FFF	2	2530	1225	1400	2.06	18.1 (+/- 4.8)	98.8	1.19
P4, V1	lung	37.5	3 x 10 Gy @84%	X6FFF	2	3018	1372	1400	2.2	15.5 (+/- 3.9)	98.7	1.07
P4, V2	lung	37.7	3 x 10 Gy @84%	X6FFF	2	2309	1346	1400	1.72	12.2 (+/-2.1)	98.6	1.07
P5	lung	9.8	4 x 10 Gy @89%	X6FFF	2	3074	1389	1400	2.22	19.6 (+/- 3.4)	99.4	1.16
P6	lung	64	10 x 6 Gy @85%	X6FFF	3	1129	912	1400	1.24	19.2 (+/-3.2)	99.6	1.14
P7	lung	18.7	15 x 3.3 Gy @85%	X6FFF	2	902	442	600	2.04	15.5 (+/- 3.9)	99.6	1.23
P8, V1	lung	14.1	12 x 4 Gy @79%	X6FFF	2	1079	941	1400	1.14	21.0 (+/- 8.4)	97.4	1.47
P8, V2	lung	5.9	11 x 4 Gy @87%	X6FFF	2	1116	904	1400	1.24	19.3 (+/- 3.2)	97.5	1.09
P9	liver	36.3	10 x 5 Gy @85%	X6FFF	2	956	592	600	1.62	18.1 (+/- 3.9)	100	1.11
P10	liver	283.5	10 x 4 Gy @80%	X6FFF	2	1114	801	1000	1.41	26.5 (+/-3.3)	99.1	1.21
P11	pancreas	131.8	2 x 6 Gy @78%	X6FFF	1	1258	1224	1400	2.06	23.2 (+/- 2.9)	99.1	0.98
P12	pancreas	24	10 x 5 Gy @87%	X6FFF	1	1079	1372	1400	0.79	25.8 (+/- 4.3)	100	1.31
P13	lung	27.4	8 x 7.5 Gy @73%	X6FFF	2	1704	830	1400	2.06	13.8 (+/- 3.2)	100	1.05
P14	lung	32.7	12 x 4 Gy @72%	X6FFF	2	1082	545	1400	2.02	15.0 (+/- 3.0)	99.1	1.04
P15	lung	24.4	4 x 12 Gy @71%	X6FFF	3	4017	1376	1400	2.89	16.1 (+/- 2.8)	99.8	1
P16	liver	42.9	4 x 10 Gy @75%	X6FFF	2	2139	1374	1400	1.55	18.7 (+/- 5.7)	98.4	0.97
P17	lung	53.8	4 x 10 Gy @85%	X6FFF	2	2263	1355	1400	1.66	17.6 (+/- 3.6)	100	1.04
P18	pancreas	40.9	2 x 6 Gy @76%	X6FFF	2	1760	1056	1400	2.04	18.3 (+/- 4.0)	98.9	1
P19	pancreas	30.2	2 x 6 Gy @75%	X10FFF	2	1851	1842	2400	1.05	17.9 (+/- 1.2)	97.8	0.99
P20	liver	131.8	4 x 12 Gy @80%	X6FFF	2	3860	1396	1400	2.78	15.3 (+/-3.3)	99.5	0.98
P21	lung	19.6	4 x 12 Gy @79%	X6FFF	4	3974	1302	1400	3.01	14.0 (+/- 2.1)	99.4	1.02
P22	adrenal	53.5	3 x 10 Gy @78%	X10FFF	2	3813	1860	2400	2.03	22.5 (+/-5.1)	98.9	1.01
P23	Lung	22.6	4 x 12 Gy @84%	X6 FFF	2	5668	1396	1400	3.36	13.5 (+/- 2.7)	97.9	1.2
P24	adrenal	77.9	4 x 10 Gy @88%	X6 FFF	2	3172	1198	1200	2.65	19.7 (+/- 4.1)	99.6	1.02
P25	lung	40.7	10 x 5 Gy @79%	X6FFF	2	1364	993	1400	1.38	16.2 (+/- 3.9)	99.2	1.06
P26	lung	61.7	5 x 7.5 Gy @78%	X10FFF	2	2170	1076	2400	2.02	18.0 (+/- 2.4)	98.3	1.02

min). CBCT acquisition required 1.8 min (1SD = 0.5 min) and 6.0 min (1SD =2.8 min) were needed for the tumor match for lung patients, and 9.6 min (1SD = 3.2 min) for abdominal patients (Figure 6.1). Treatment beam-on time was on average 1.6 min (1SD = 0.6 min) with the total treatment times recorded at 17.2 min (1SD = 3.4 min) and 20.6 min (1SD = 3.7 min) in patients with tumors of the lung and upper abdomen, respectively (Table 6.1 and Figure 6.1). Figure 6.2 shows the

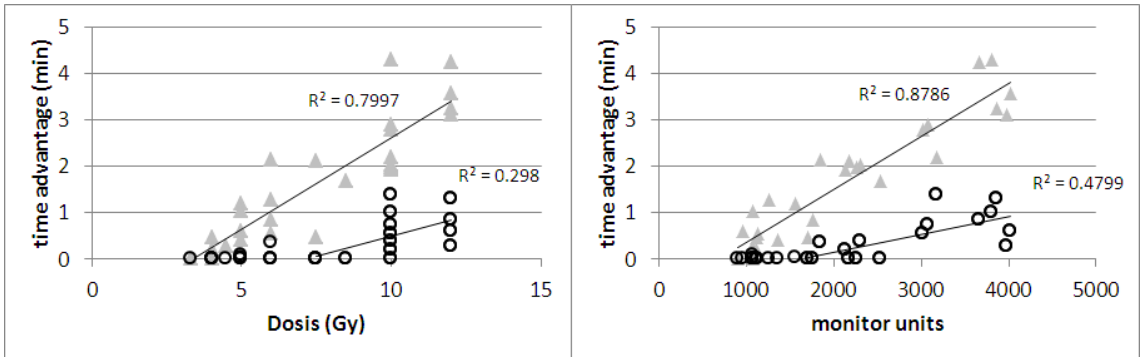

Figure 6.2: Dependency of the difference in delivery time on the dose (left) and on the monitor units (right) using X6 beam compared to X6FFF beam (grey triangle) and using X6FFF compared to X10FFF (black circles). X6FFF saves time if more than 1000 MU are needed to deliver the plan or if a dose larger than 4 Gy is given. X10FFF saves time compared to X6FFF if more than 2000 MU are needed or the dose is larger than 10 Gy.

differences in beam-on time using the X6FFF beam compared to a X6 beam, as well the difference between X10FFF and X6FFF. From a dose of approximately 4 Gy or 1000 MU, the X6FFF beam allows more rapid treatment delivery compared to the X6 beam. The time advantage increases with increasing number of monitor units ($R2 = 0.88$, $p < 0.01$) and increasing dose ($R2 = 0.80$, $p < 0.01$). The use of the X10FFF beams has advantages for doses above 10 Gy ($p=0.03$) or monitor units above 2000 MUs compared to X6FFF beams ($p < 0.01$). There was no significant dependency of time advantage using X6FFF or X10FFF beam on the size of the treated volume ($R2 = 0.01$, $p = 0.85$).

6.4.4 Intra-fractional stability

The average 3D vector of the patient and baseline (tumor in respect to the bones) shifts during treatment were 2.0 mm (1SD = 0.8) and 1.9 mm (1SD = 0.5 mm), the total tumor displacement was 2.0 mm (1SD = 1.0 mm) in all patients and 2.1 mm (1SD = 1.2 mm) in patients with lung tumors. Figure 6.3 shows patient and baseline shifts for lung and abdominal treatments. Intra-fractional motion was similar for lung and abdomen patients. The maximal shift observed was 5.2 mm. Shifts in lateral and longitudinal direction were non-systematic, whereas there was

a slight systematic drift in vertical direction (mean shift 0.54 mm, $p < 0.01$), due to sagging and relaxing of the patient in the vacuum bag (Figure 6.3). For stereotactic

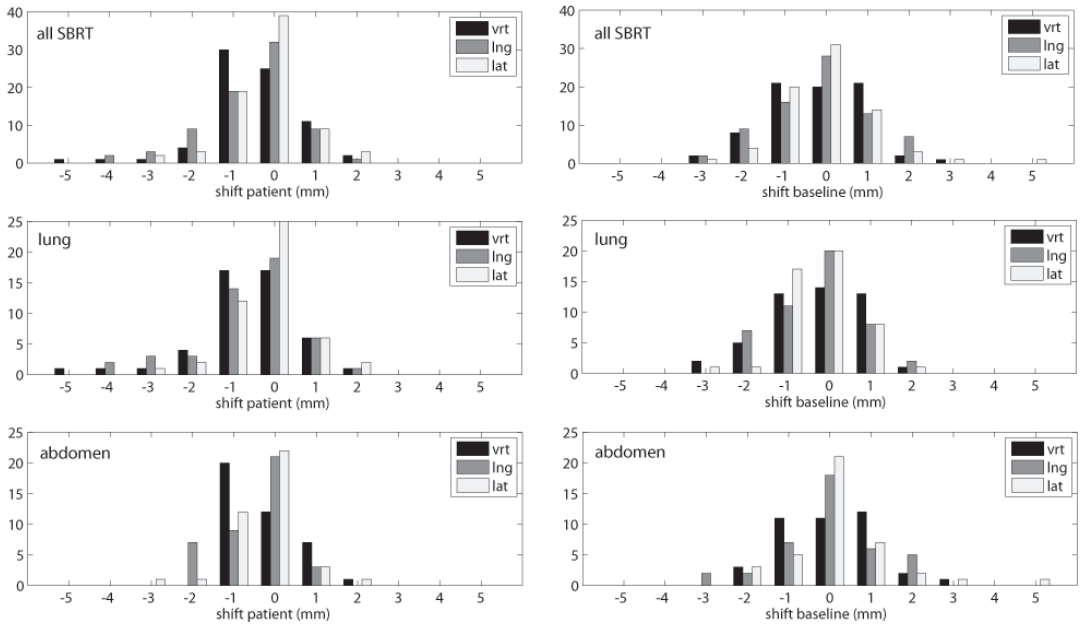

Figure 6.3: Patient (bony anatomy) and baseline (tumor in respect to the bones) shifts for lung and abdominal treatments. Intra-fractional motion was similar for patients with lung and abdominal tumors. The maximal shift observed was 4.2 mm. Shifts in lateral and longitudinal direction were non systematic whereas there was a slight systematic drift in vertical direction (mean shift 0.43 mm, $p < 0.01$), due to sagging and relaxing of the patient in the vacuum bag.

radiotherapy with large single fractions, minimal ITV to PTV margins are generally used. Derived from our calculated random and systematic errors (compare table 6.2 and 6.3) according to Van Herk's formula, ITV to PTV margins of 6 mm should be used if the described technique is applied. No dependency of the shifts on the beam-on time was found ($R^2 = 0.09$, $p = 0.78$).

6.5 Discussion

Here we reported our experience with the clinical application of stereotactic VMAT using X6FFF or X10 FFF beams at maximum dose rate. We showed that FFF beams at maximum dose rate substantially shorten beam-on time; in addition, we found minimal patient and target shift during treatment.
In our series, most patients had metastasized cancers and were heavily pretreated with surgery and chemotherapy. Accordingly, the doses prescribed in Gray represent an individualized treatment approach dependent on the individual patient situation

Table 6.2: Group mean (GM), systematic Σ and random σ errors for baseline (tumor in respect to bones), patient (bony anatomy) and tumor (total= baseline + patient) shifts. Margins M1 (only intrafractional motion) and M2 (intra-fractional motion + 2 mm contouring) for lung tumors calculated according to Van Herks formula.

lung		**GM (mm)**	**S (mm)**	**s (mm)**	**M1 (mm)**	**M2 (mm)**
tumor baseline bone	vrt	-0.54	0.6	1.18		
	lng	-0.77	0.91	0.51		
	lat	0.05	0.62	0.58		
	vrt	-0.4	0.67	0.37		
	lng	-0.35	0.53	0.46		
	lat	-0.43	0.77	0.59		
	vrt	-0.94	0.99	1.08	3.23	6.33
	lng	-1.12	0.98	0.66	2.74	5.86
	lat	-0.38	0.54	0.81	1.77	5.6

Table 6.3: Group mean (GM), systematic Σ and random σ errors for baseline (tumor in respect to bones), patient (bony anatomy) and tumor (total= baseline + patient) shifts. Margins M1 (only intrafractional motion) and M2 (intra-fractional motion + 2 mm contouring) for abdominal tumors calculated according to Van Herks formula.

abdomen		**GM (mm)**	**S (mm)**	**s (mm)**	**M1 (mm)**	**M2 (mm)**
tumor baseline bone	vrt	0.02	0.31	0.42		
	lng	-1.02	0.79	0.34		
	lat	-0.28	0.59	0.38		
	vrt	-0.06	0.26	0.64		
	lng	0.25	0.54	0.35		
	lat	0.32	0.57	0.71		
	vrt	-0.04	0.29	0.93	1.3	5.62
	lng	-0.77	0.48	0.47	1.34	5.28
	lat	0.03	0.45	0.45	1.27	5.26

and the tolerance of the remaining surrounding organ. In patients with high morbidity, treatment efficiency is important because these patients are not able to endure long treatment sessions.
We demonstrated that the X6FFF beam provided a time efficient treatment and was therefore a good choice for our patient cohort. X10FFF had a small additional benefit for patients receiving more than 10 Gy. However, the use of the higher dose rate of the X10FFF beam below 10 Gy does not translate into a time advantage due to the limited speed of the gantry (1 min/arc) [139]. A recent treatment planning study from our department indicates that X6FFF beams give superior plans for SBRT of lung tumors, compared to X6 and X10FFF. Therefore, our departmental policy is to treat lung volumes with X6FFF beams. We did not find a correlation between the time advantage of using FFF beams and the size of the treated volume. However, most of the patients had a PTV of similar size and only three patients had a volume larger than 100 ccm. The inclusion of more patients with larger volumes may change the result. As discussed in [139], the integral dose of FFF beams decreases with increasing volume and therefore it is expected that from a field size above 100 ccm, the number of MUs for FFF beams increases and the time advantage decreases.
The devices used for patient stabilization and the time of treatment delivery are thought to influence treatment accuracy. Using a stereotactic body frame (SBF) for immobilization of patients treated with SBRT, the 3D vectors of patient shift analyzed by pre and post treatment CBCT was 2.1 mm [45] and tumor drift was 2.3 mm (+/- 1.6 mm) [16] or, in a similar study, 5.2 mm (maximum 14.9 mm) [45]. The latter studies did not correlate stability with treatment time. Hoogeman et al. immobilized patients with vacuum bags and demonstrated significant patient shifts if the time span between measurements exceeded 15 minutes [51]. The importance of treatment time for patient stability was shown by a clinical study of patients with lung tumors treated with SBRT in which the mean patient shift was 5.3 mm if treatment lasted longer than 34 min, and only 2.2 mm if treatment time was shorter than 34 min [103]. In a recently published study Dahele et al. analyzed stability of the patient spine before and after RapidArc SBRT. Mean treatment time was 4.2 min and spine shifts were in the submm range [21]. However spine shift alone might not reflect bony shift of the whole thorax or, for example, of the sternum, when the patient relaxes. In our study, the mean beam on time was 1.6 min, the patient shift was within the submillimeter range and the 3D vector of the total tumor displacement was 2.0 mm, if all patients were considered, and 2.1 mm for tumors in the lung. These values represent an excellent level of patient stability for this technique, which can be at least in part attributed to the shortened beam-on times due to the use of FFF beams and volumetric arc treatment delivery. We did not find a dependency of the beam-on time on the stability of the patient. This is mainly due to the small range of beam on times between 0.84 min to 3.5 min. The high level of patient stability supports the use of small ITV to PTV margins (in our case 6 mm), which further benefit the patient by potentially reducing toxicity.

Of clinical concern is a potential increase in toxicity when using FFF beams with unprecedented high dose rates for the treatment of patients [79, 117]. However, FFF beams are increasingly used and first clinical studies in patients treated with SBRT did not result in unexpected toxicity [111]. Furthermore, as SBRT treatment volumes are small and toxicity is usually mild, it seems unlikely that toxicity will be significantly increased by using FFF beams for SBRT. In summary, our early clinical experience indicates that the use of FFF beams at high dose rate for extracranial stereotactic radiotherapy of patients with tumors in the lung, or abdomen, is very efficient. The X6FFF beam is generally a good choice for high dose per fraction, whereas there is only an additional benefit for the X10FFF beam (compared to the X6FFF beam) at doses above 10 Gy per fraction.

Chapter 7

Development and evaluation of a prototype tracking system using the treatment couch *

7.1 Abstract

Objective: Tumor motion increases safety margins around the clinical target volume and leads to an increased dose to the surrounding healthy tissue. We have developed and evaluated a treatment couch tracking system to counter steer respiratory tumor motion. Three different motion detection sensors with different lag times were evaluated.
Materials and Methods: The couch tracking system consists of a motion detection sensor, which can be the topometrical system Topos, the respiratory gating system RPM or the laser triangulation system and the Protura treatment couch. The control system was implemented in the block diagram environment Simulink. To achieve real time performance the Simulink models were executed on a real time engine, provided by Real-Time Windows Target. To achieve high control performance with good reference tracking and good disturbance rejection, a proportional-integral control system was implemented. The lag time of the couch tracking system using the three different motion detection sensors was determined with a step function of 2 cm on the position reference signal.
The geometrical accuracy of the system was evaluated by measuring the mean absolute deviation from the reference (static position) during motion tracking. A hexapod system was moving according to 7 respiration patterns previously acquired with the RPM system as well as according to a $\sin^6$ function with two different frequencies (0.33 Hz and 0.17 Hz) and the treatment table compensated the motion.
Results: A prototype system for treatment couch tracking of respiratory motion was successfully developed. We found that short delay times are needed to be able

*This chapter has been submitted for publication in Medical Physics (Lang et al).

to track all respiration frequencies. The laser based tracking system with a small lag time of 60 ms could track all respiration patterns. An increase in delay time from 60 ms to 130 ms (RPM based system) resulted in a poor tracking performance for the $\sin^6$ pattern (frequency 0.33 Hz). The Topos based tracking system with the largest lag time of 300 ms was only able to track four respiration patterns. For the four patient respiration patterns, which could be tracked by all three systems, a mean absolute deviation of 0.19 mm was achieved using the laser sensor, 0.45 mm using the RPM system and 0.52 mm using the TOPOS system.
Conclusion: Couch tracking with the Protura treatment couch is achievable. To reliably track all possible respiration patterns without prediction filters a short lag time below 100 ms is needed. More scientific work is necessary to extend our prototype to tracking of internal motion.

7.2 Introduction

Modern accelerators achieve sub-millimeter accuracy. However, not all tumors are stable during the treatment session. Tumors in the lung can move up to 16 mm [114], in the liver up to 34 mm [110] and the thoracic wall moves up to 14 mm [105] due to respiratory motion. In these cases tumor motion management is needed to accurately irradiate the tumor while sparing healthy tissue. This becomes important for large treatment volumes, where dose to the surounding tissue is a limiting factor and for hypofractionation, where high doses are applied in a small number of treatment fractions.
The three motion management techniques currently used in the clinical setting are motion encompassing treatment, gating and tracking. In comparison to motion encompassing treatment, gating allows treatment to a smaller volume; however, at the cost of substantially increased treatment time. The most sophisticated treatment technique appears to be tracking because it confines the high dose to the tumor (small volume) and is time efficient.
Tracking can be achieved by tracing the target volume dynamically with the radiation beam. This was first implemented in a robotic radiosurgery system, the CyberKnife system [2], and has been further realized by the use of a dynamic multi leaf collimator (MLC) [89] and the gimbaled head of the VERO system (BrainLab, Germany) [25]. Another possibility is to leave the treatment beam undisturbed but to move the treatment couch to achieve a stable tumor position. Several visibility studies have been performed showing the capability of different couch systems to perform tracking. In 2005 D'Souza et al [27] presented a couch tracking system based on a hexapod, which could perform tracking for slow respiration periods of 16s. More recently Buzurovic et al [18], Haas et al [46] and Wilbert et al [135] have developed more advanced couch control systems using proportional integral derivative feedback systems. However, none of these couch tracking systems is used in clinical routine. More research is needed to define optimal tracking settings and

demonstrate the clinical benefit of couch tracking. We've developed a prototype system for one-dimensional treatment couch tracking which works with the clinically available Protura treatment couch and is integrated into a clinical linear accelerator. To our knowledge the capability of couch tracking for this system has not yet been shown. Geometric as well as dosimetric accuracy was analysed using three different motion detection systems with different delay times. This enabled us to show the effect of different delay times on the tracking performance, which to our knowledge has not yet been evaluated.

7.3 Materials and Methods

Figure 7.1 shows the components of the tracking system. A phantom which moved in the vertical direction was imaged and tracked. The system consisted of a motion detection sensor, which could be the topometrical system Topos (CyberTechnologies), the respiratory gating system RPM (Varian Medical Systems) or the laser triangulation system (MicroEpsilon) and the treatment couch Protura (Civco Medical Systems).

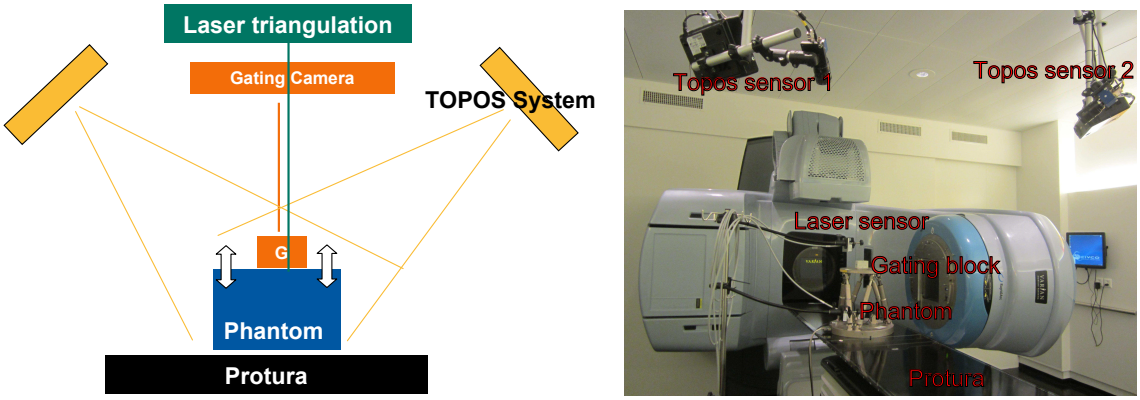

Figure 7.1: Components of the couch tracking system: A phantom performs a one-dimensional respiration pattern. The respiration is detected by the RPM gating system, the TOPOS system or the laser sensor. The Protura treatment couch compensates the breathing motion.

7.3.1 Motion detection sensors

Three different position detection sensors were integrated into the control system for the treatment couch tracking.

Topometrical Surface detection

A prototype of the topometrical surface detections system Topos (Cyber Technologies, Ingolstaft, Germany) previously described by Lindl et al [76] was used for the acquisition of the respiratory signal. It was composed of two beamers which projected structered white light onto the patient and two cameras, which acquired the images under a certain observation angle (Figure 7.2). It used phase measuring triangulation. The surface was calculated on the Topos server and the information was passed on to the Topos client via TCP/IP. The Topos client calculated the respiration signal and transmitted it to Matlab (MathWorks, Massachusetts, USA) via a .net named pipe.

Topos imaged the motion of the patient surface within a volume of 40x50x50 cm^3.

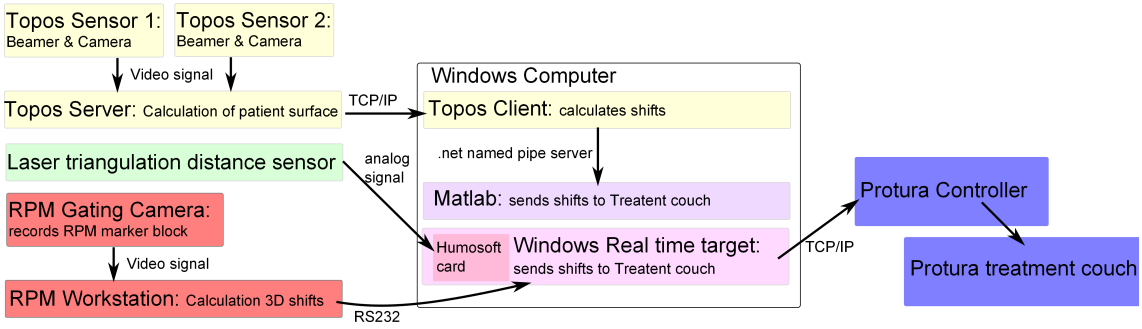

Figure 7.2: Schematic drawing of a couch tracking system

For the acquisition of the respiratory motion a volume of 5x5x5 cm^3 was defined and the motion of the surface in this volume was tracked. The three dimensional vector of the respiratory motion was written to a named pipe. The measuring rate of the system was 10 Hz, the delay time was approximated by Lindl et al to be 250 ms [76]. The accuracy in vertical direction was below 0.5 mm [76].

Single Point Infrared detection

The commercially available respiratory gating system RPM (Varian Medical Systems, Paolo Alto, USA) was used in a non-clinical mode. A 6-point marker block was detected in three dimensions using an infrared camera system (gating camera). The non-clinical mode allowed the transmission of the marker blocks's three dimensional position to the serial port of the RPM workstation. This signal could be further used for couch tracking (Figure 7.2). The measuring rate of the system was 25 Hz.

Laser triangulation measurement

The third position detection sensors used, was the laser triangulation displacement sensor opto NCDT 1302-100 (Micro Epsilon, Brownland, USA). The semiconductor

laser had a wavelength of 630 nm and a power less than 1 Watt. It had a one dimensional measurement range of 100 mm and was installed 100 mm above the surface of the respiratory phantom. The measuring rate of the system was 750 Hz and it had a resolution of 50 um.

7.3.2 Treatment couch

Treatment couch tracking was performed using the 6 degree of freedom (DoF) couch Protura (Civco Medical Systems, Iowa, USA)). The system used for our investigation is installed on a Trilogy linear accelerator (Varian Medical Systems, Paolo Alto, USA) used for clinical routine. The controller of the couch could be addressed using a dynamic link library (dll). The only difference between research mode and clinical mode was a modified firmware for the research mode to reduce delay times. In research mode, sending of commands via the dll took 0.9 ms. The request of information from the controller took 21.8 ms. The maximum allowed speed of the couch was 16 mm/s. The Protura couch is able to track in 6DoF, however at the moment the system was implemented for 1DoF tracking (vertical).

7.3.3 Control system

The controller was implemented in the block diagram environment Simulink (MathWorks, Massachusetts, USA). To achieve a high control performance with good reference tracking and good disturbance rejection, a proportional-integral controller according to the following equation was implemented:

$$z(t) = k_p \cdot u(t) + k_i \cdot (u(t) - u(t-1)) \tag{7.1}$$

$z(t)$ is the controller output in vertical direction at the discrete time t, $u(t)$ is the controller input, k_p is the proportional gain and k_i the integral gain. The proportional and integral gain were determined using Ziegler and Nichols tuning rules. To ensure that the tracking system worked in real time conditions, the Simulink models were executed on a real time engine, provided by Real-Time Windows target. Different filter designs for the three motion detection sensors were implemented to smooth the measured input signal. For the Topos based and the RPM based tracking system a finite impuls response (FIR) filter was used, for the laser based system a infinite impulse response (IIR) filter was implemented.

7.3.4 Evaluation of the tracking accuracy

The lag time of the couch tracking system using the three different imaging systems was determined using a step function of 2 cm. The time between the initiation of the step and the reaction of the imaging system was measured. The geometrical accuracy of the system was evaluated by measuring the residual signal, when tracking

was active. A hexapod system (Physics Instruments, Germany) was moved according to a $\sin^6$ function with two different frequencies (0.33 Hz and 0.17 Hz) and the treatment table compensated for the motion. The $\sin^6$ function to simulate breathing was chosen based on the work of Lujan et al [80]. Additionally, the hexapod system was moving according to 7 different respiration patterns of patients previously acquired with the RPM system during 4 dimensional computer tomography (4DCT). Mean frequency and amplitude of these patterns are summarized in table 7.1. The geometrical accuracy of the system was evaluated by measuring the mean

Table 7.1: Characteristics of respiratory pattern of seven patients: Respiration period T with standard deviation (SD), respiration peak to peak amplitude A with SD and the baseline drift of the patient due to relaxation normalized to 100 s.

pattern	T (s)	SD(T) (s)	A (mm)	SD(A) (mm)	drift (mm/100s)
1	8.69	0.84	10.21	0.76	6.9
2	8.32	0.75	10.65	1.21	7.6
3	6.79	1.59	10.38	4.03	0.7
4	6.06	0.53	4.91	0.87	1.3
5	5.56	1.38	5.34	1.13	0.8
6	5.51	1.41	0.35	0.94	0.9
7	3.49	0.28	5.33	0.75	2.6
$\sin^6$ 1	6.00	0.00	10.00	0.00	0.0
$\sin^6$ 1	3.00	0.00	10.00	0.00	0.0

absolute deviation from the reference position (static position), when tracking was applied. We considered the tracking as successful if the deviation was reduced by a factor of two between no tracking and tracking applied. The factor of 2 was chosen because if the reduction was less then 2 the system was likely to oscillate due to the breathing with a higher frequency than the breathing frequency. This we considered as disturbing for the patient.
Additionally the dosimetric effect of using tracking to compensate respiration compared to no tracking applied was investigated. Gafchromic films were irradiated for 60 s with and without tracking of one respiration pattern (pattern 4, using the laser based tracking system) with an open 2x2 cm^2 field at gantry angle of 90°. The broadening of the penumbra compared to static fields was evaluated.

7.4 Results

7.4.1 Lag times of the different systems

Figure 7.3 shows the response on a step function (20 mm) of the tracking system with the three different motion detection sensors. The laser system worked with a

high sampling rate of 750 Hz and has according to the manufacturer a lag time of below 1 ms. From the response on the step function a lag time of 57 ms of the total system (laser position acquisition and couch tracking) could be derived. Therefore the lag time of the Protura couch was approximately 56 ms. The lag time of the RPM system was 74 ms and of the TOPOS 244 ms. The total lag time of the Protura couch combined with the RPM system was 130 ms and combined with the TOPOS system 300 ms.

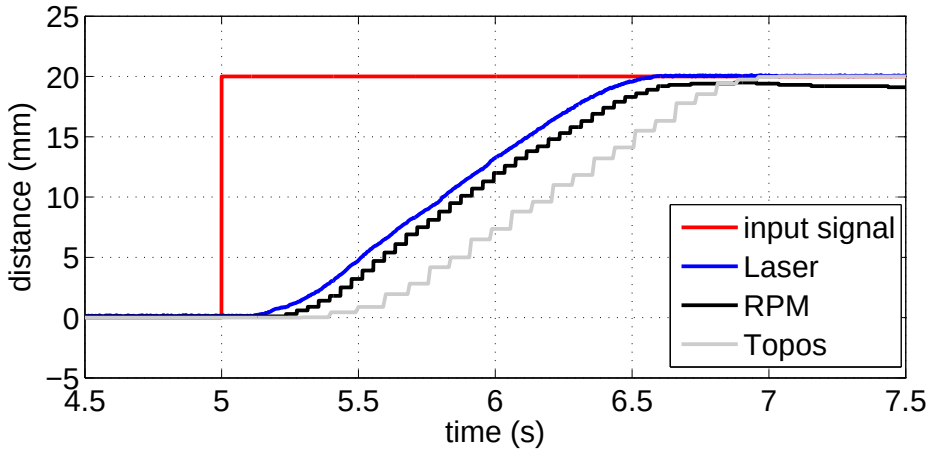

Figure 7.3: Response of the couch tracking system on a step function. The delay was different for the three different image acquisition systems.

7.4.2 Geometric and dosimetric accuracy

Figure 7.4 shows three different respiration patterns and the residual motion when tracking was applied. All three patterns could be tracked reliably if the laser based tracking approach was used for distance measurements. Pattern 3 (bottom) could not be tracked reliably (reduction in mean absolute deviation of less then a factor of two), when the Topos sensor was used. If the RPM sensor was used, the residual mean absolute deviation was reduced by a factor of 2.8 compared to a reduction of 10.56 if the laser sensor was used. Patterns 1 and 4 could be tracked by all three systems. Table 7.2 summarizes the residual motion for all seven respiration patterns. The laser based tracking system and the RPM based system could track all seven respiration patterns, the Topos based system was only able to track 4 out of the 7 patterns. Similarly, the tracking system based on the laser sensor could track both frequencies (0.33 Hz and 0.17 Hz) of the $\sin^6$ function and the tracking system based on the RPM sensor and the TOPOS sensor could only track the slower frequency.

Patient motion leads to broadening of the penumbra and an underdosage at the field edges (Figure 7.5 and Figure 7.6). Tracking can correct for this motion and the associated broadening of the penumbra. The increase in the penumbra of the profile

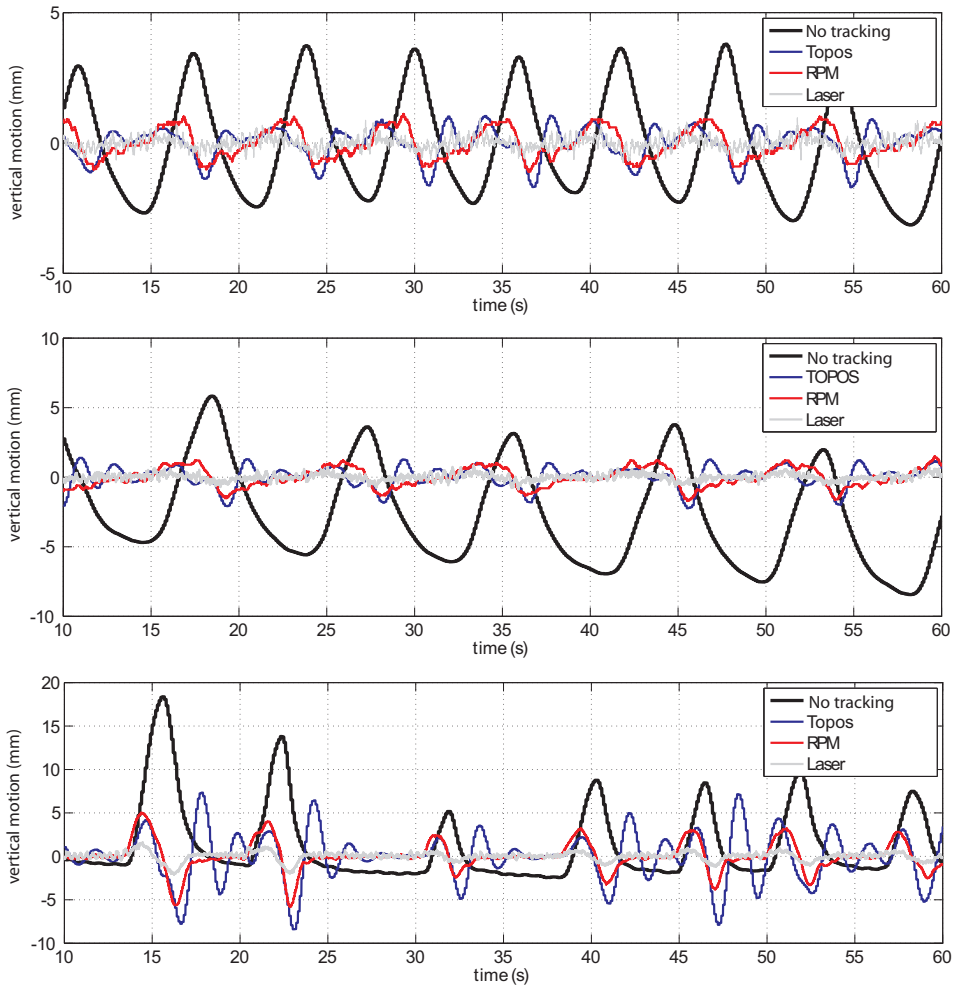

Figure 7.4: Respiration signal and residual signals, if tracking is applied using the three different motion detection sensors. top: Pattern 4, middle: Pattern 1, bottom: Pattern 3

for a motion of 6 mm was 1.4 mm. With tracking applied there was no increase in the penumbra (Figure 7.6)

7.5 Discussion and Conclusion

A one dimensional treatment couch tracking system, which could compensate for respiratory motion of the patient, was developed and evaluated. The respiratory motion was detected by three different surface detection systems with different delay times. We found that short delay times are needed to be able to track all the respiration frequencies. The laser based tracking system with a small lag time of approximatly 60 ms could track all the respiration patterns. An increase in delay time from 60 ms to 130 ms resulted in an inadequate tracking performance for the

Table 7.2: Mean deviation from the baseline without tracking applied and with the three different tracking systems. If tracking was not possible it is marked with NP.

Pattern	mean deviation (mm)			
	No tracking	Laser sensor	RPM	Topos
1	3.93	0.20	0.54	0.65
2	3.94	0.21	0.50	0.51
3	3.87	0.37	1.38	NP
4	1.84	0.17	0.45	0.47
5	2.09	0.23	0.65	NP
6	1.68	0.17	0.35	0.44
7	1.65	0.51	0.77	NP
$\sin^6$ 1	3.70	0.21	0.43	0.97
$\sin^6$ 2	3.70	0.47	NP	NP

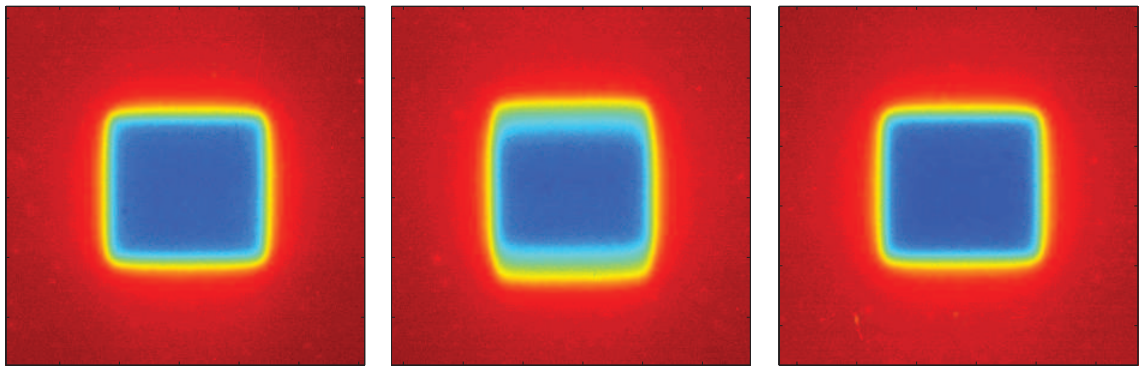

Figure 7.5: Comparison of an open field, radiated on a gafchromic film in a moving phantom (middle), on a static phantom (left) and on a moving phantom with tracking applied (right).

$\sin^6$ pattern (frequency 0.33 Hz). The system with the largest lag time of 300 ms was only able to track 4 of the breathing patterns. Prediction filters might be an option to improve the accuracy of the this system. Buzurovic et al [17] and Qiu et al [104] have shown that prediction filters improve the tracking accuracy for lag times between 125 ms - 250 ms.
For the four patient respiration patterns, which could be tracked by all three systems, a mean absolute deviation of 0.19 mm was achieved using the laser sensor, 0.45 mm using the RPM system and 0.52 mm using the TOPOS system. For all seven patient patterns tested, a mean absolute deviation of 0.27 mm was achieved using the laser sensor and of 0.65 mm using the RPM system. Similarly, Buzurovic et al [18] showed an accuracy of 0.18 mm for an experimental couch in combination with the Align RT system (VisionRT, London, UK). The results are difficult to compare because different respiration patterns were used, but are non the less in the same

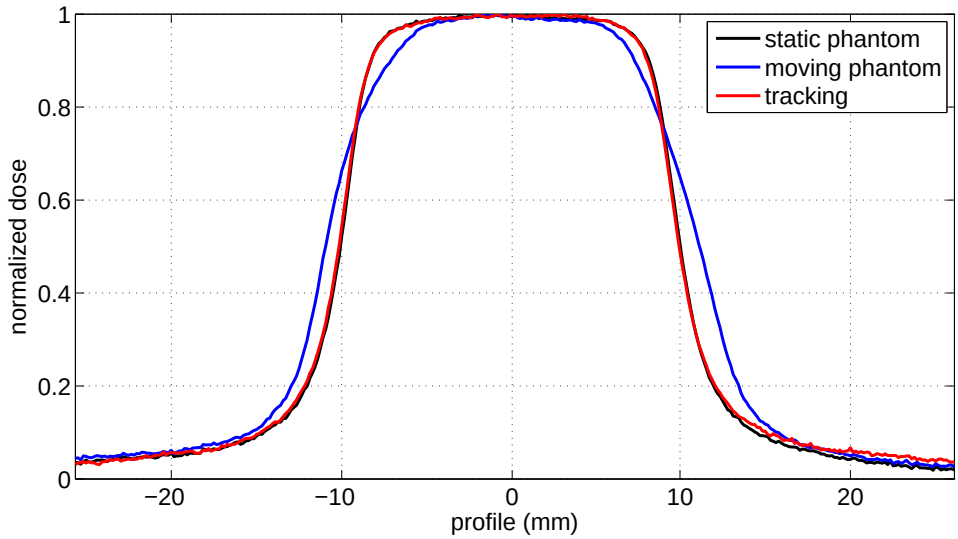

Figure 7.6: Profiles of an open field (2x2 cm^2) along the direction of respiration motion, acquired with gafchromic films. Black: static phantom, no motion, blue: phantom in motion, no tracking, red: phantom in motion, tracking

order of magnitude. Lee et al [74] found a root mean square error of 2.34 mm for their experimental couch in combination with Align RT. The larger error probably results due to their large lag time of 251 ms.
One limiting performance factor of our system was the speed of the couch. We were limited to a velocity of 16 mm/s. For respiratory pattern 3 it was not possible to follow the fast respiratory motion of the patient with this velocity. Souza et al [27] had a similar problem, their experimental couch system could not track breathing cycle times of 4s due to the limited speed of the treatment couch. Buzurovic et al [19] used an Elekta Precise Table™ with a maximum speed of 50 mm/s and did not experience any limitations with this velocity. However, patient tolerance for couch tracking should be assessed for different velocities and accelerations to define a maximum tolerable speed. Motion sickness due to the tracking of the couch might be an issue. Only very limited data exists on this topic [28, 120, 134].
All three motion detection systems detected the surface of the patient. This makes our tracking approach a suitable tool for the tracking of breast or thoracic wall tumors. However at the same time it is a limitation because motion of lung or liver tumors cannot be tracked only based on surface detection systems. A correlation model between internal and external motion, or an imaging modality which images internal motion would be needed. Similarly for prostate or vertebral tumors, an imaging technique, such as RF transponder localisation, MV or kV imaging during treatment is needed to quantify intrafractional motion. The discussed imaging modalities or a correlation model could be easily added to our existing couch tracking system to make it more universal.

Chapter 8

Conclusions and future work

Precise Radiotherapy of hypo-fractionated treatments of moving tumors applied by a linear accelerator was the topic of this PhD thesis. Hypofractionated radiotherapy is currently an area of clinical research. Clinical trials are looking into giving higher doses of radiation per fraction, but giving fewer fractions. The goal is to find out if the tumor can be better controlled in this way or if the treatment time can be shortened with the same or better clinical outcome. However for moving tumors, large safety margins need to be applied to cover the tumor volume with the full dose. This leads to a large amount of healthy tissue being irradiated with high doses and eventually increases side effects. Therefore to safely apply hypofractionated treatments to moving structures, motion management techniques are needed, to reduce safety margins and high doses to healthy tissue. Two approaches to reduce intrafractional motion to be able increase the dose per fraction are implemented and evaluated within the frame of this thesis. First flattening filter free beams were implemented for clinical use (Chapter3-5). Flattening filter free beams have an increased dose rate (Chapter 3) compared to conventional beams, which leads to reduced treatment times and reduced intrafractional motion as was shown in Chapter 6. The use of flattening filter free beams has the potential to reduce patient motion as well as prostate motion, however for periodic respiratory motion there is no benefit expected. In Chapter 7 the reduction of safety margins for respiratory motion was addressed. The compensation was performed by countersteering the respiratory motion with the treatment couch.
Below, results and conclusions from Chapter 3-7 will be discussed.
In Chapter 3 it was shown that air-vented ionization chambers can be reliably used for relative dosimetry of flattening filter free beams. The Markus chamber demonstrated the largest ion collection efficiency (0.994 @ DPP = 1.7 mGy, X10FFF beam). The order of correction for reference dosimetry is given within Chapter 3. However, liquid ionization chambers appear to be unsuitable for dosimetry in unflattened beams due to their decreased ion collection efficiency.
As a result of the planning study in Chapter 4 it was found that FFF beams resulted in dose distributions similar to flattened beams. Additionally, it was shown

that the mean body dose was a function of beam energy and decreased with increasing mean beam energy. X10FFF beam provided the best solution, sparing rectum and bladder and minimizing whole body dose. Moreover the planning study showed that the number of MU increased for X6FFF and X10FFF by 7.7% and 1.2%. FFF beams lead to a time efficient treatment delivery, particularly when combined with hypofractionated VMAT.
In Chapter 5 the dosimetric accuracy of flattening filter free beam delivery for IMRT and VMAT techniques was shown. Dose delivery was equally accurate for IMRT and RA delivery as well as for the two beams evaluated. Additionally in the study in Chapter 5 a set of QA devices suitable for use in high dose rate flattening filter free beams was presented.
The study on the clinical application of FFF beams described in Chapter 6 showed that SBRT using FFF beams is time efficient. Mean beam-on time was 1.6 min and total treatment time 17.2 min. The high level of patient stability supported the use of small ITV to PTV margins (in our case 6 mm), which benefit the patient by potentially reducing toxicity.
In the last Chapter of the thesis (Chapter 7) the technical realisation of a couch tracking system was explained and the system was evaluated and characterized. Three different motion detection sensors with different lag times were used and compared. A lag time below 100 ms is needed to reliably track all possible breathing motion if no prediction filters are used.
Interest in FFF technology with dose rates of up to 24 Gy/min is resulting from the expectation that it will allow faster treatment delivery. This might lead to reduced intra-fractional motion of the patient. Additionally a reduced dose outside the field is expected. Flattening filter free beams are clinically available since March 2010, since then over 40 scientific studies have been published on FFF technology. Many clinics have already introduced FFF beams into the clinics, showing excellent results concerning treatment efficiency and outcome [111, 87]. Within the frame of this thesis four studies on FFF technology were performed, which are in line with other publications showing the efficiency and safety of the FFF beams. Several other publications have based their research on our findings on the safe delivery of FFF beams.
Flattening filter free beams are mainly used for hypo-fractionated treatments [83, 95, 102]. Together with my colleagues I have performed two studies showing the application of FFF beams for hypofractionated treatments of the prostate and the lung (Chapter 4 and 6). Similar to Mancosu et al, Ong et al and Prendergast et al [83, 95, 102], we have shown an increased treatment efficiency for both treatment sites. For lung and liver patients this lead to excellent stability of the patient during the treatment delivery (Chapter 6). However dosimterically we found only slight improvements compared to treatments with flattened beams. This is in agreement with the results of other researchers [123, 95].
The use of flattening filter free beams has the potential to reduce motion of the patient (Chapter 6) as well as prostate motion, however for periodic respiratory motion

there is no benefit, as was recently shown by Ong et al [93]. This shows the need of intra-fractional motion management. The three motion management techniques currently used in clinical settings are motion encompassing treatment, gating and tracking. In comparison to motion encompassing treatments, gating allows the treatment to a smaller volume at the cost however of substantially increased treatment time. The most sophisticated treatment technique appears to be tracking because it confines the high dose to the tumor (small volume) and is time efficient. Within the frame of my thesis a couch tracking system was developed which can compensate for respiratory motion of the patient. The respiratory motion is detected by three different surface detection systems. This makes it a suitable tool for tracking of breast and thoracic wall tumors. However at the same time it is a limitation, because tumor motion of lung or liver tumors cannot be tracked only based on surface detection systems. A correlation model between internal and external motion or internal motion imaging would be needed. Similarly for prostate or vertebral tumors, MV or kV imaging during treatment is needed to quantify intra-fractional motion. The discussed imaging modalities or a correlation model can be easily added to our existing couch tracking system in order to make it more universal. In a next step, patient tolerance concerning couch tracking should be assessed. Motion sickness due to the tracking of the couch might be an issue. Only very limited data exists on this topic [28, 120]. A large patient and volunteer study would be needed to address the issue. Currently we are working on the implementation of prediction filters to further reduce the residual motion during respiration and on a correlation model to correlate the internal liver motion with the external motion. The field of intra-fractional motion managment is large and many more PhD thesis will be needed to satisfactorily cover all issues. However within the frame of this thesis two key issue how intra-fractional motion can be managed were addressed.

Bibliography

[1] L. R. Aarup, A. E. Nahum, C. Zacharatou, T. Juhler-Nøttrup, T. Knöös, H. Nyström, L. Specht, E. Wieslander, and S. S. Korreman. The effect of different lung densities on the accuracy of various radiotherapy dose calculation methods: implications for tumour coverage. *Radiotherapy and Oncology*, 91(3):405–414, 2009.

[2] J. R. Adler Jr, M. J. Murphy, S. D. Chang, and S. L. Hancock. Image-guided robotic radiosurgery. *Neurosurgery*, 44(6):1299–1306, 1999.

[3] S. Agostinelli, S. Garelli, M. Piergentili, and F. Foppiano. Response to high-energy photons of ptw31014 pinpoint ion chamber with a central aluminum electrode. *Medical Physics*, 35:3293–3301, 2008.

[4] P. R. Almond, P. J. Biggs, B. Coursey, W. Hanson, M. S. Huq, R. Nath, and D. Rogers. Aapm's tg-51 protocol for clinical reference dosimetry of high-energy photon and electron beams. *Medical physics*, 26:1847, 1999.

[5] J. M. Balter, J. N. Wright, L. J. Newell, B. Friemel, S. Dimmer, Y. Cheng, J. Wong, E. Vertatschitsch, and T. P. Mate. Accuracy of a wireless localization system for radiotherapy. *International Journal of Radiation Oncology* Biology* Physics*, 61(3):933–937, 2005.

[6] J. L. Bedford, Y. K. Lee, P. Wai, C. P. South, and A. P. Warrington. Evaluation of the delta4 phantom for imrt and vmat verification. *Physics in medicine and biology*, 54(9):N167, 2009.

[7] S. Bentzen, R. Agrawal, E. Aird, J. Barrett, P. Barrett-Lee, J. Bliss, J. Brown, J. Dewar, H. Dobbs, J. Haviland, et al. The uk standardisation of breast radiotherapy (start) trial a of radiotherapy hypofractionation for treatment of early breast cancer: a randomised trial. *The lancet oncology*, 9(4):331, 2008.

[8] S. M. Bentzen, L. S. Constine, J. O. Deasy, A. Eisbruch, A. Jackson, L. B. Marks, R. K. Ten Haken, and E. D. Yorke. Quantitative analyses of normal tissue effects in the clinic (quantec): an introduction to the scientific issues. *International Journal of Radiation Oncology* Biology* Physics*, 76(3):S3–S9, 2010.

[9] C. Bert, K. G. Metheany, K. P. Doppke, A. G. Taghian, S. N. Powell, and G. T. Chen. Clinical experience with a 3d surface patient setup system for alignment of partial-breast irradiation patients. *International Journal of Radiation Oncology* Biology* Physics*, 64(4):1265–1274, 2006.

[10] BfS. Statistik schweiz - todesfälle: Anzahl, entwicklung und ursachen 2010, 2010.

[11] J. Boag. *Ionization chambers Radiation Dosimetry vol II*. London: Academic, 1966.

[12] J. Boag and J. Currant. Current collection and ionic recombination in small cylindrical ionization chambers exposed to pulsed radiation. *British Journal of Radiology*, 53:471–478, 1980.

[13] S. L. Brown, A. Rodger, C. G. Orton, et al. Hypofractionation is a proven safe and effective modality for postoperative whole-breast radiotherapy for early breast cancer patients. *Medical physics*, 36:1927, 2009.

[14] G. Bruggmoser, R. Saum, A. Schmachtenberg, F. Schmid, and E. Schüle. Determination of the recombination correction factor ks for specific plane-parallel and cylindrical ionization chambers in pulsed photon and electron beams. *Physics in Medicine and Biology*, 52:N35–N50, 2007.

[15] J. Burns and K. Rosser. Saturation correction for the ne 2560/1 dosemeter in photon dosimetry. *Physics in Medicine and Biology*, 35(5):687, 1990.

[16] L. E. Butler, K. M. Forster, C. W. Stevens, C. Bloch, H. H. Liu, S. L. Tucker, R. Komaki, Z. Liao, and G. Starkschall. Dosimetric benefits of respiratory gating: a preliminary study. *Journal of Applied Clinical Medical Physics*, 5(1), 2004.

[17] I. Buzurovic, K. Huang, T. K. Podder, and Y. Yu. Comparison between acceleration-enhanced adaptive filters and neural network filters for respiratory motion prediction. In *Neural Network Applications in Electrical Engineering (NEUREL), 2012 11th Symposium on*, pages 181–184. IEEE, 2012.

[18] I. Buzurovic, K. Huang, Y. Yu, and T. Podder. A robotic approach to 4d real-time tumor tracking for radiotherapy. *Physics in Medicine and Biology*, 56(5):1299, 2011.

[19] I. Buzurovic, Y. Yu, M. Werner-Wasik, T. Biswas, P. Anne, A. Dicker, and T. Podder. Implementation and experimental results of 4d tumor tracking using robotic couch. *Medical physics*, 39:6957, 2012.

[20] J. Cashmore, M. Ramtohul, and D. Ford. Lowering whole-body radiation doses in pediatric intensity-modulated radiotherapy through the use of unflattened photon beams. *International Journal of Radiation Oncology* Biology* Physics*, 80(4):1220–1227, 2011.

[21] M. Dahele, W. Verbakel, J. Cuijpers, B. Slotman, and S. Senan. An analysis of patient positioning during stereotactic lung radiotherapy performed without rigid external immobilization. *Radiotherapy and Oncology*, 104(1):28–32, 2012.

[22] A. Dasu, P.-O. Löfroth, and G. Wickman. Liquid ionization chamber measurements of dose distributions in small 6 mv photon beams. *Physics in medicine and biology*, 43(1):21, 1998.

[23] D. Dearnaley, I. Syndikus, G. Sumo, M. Bidmead, D. Bloomfield, C. Clark, A. Gao, S. Hassan, A. Horwich, R. Huddart, et al. Conventional versus hypofractionated high-dose intensity-modulated radiotherapy for prostate cancer: preliminary safety results from the chhip randomised controlled trial. *The lancet oncology*, 2011.

[24] F. DeBlois, C. Zankowski, and E. B. Podgorsak. Saturation current and collection efficiency for ionization chambers in pulsed beams. *Medical physics*, 27:1146, 2000.

[25] T. Depuydt, D. Verellen, O. Haas, T. Gevaert, N. Linthout, M. Duchateau, K. Tournel, T. Reynders, K. Leysen, M. Hoogeman, G. Storme, and M. D. Ridder. Geometric accuracy of a novel gimbals based radiation therapy tumor tracking system. *Radiotherapy and Oncology*, 98(3):365 – 372, 2011.

[26] K. Derikum and M. Roos. Measurement of saturation correction factors of thimble-type ionization chambers in pulsed photon beams. *Physics in Medicine and Biology*, 38(6):755, 1993.

[27] W. D'Souza, S. A. Naqvi, and X. Y. Cedric. Real-time intra-fraction-motion tracking using the treatment couch: a feasibility study. *Physics in medicine and biology*, 50(17):4021, 2005.

[28] W. D. D'Souza, K. T. Malinowski, S. Van Liew, G. D'Souza, K. Asbury, T. J. McAvoy, M. Suntharalingam, and W. F. Regine. Investigation of motion sickness and inertial stability on a moving couch for intra-fraction motion compensation. *Acta Oncologica*, 48(8):1198–1203, 2009. PMID: 19863229.

[29] A. Dutreix. Keynote address: Prescription, precision, and decision in treatment planning. *International Journal of Radiation Oncology*Biology*Physics*, 13(9):1291 – 1296, 1987.

[30] V. Feygelman, G. Zhang, C. Stevens, and B. E. Nelms. Evaluation of a new vmat qa device, or the "x" and "o" array geometries. *Journal of Applied Clinical Medical Physics*, 12(2), 2011.

[31] C. Fiorino, I. Dell'Oca, A. Pierelli, S. Broggi, E. De Martin, N. Di Muzio, B. Longobardi, F. Fazio, R. Calandrino, et al. Significant improvement in normal tissue sparing and target coverage for head and neck cancer by means of helical tomotherapy. *Radiotherapy and oncology: journal of the European Society for Therapeutic Radiology and Oncology*, 78(3):276, 2006.

[32] A. Fogliata, A. Clivio, P. Fenoglietto, J. Hrbacek, S. Kloeck, P. Lattuada, P. Mancosu, G. Nicolini, E. Parietti, G. Urso, et al. Quality assurance of rapidarc in clinical practice using portal dosimetry. *British Journal of Radiology*, 84(1002):534–545, 2011.

[33] A. Fogliata, G. Nicolini, A. Clivio, E. Vanetti, and L. Cozzi. Accuracy of acuros xb and aaa dose calculation for small fields with reference to rapidarc® stereotactic treatments. *Medical physics*, 38:6228, 2011.

[34] A. Fogliata, G. Nicolini, A. Clivio, E. Vanetti, P. Mancosu, and L. Cozzi. Dosimetric validation of the acuros xb advanced dose calculation algorithm: fundamental characterization in water. *Physics in medicine and biology*, 56(6):1879, 2011.

[35] A. Fogliata, E. Vanetti, D. Albers, C. Brink, A. Clivio, T. Knöös, G. Nicolini, and L. Cozzi. On the dosimetric behaviour of photon dose calculation algorithms in the presence of simple geometric heterogeneities: comparison with monte carlo calculations. *Physics in medicine and biology*, 52(5):1363, 2007.

[36] D. Followill, P. Geis, A. Boyer, et al. Estimates of whole-body dose equivalent produced by beam intensity modulated conformal therapy. *International journal of radiation oncology, biology, physics*, 38(3):667, 1997.

[37] D. E. Freeman, C. R. King, et al. Stereotactic body radiotherapy for low-risk prostate cancer: five-year outcomes. *Radiation Oncology*, 6(3), 2011.

[38] W. Fu, J. Dai, Y. Hu, D. Han, and Y. Song. Delivery time comparison for intensity-modulated radiation therapy with/without flattening filter: a planning study. *Physics in medicine and biology*, 49(8):1535, 2004.

[39] D. Georg, T. Knöös, and B. McClean. Current status and future perspective of flattening filter free photon beams. *Medical physics*, 38:1280, 2011.

[40] D. Georg, G. Kragl, S. Af Wetterstedt, P. McCavana, B. McClean, and T. Knöös. Photon beam quality variations of a flattening filter free linear accelerator. *Medical physics*, 37:49, 2010.

[41] D. P. Gierga, J. Brewer, G. C. Sharp, M. Betke, C. G. Willett, and G. T. Chen. The correlation between internal and external markers for abdominal tumors: implications for respiratory gating. *International Journal of Radiation Oncology* Biology* Physics*, 61(5):1551–1558, 2005.

[42] N. Giorgia, F. Antonella, V. Eugenio, C. Alessandro, A. Filippo, C. Luca, et al. What is an acceptably smoothed fluence? dosimetric and delivery considerations for dynamic sliding window imrt. *Radiat Oncol*, 2:42, 2007.

[43] P. Giraud, E. Yorke, E. C. Ford, R. Wagman, G. S. Mageras, H. Amols, C. C. Ling, and K. E. Rosenzweig. Reduction of organ motion in lung tumors with respiratory gating. *Lung Cancer*, 51(1):41–51, 2006.

[44] I. S. Grills, G. Hugo, L. L. Kestin, A. P. Galerani, K. K. Chao, J. Wloch, D. Yan, et al. Image-guided radiotherapy via daily online cone-beam ct substantially reduces margin requirements for stereotactic lung radiotherapy. *International journal of radiation oncology, biology, physics*, 70(4):1045–1056, 2008.

[45] M. Guckenberger, J. Meyer, J. Wilbert, A. Richter, K. Baier, G. Mueller, and M. Flentje. Intra-fractional uncertainties in cone-beam ct based image-guided radiotherapy (igrt) of pulmonary tumors. *Radiotherapy and oncology*, 83(1):57–64, 2007.

[46] O. C. L. Haas, P. Skworcow, D. Paluszczyszyn, A. Sahih, M. Ruta, and J. A. Mills. Couch-based motion compensation: modelling, simulation and real-time experiments. *Physics in Medicine and Biology*, 57(18):5787, 2012.

[47] E. J. Hall. Intensity-modulated radiation therapy, protons, and the risk of second cancers. *International Journal of Radiation Oncology Biology Physics*, 65(1):1–7, 2006.

[48] J. Havercroft and S. Klevenhagen. Ion recombination corrections for plane-parallel and thimble chambers in electron and photon radiation. *Physics in medicine and biology*, 38(1):25, 1993.

[49] L. Hoffmann. Implementation and experimental validation of the high dose rate stereotactic treatment mode at varian accelerators. *Acta Oncologica*, 48(2):201–208, 2009.

[50] J. D. Hoisak, K. E. Sixel, R. Tirona, P. C. Cheung, and J.-P. Pignol. Correlation of lung tumor motion with external surrogate indicators of respiration. *International Journal of Radiation Oncology* Biology* Physics*, 60(4):1298–1306, 2004.

[51] M. S. Hoogeman, J. J. Nuyttens, P. C. Levendag, and B. J. Heijmen. Time dependence of intrafraction patient motion assessed by repeat stereoscopic imaging. *International Journal of Radiation Oncology* Biology* Physics*, 70(2):609–618, 2008.

[52] S. Hossain, P. Xia, C. Chuang, L. Verhey, A. R. Gottschalk, G. Mu, and L. Ma. Simulated real time image guided intrafraction tracking-delivery for hypofractionated prostate imrt. *Medical physics*, 35:4041, 2008.

[53] J. Hrbacek, S. Lang, and S. Klöck. Commissioning of photon beams of a flattening filter-free linear accelerator and the accuracy of beam modeling using an anisotropic analytical algorithm. *International Journal of Radiation Oncology* Biology* Physics*, 80(4):1228–1237, 2011.

[54] ICRU. Report 24. determination of absorbed dose in a patient irradiated by means of x or gamma rays in radiotherapy procedures. *International Commission on Radiation Units and Measurements*, 1976.

[55] ICRU. Report 50. prescribing, recording, and reporting photon beam therapy. *International Commission on Radiation Units and Measurements*, 1993.

[56] ICRU. Report 62. prescribing, recording, and reporting photon beam therapy. *International Commission on Radiation Units and Measurements*, 1999.

[57] S. B. Jiang et al. Technical aspects of image-guided respiration-gated radiation therapy. *Medical Dosimetry*, 31(2):141–151, 2006.

[58] J.-Y. Jin, M. Ajlouni, Q. Chen, F.-M. S. Kong, S. Ryu, and B. Movsas. Quantification of incidental dose to potential clinical target volume (ctv) under different stereotactic body radiation therapy (sbrt) techniques for non-small cell lung cancer – tumor motion and using internal target volume (itv) could improve dose distribution in {CTV}. *Radiotherapy and Oncology*, 85(2):267 – 276, 2007.

[59] J.-Y. Jin, F.-M. Kong, I. J. Chetty, M. Ajlouni, S. Ryu, R. Ten Haken, and B. Movsas. Impact of fraction size on lung radiation toxicity: hypofractionation may be beneficial in dose escalation of radiotherapy for lung cancers. *International Journal of Radiation Oncology* Biology* Physics*, 76(3):782–788, 2010.

[60] B. Johansson and G. Wickman. General collection efficiency for liquid isooctane and tetramethylsilane used as sensitive media in a parallel-plate ionization chamber. *Physics in medicine and biology*, 42(1):133, 1997.

[61] B. Johansson, G. Wickman, and J. Bahar-Gogani. General collection efficiency for liquid isooctane and tetramethylsilane in pulsed radiation. *Physics in Medicine and Biology*, 42(10):1929, 1997.

[62] A. W. Katz, M. Carey-Sampson, A. G. Muhs, M. T. Milano, M. C. Schell, and P. Okunieff. Hypofractionated stereotactic body radiation therapy (sbrt) for limited hepatic metastases. *International Journal of Radiation Oncology* Biology* Physics*, 67(3):793–798, 2007.

[63] F. M. Khan and F. Khan. *The physics of radiation therapy*, volume 3. Lippincott Williams & Wilkins Philadelphia, 2003.

[64] J. Kim, N. Wen, J.-Y. Jin, N. Walls, S. Kim, H. Li, L. Ren, Y. Huang, A. Doemer, K. Faber, T. Kunkel, A. Balawi, K. Garbarino, K. Levin, S. Patel, M. Ajlouni, B. Miller, T. Nurushev, C. Huntzinger, R. Schulz, I. Chetty, B. Movsas, and S. Ryu. Clinical commissioning and use of the novalis tx linear accelerator for srs and sbrt. *Journal of Applied Clinical Medical Physics*, 13(3), 2012.

[65] G. Kragl, S. af Wetterstedt, B. Knäusl, M. Lind, P. McCavana, T. Knöös, B. McClean, and D. Georg. Dosimetric characteristics of 6 and 10mv unflattened photon beams. *Radiotherapy and Oncology*, 93(1):141–146, 2009.

[66] G. Kragl, F. Baier, S. Lutz, D. Albrich, M. Dalaryd, B. Kroupa, T. Wiezorek, T. Knöös, and D. Georg. Flattening filter free beams in sbrt and imrt: dosimetric assessment of peripheral doses. *Zeitschrift für Medizinische Physik*, 21(2):91–101, 2011.

[67] S. F. Kry, O. N. Vassiliev, and R. Mohan. Out-of-field photon dose following removal of the flattening filter from a medical accelerator. *Physics in medicine and biology*, 55(8):2155, 2010.

[68] F. J. Lagerwaard, O. W. Meijer, E. A. van der Hoorn, W. F. Verbakel, B. J. Slotman, and S. Senan. Volumetric modulated arc radiotherapy for vestibular schwannomas. *International Journal of Radiation Oncology* Biology* Physics*, 74(2):610–615, 2009.

[69] S. Lang, J. Hrbacek, A. Leong, and S. Klöck. Ion-recombination correction for different ionization chambers in high dose rate flattening-filter-free photon beams. *Physics in Medicine and Biology*, 57(9):2819, 2012.

[70] S. Lang, G. Reggiori, J. P. Vaqué, C. Calle, J. Hrbacek, S. Klöck, M. Scorsetti, L. Cozzi, and P. Mancosu. Pretreatment quality assurance of flattening filter free beams on 224 patients for intensity modulated plans: A multicentric study. *Medical physics*, 39:1351, 2012.

[71] S. Lang and O. Riesterer. Modern techniques in radiation oncology. *SPG Mitteilungen*, 40, November 2013.

[72] S. Lang, B. Shrestha, S. Graydon, F. Cavelaars, C. Linsenmeier, J. Hrbacek, S. Klöck, G. Studer, and O. Riesterer. Clinical application of flattening filter free beams for extracranial stereotactic radiotherapy. *Radiotherapy and Oncology*, 2013.

[73] F. Leborgne and J. Fowler. Late outcomes following hypofractionated conformal radiotherapy vs. standard fractionation for localized prostate cancer: a nonrandomized contemporary comparison. *International Journal of Radiation Oncology* Biology* Physics*, 74(5):1441–1446, 2009.

[74] S. Lee, K.-H. Chang, J. B. Shim, Y. Cao, C. K. Lee, S. J. Cho, D. S. Yang, Y. J. Park, W. S. Yoon, and C. Y. Kim. Evaluation of mechanical accuracy for couch-based tracking system (cbts). *Journal of Applied Clinical Medical Physics*, 13(6), 2012.

[75] S.-X. Liang, X.-D. Zhu, H.-J. Lu, C.-Y. Pan, F.-X. Li, Q.-F. Huang, A.-Y. Wang, L. Chen, X.-L. Fu, and G.-L. Jiang. Hypofractionated three-dimensional conformal radiation therapy for primary liver carcinoma. *Cancer*, 103(10):2181–2188, 2005.

[76] B. L. Lindl, R. G. Müller, S. Lang, M. D. H. Lablanca, and S. Klöck. Topos: A new topometric patient positioning and tracking system for radiation therapy based on structured white light. *Medical physics*, 40:042701, 2013.

[77] W. Liu, R. Wiersma, W. Mao, G. Luxton, and L. Xing. Real-time 3d internal marker tracking during arc radiotherapy by the use of combined mv–kv imaging. *Physics in medicine and biology*, 53(24):7197, 2008.

[78] W. Liu, R. D. Wiersma, and L. Xing. Optimized hybrid megavoltage-kilovoltage imaging protocol for volumetric prostate arc therapy. *International Journal of Radiation Oncology* Biology* Physics*, 78(2):595–604, 2010.

[79] I. Lohse, S. Lang, J. Hrbacek, S. Scheidegger, S. Bodis, N. S. Macedo, J. Feng, U. M. Lütolf, and K. Zaugg. Effect of high dose per pulse flattening filter-free beams on cancer cell survival. *Radiotherapy and Oncology*, 101(1):226–232, 2011.

[80] A. E. Lujan, E. W. Larsen, J. M. Balter, and R. K. Ten Haken. A method for incorporating organ motion due to breathing into 3d dose calculations. *Medical physics*, 26:715, 1999.

[81] W. Lutz, K. R. Winston, and N. Maleki. A system for stereotactic radiosurgery with a linear accelerator. *International Journal of Radiation Oncology* Biology* Physics*, 14(2):373–381, 1988.

[82] V. Macías and A. Biete. Hypofractionated radiotherapy for localised prostate cancer. review of clinical trials. *Clinical and Translational Oncology*, 11(7):437–445, 2009.

[83] P. Mancosu, S. Castiglioni, G. Reggiori, M. Catalano, F. Alongi, C. Pellegrini, S. Arcangeli, A. Tozzi, F. Lobefalo, A. Fogliata, et al. Stereotactic body radiation therapy for liver tumours using flattening filter free beam: dosimetric and technical considerations. *Radiation Oncology*, 7(1):1–8, 2012.

[84] L. Masi, F. Casamassima, R. Doro, and P. Francescon. Quality assurance of volumetric modulated arc therapy: Evaluation and comparison of different dosimetric systems. *Medical physics*, 38:612, 2011.

[85] M. J. Menten, M. Guckenberger, C. Herrmann, A. Krauss, S. Nill, U. Oelfke, and J. Wilbert. Comparison of a multileaf collimator tracking system and a robotic treatment couch tracking system for organ motion compensation during radiotherapy. *Medical Physics*, 39(11):7032–7041, 2012.

[86] A. Mozumder. Effect of an external electric field on the yield of free ions. i general results from the onsager theory. *The Journal of Chemical Physics*, 60:4300, 1974.

[87] P. Navarria, A. M. Ascolese, P. Mancosu, F. Alongi, E. Clerici, A. Tozzi, C. Iftode, G. Reggiori, S. Tomatis, M. Infante, et al. Volumetric modulated arc therapy with flattening filter free (fff) beams for stereotactic body radiation therapy (sbrt) in patients with medically inoperable early stage non small cell lung cancer (nsclc). *Radiotherapy and Oncology*, 2013.

[88] A. J. Nederveen, U. A. Heide, H. Dehnad, R. J. A. Moorselaar, P. Hofman, and J. J. Lagendijk. Measurements and clinical consequences of prostate motion during a radiotherapy fraction. *International Journal of Radiation Oncology* Biology* Physics*, 53(1):206–214, 2002.

[89] T. Neicu, H. Shirato, Y. Seppenwoolde, and S. B. Jiang. Synchronized moving aperture radiation therapy (smart): average tumour trajectory for lung patients. *Physics in medicine and biology*, 48(5):587, 2003.

[90] A. W. Ng, S. Y. Tung, and V. Y. Wong. Hypofractionated stereotactic radiotherapy for medically inoperable stage i non-small cell lung cancer: report on clinical outcome and dose to critical organs. *Radiotherapy and oncology*, 87(1):24–28, 2008.

[91] J. O'Daniel, S. Das, Q. J. Wu, and F.-F. Yin. Volumetric-modulated arc therapy: Effective and efficient end-to-end patient-specific quality assurance. *International Journal of Radiation Oncology* Biology* Physics*, 82(5):1567–1574, 2012.

[92] C. L. Ong, J. P. Cuijpers, S. Senan, B. J. Slotman, and W. F. Verbakel. Impact of the calculation resolution of aaa for small fields and rapidarc treatment plans. *Medical Physics*, 38:4471, 2011.

[93] C. L. Ong, M. Dahele, B. J. Slotman, and W. F. Verbakel. Dosimetric impact of the interplay effect during stereotactic lung radiation therapy delivery using flattening filter-free beams and volumetric modulated arc therapy. *International Journal of Radiation Oncology* Biology* Physics*, 86(4):743–748, 2013.

[94] C. L. Ong, W. F. Verbakel, J. P. Cuijpers, B. J. Slotman, F. J. Lagerwaard, and S. Senan. Stereotactic radiotherapy for peripheral lung tumors: a comparison of volumetric modulated arc therapy with 3 other delivery techniques. *Radiotherapy and Oncology*, 97(3):437–442, 2010.

[95] C. L. Ong, W. F. Verbakel, M. Dahele, J. P. Cuijpers, B. J. Slotman, and S. Senan. Fast arc delivery for stereotactic body radiotherapy of vertebral and lung tumors. *International Journal of Radiation Oncology* Biology* Physics*, 83(1):e137–e143, 2012.

[96] D. A. Palma, W. F. Verbakel, K. Otto, and S. Senan. New developments in arc radiation therapy: a review. *Cancer treatment reviews*, 36(5):393–399, 2010.

[97] J. Pardo, L. Franco, F. Gomez, A. Iglesias, R. Lobato, J. Mosquera, A. Pazos, J. Pena, M. Pombar, A. Rodríguez, et al. Free ion yield observed in liquid isooctane irradiated by γ rays. comparison with the onsager theory. *Physics in medicine and biology*, 49(10):1905, 2004.

[98] J. Pardo-Montero and F. Gómez. Determining charge collection efficiency in parallel-plate liquid ionization chambers. *Physics in medicine and biology*, 54(12):3677, 2009.

[99] E. Parsai, D. Pearson, and T. Kvale. Consequences of removing the flattening filter from linear accelerators in generating high dose rate photon beams for clinical applications: A monte carlo study verified by measurement. *Nuclear Instruments and Methods in Physics Research Section B: Beam Interactions with Materials and Atoms*, 261(1):755–759, 2007.

[100] J. M. Pawlowski, E. S. Yang, A. W. Malcolm, C. W. Coffey, and G. X. Ding. Reduction of dose delivered to organs at risk in prostate cancer patients via image-guided radiation therapy. *International journal of radiation oncology, biology, physics*, 76(3):924–934, 2010.

[101] C. Perez, L. Brady, and J. Roti. *Principles and Practice of Radiation Oncology*, volume 33. Lippincott-Raven, Philidelphia, 1998.

[102] B. M. Prendergast, J. B. Fiveash, R. A. Popple, G. M. Clark, E. M. Thomas, D. J. Minnich, R. Jacob, S. A. Spencer, J. A. Bonner, and M. C. Dobelbower. Flattening filter-free linac improves treatment delivery efficiency in stereotactic body radiation therapy. *Journal of Applied Clinical Medical Physics*, 14(3), 2013.

[103] T. G. Purdie, J.-P. Bissonnette, K. Franks, A. Bezjak, D. Payne, F. Sie, M. B. Sharpe, and D. A. Jaffray. Cone-beam computed tomography for on-line image guidance of lung stereotactic radiotherapy: localization, verification, and intrafraction tumor position. *International Journal of Radiation Oncology* Biology* Physics*, 68(1):243–252, 2007.

[104] P. Qiu, W. D D'Souza, T. J. McAvoy, and K. R. Liu. Inferential modeling and predictive feedback control in real-time motion compensation using the treatment couch during radiotherapy. *Physics in medicine and biology*, 52(19):5831, 2007.

[105] S. Quirk, N. Becker, and W. Smith. External respiratory motion analysis and statistics for patients and volunteers. *Journal of Applied Clinical Medical Physics*, 14(2), 2013.

[106] G. Reggiori, P. Mancosu, S. Castiglioni, F. Alongi, C. Pellegrini, F. Lobefalo, M. Catalano, A. Fogliata, S. Arcangeli, P. Navarria, et al. Can volumetric modulated arc therapy with flattening filter free beams play a role in stereotactic body radiotherapy for liver lesions? a volume-based analysis. *Medical Physics*, 39:1112, 2012.

[107] G. Reggiori, P. Mancosu, A. Tozzi, M. C. Cantone, S. Castiglioni, P. Lattuada, F. Lobefalo, L. Cozzi, A. Fogliata, P. Navarria, et al. Cone beam ct pre-and post-daily treatment for assessing geometrical and dosimetric intrafraction variability during radiotherapy of prostate cancer. *Journal of Applied Clinical Medical Physics*, 12(1), 2010.

[108] P. Remeijer, C. Rasch, J. V. Lebesque, and M. van Herk. A general methodology for three-dimensional analysis of variation in target volume delineation. *Medical physics*, 26:931, 1999.

[109] M. Ritter, J. Forman, P. Kupelian, C. Lawton, and D. Petereit. Hypofractionation for prostate cancer. *Cancer journal (Sudbury, Mass.)*, 15(1):1, 2009.

[110] T. Rohlfing, C. R. Maurer Jr, W. G. O'Dell, and J. Zhong. Modeling liver motion and deformation during the respiratory cycle using intensity-based nonrigid registration of gated mr images. *Medical physics*, 31:427, 2004.

[111] M. Scorsetti, F. Alongi, S. Castiglioni, A. Clivio, A. Fogliata, F. Lobefalo, P. Mancosu, P. Navarria, V. Palumbo, C. Pellegrini, et al. Feasibility and early clinical assessment of flattening filter free (fff) based stereotactic body radiotherapy (sbrt) treatments. *Lung*, 34:48, 2011.

[112] J. Seco, X.-Q. Lu, K. Ebe, C. Mayo, D. Ionascu, B. Winey, N. Giakoumakis, M. Aristophanous, R. Berbeco, J. Rottman, et al. Use of a realistic breathing lung phantom to evaluate dose delivery errors. *Medical physics*, 37:5850, 2010.

[113] R. Shaffer, W. Morris, V. Moiseenko, M. Welsh, C. Crumley, S. Nakano, M. Schmuland, T. Pickles, and K. Otto. Volumetric modulated arc therapy and conventional intensity-modulated radiotherapy for simultaneous maximal intraprostatic boost: a planning comparison study. *Clinical oncology*, 21(5):401–407, 2009.

[114] S. Shimizu, H. Shirato, S. Ogura, H. Akita-Dosaka, K. Kitamura, T. Nishioka, K. Kagei, M. Nishimura, and K. Miyasaka. Detection of lung tumor movement in real-time tumor-tracking radiotherapy. *International Journal of Radiation Oncology* Biology* Physics*, 51(2):304–310, 2001.

[115] D. Skarsgard, P. Cadman, A. El-Gayed, R. Pearcey, P. Tai, N. Pervez, J. Wu, et al. Planning target volume margins for prostate radiotherapy using daily electronic portal imaging and implanted fiducial markers. *Radiat Oncol*, 5(52):41–50, 2010.

[116] J.-J. Sonke, M. Rossi, J. Wolthaus, M. van Herk, E. Damen, and J. Belderbos. Frameless stereotactic body radiotherapy for lung cancer using four-dimensional cone beam ct guidance. *International Journal of Radiation Oncology* Biology* Physics*, 74(2):567–574, 2009.

[117] B. S. Sørensen, A. Vestergaard, J. Overgaard, and L. H. Præstegaard. Dependence of cell survival on instantaneous dose rate of a linear accelerator. *Radiotherapy and Oncology*, 101(1):223–225, 2011.

[118] S. Stathakis, C. Esquivel, A. Gutierrez, C. R. Buckey, and N. Papanikolaou. Treatment planning and delivery of imrt using 6 and 18mv photon beams without flattening filter. *Applied Radiation and Isotopes*, 67(9):1629–1637, 2009.

[119] K. Stewart, A. Elliott, and J. Seuntjens. Development of a guarded liquid ionization chamber for clinical dosimetry. *Physics in medicine and biology*, 52(11):3089, 2007.

[120] R. A. Sweeney, W. Arnold, E. Steixner, M. Nevinny-Stickel, and P. Lukas. Compensating for tumor motion by a 6-degree-of-freedom treatment couch: Is patient tolerance an issue? *International Journal of Radiation Oncology*Biology*Physics*, 74(1):168 – 171, 2009.

[121] H. Tölli, R. Sjögren, and M. Wendelsten. A two-dose-rate method for general recombination correction for liquid ionization chambers in pulsed beams. *Physics in medicine and biology*, 55(15):4247, 2010.

[122] M. van Herk, P. Remeijer, C. Rasch, J. V. Lebesque, et al. The probability of correct target dosage: dose-population histograms for deriving treatment margins in radiotherapy. *International journal of radiation oncology, biology, physics*, 47(4):1121, 2000.

[123] O. N. Vassiliev, S. F. Kry, J. Y. Chang, P. A. Balter, U. Titt, and R. Mohan. Stereotactic radiotherapy for lung cancer using a flattening filter free clinac. *Journal of Applied Clinical Medical Physics*, 10(1), 2009.

[124] O. N. Vassiliev, S. F. Kry, D. A. Kuban, M. Salehpour, R. Mohan, and U. Titt. Treatment-planning study of prostate cancer intensity-modulated radiotherapy with a varian clinac operated without a flattening filter. *International Journal of Radiation Oncology* Biology* Physics*, 68(5):1567–1571, 2007.

[125] O. N. Vassiliev, U. Titt, S. F. Kry, F. Pönisch, M. T. Gillin, and R. Mohan. Monte carlo study of photon fields from a flattening filter-free clinical accelerator. *Medical physics*, 33:820, 2006.

[126] O. N. Vassiliev, U. Titt, F. Pönisch, S. F. Kry, R. Mohan, and M. T. Gillin. Dosimetric properties of photon beams from a flattening filter free clinical accelerator. *Physics in medicine and biology*, 51(7):1907, 2006.

[127] M. Wagar, R. Berbeco, A. Reisner, B. Winey, D. Schofield, D. Ionascu, A. M. Allen, R. Popple, T. Lingos, et al. Evaluation of the interplay effect when using rapidarc to treat targets moving in the craniocaudal or right-left direction. *Medical physics*, 37:4, 2010.

[128] R. Wagman, E. Yorke, E. Ford, P. Giraud, G. Mageras, B. Minsky, and K. Rosenzweig. Respiratory gating for liver tumors: use in dose escalation. *International Journal of Radiation Oncology* Biology* Physics*, 55(3):659–668, 2003.

[129] D. Wagner, H. Vorwerk, et al. Two years experience with quality assurance protocol for patient related rapid arc treatment plan verification using a two dimensional ionization chamber array. *Radiat. Oncol*, 6(21):1–8, 2011.

[130] L. Wang, K. N. Kielar, E. Mok, A. Hsu, S. Dieterich, and L. Xing. An end-to-end examination of geometric accuracy of igrt using a new digital accelerator equipped with onboard imaging system. *Physics in Medicine and Biology*, 57(3):757, 2012.

[131] E. Wüest. Sterbeziffern für 30 wichtige todesursachen nach geschlecht in der schweiz, 2012.

[132] T. J. Whelan, J.-P. Pignol, M. N. Levine, J. A. Julian, R. MacKenzie, S. Parpia, W. Shelley, L. Grimard, J. Bowen, H. Lukka, et al. Long-term results of hypofractionated radiation therapy for breast cancer. *New England Journal of Medicine*, 362(6):513–520, 2010.

[133] G. Wickman and H. Nystrom. The use of liquids in ionization chambers for high precision radiotherapy dosimetry. *Physics in Medicine and Biology*, 37(9):1789, 1992.

[134] J. Wilbert, K. Baier, A. Richter, C. Herrmann, L. Ma, M. Flentje, and M. Guckenberger. Influence of continuous table motion on patient breathing patterns. *International Journal of Radiation Oncology* Biology* Physics*, 77(2):622–629, 2010.

[135] J. Wilbert, J. Meyer, K. Baier, M. Guckenberger, C. Herrmann, R. Hess, C. Janka, L. Ma, T. Mersebach, A. Richter, M. Roth, K. Schilling, and M. Flentje. Tumor tracking and motion compensation with an adaptive tumor tracking system (atts): System description and prototype testing. *Medical Physics*, 35(9):3911–3921, 2008.

[136] T. R. Willoughby, P. A. Kupelian, J. Pouliot, K. Shinohara, M. Aubin, M. Roach III, L. L. Skrumeda, J. M. Balter, D. W. Litzenberg, S. W. Hadley, et al. Target localization and real-time tracking using the calypso 4d localization system in patients with localized prostate cancer. *International Journal of Radiation Oncology* Biology* Physics*, 65(2):528–534, 2006.

[137] J. W. Wong, M. B. Sharpe, D. A. Jaffray, V. R. Kini, J. M. Robertson, J. S. Stromberg, and A. A. Martinez. The use of active breathing control (abc) to reduce margin for breathing motion. *International Journal of Radiation Oncology* Biology* Physics*, 44(4):911–919, 1999.

[138] M. Xi, M.-Z. Liu, X.-W. Deng, L. Zhang, X.-Y. Huang, H. Liu, Q.-Q. Li, Y.-H. Hu, L. Cai, and N.-J. Cui. Defining internal target volume (itv) for hepatocellular carcinoma using four-dimensional ct. *Radiotherapy and Oncology*, 84(3):272–278, 2007.

[139] D. R. Zwahlen, S. Lang, J. Hrbacek, C. Glanzmann, S. Kloeck, Y. Najafi, T. Streller, G. Studer, K. Zaugg, and U. M. Luetolf. The use of photon beams of a flattening filter-free linear accelerator for hypofractionated volumetric modulated arc therapy in localized prostate cancer. *International Journal of Radiation Oncology* Biology* Physics*, 2012.

List of Tables

List of Tables

List of Figures

Curriculum Vitae

Personal data

Name	**Lang**
First name	**Stephanie**
Date of birth	**07.01.1983**
Nationality	**German**

Education

1989–1993	**Elementary school in Geislingen (D)**
1994–2002	**Secondary school in Balingen (D), Abitur in 2002**
2002–2008	**University of Konstanz (D), Master in Physics in 2008**
2010–2012	**Technical University of Zürich (CH), Masterof Advanced Studies in Medical Physics in 2012**
2010–2013	**University of Zürich (CH), PhD Studies in Medical Physics**

Work Experience

2009–2013	**Medical Physicist at the University Hospital in Zürich**

Zürich, September 2013 Stephanie Lang

Publications

[A] S. Lang and O. Riesterer
Modern Techniques in Radiation Oncology
accepted for publication in SPG Mitteilungen **40** (2013)

[B] B. Lindl, R.G. Müller, S. Lang, M.D. Lablanca, S. Klöck
TOPOS: A new topometric patient positioning and tracking system for radiation therapy based on structured white light
Med Phys **40**, 42701 (2013)

[C] S. Lang, B. Shrestha, S. Graydon, F. Cavelaars, C. Linsenmeier, J. Hrbacek, S. Klöck, G. Studer, O. Riesterer
Clinical application of flattening filter free beams for extracranial stereotactic radiotherapy
Rad Onc **106**(2), 255 (2013)

[D] S. Lang, J. Hrbacek, A. Leong, S. Klöck
Ion recombination corrections for different ionization chambers in high dose rate flattening filter free photon beams
Phys Med Biol **57**, 2819 (2012)

[E] T. Depuydt T., R. Penne, D. Verellen, J. Hrbacek, S. Lang, et al.
Computer-aided analysis of star shot films for high accuracy radiation therapy treatment units
Phys Med Biol **57**, 2997 (2012)

[F] D. Zwahlen, S. Lang, J. Hrbacek, C. Glanzmann, S.. Kloeck, Y. Najafi, G. Studer, K. Zaugg, U.M.. Luetolf
The use of photon beams of a flattening filter free linear accelerator for hypofractionated volumetric arc therapy in localized prostate cancer
Int J Radiat Oncol Biol Phys **83**, 1655 (2012)

[G] S. Lang, G. Reggiori, J. Puxeu Vaque, C. Calle, J. Hrbacek, S. Klöck, M. Scorsetti, L. Cozzi, P. Mancosu
Pretreatment quality assurance of flattening filter free beams on 224 patients for intensity modulated plans: A multicentric study
Med Phys **39**(3), 1351 (2012)

[H] J. Hrbacek, S. Lang, S. Klöck
Commissioning of photon beams of a flattening filter-free linear accelerator and the accuracy of beam modeling using an anisotropic analytical algorithm
Int J Radiat Oncol Biol Phys **80**(4), 1228 (2011)

[I] I. Lohse, S. Lang, J. Hrbacek, S. Scheidegger, S. Bodis, N.S. Macedo,J. Feng, U.M. Lütolf and K. Zaugg
Effect of high dose per pulse flattening filter-free beams on cancer cell survival
Rad Onc **101**(1), 226 (2011)

[J] M. Beck, M. Klammer, S. Lang, P. Leiderer, V.V. Kabanov, G.N. Goltsman, and J. Demsar
Energy-Gap Dynamics of Superconducting NbN Thin Films Studied by Time-Resolved Terahertz Spectroscopy
Phys Revs Letts **107**, 177007 (2011)

[K] C.M. Petrache, M. Fantuzi, D. Mengoni, D. Petrache, R.A. Bark, S. Murray, E.A. Lawrie, J. Lawrie, S. Mullins, S. Lang, S.M. Maliage, T.M. Ramashidzha, S.S. Ntshangase, I. Ragnarsson
Six-quasiparticle isomer in 140Nd
Phys Rev C **74**(3), 177007 (2006)

Acknowledgments

It has been a great pleasure for me to work at the University Hospital Zürich over the last four years. I have met a lot of interesting people, who supported myself and my work and I have made a lot of friends.

Hereby I would like to give my thanks to Dr. Stephan Klöck, who gave me the chance to work in his group on a lot of different and interesting projects. I would also like to thank him for his scientific support during my thesis and proofreading my thesis.
I would like to thank Prof. Dr. Martin Pruschy for supervising my thesis. I very much appreciated your support and that you pushed me to make my research accesible to non-physicists. I thank PD Dr. Andreas Mack for accepting to be co-examiner on my thesis and for proofreading my thesis. I thank Prof. Dr. Michael Hengartner for accepting to be co-examiner on my thesis.

I would like to thank all my physics, technicians and medical doctor colleagues. I enjoy working in this multi-disciplinary team. Special thanks to Jan Hrbacek, who supervised me during my first two years and who became a good friend. Special thanks to Dr. Daniel Zwahlen and Dr. Oliver Riesterer for involving me in different and interesting projects and assissting me with my first publications. A big thank you to Prof. Dr. Urs Lütolf for promoting and supporting my work. Special thanks to Anja, Jerome, Mariangela, Lola, Linda, Jörg, Pascal, Sabrina, Karl, Shaun, Sarah, Martina, Michelle, Michael, Stephan, Chris, Tino, Martin and Marc for creating an enjoyable work atmosphere.

Many thanks to Aidan, Alessandra, Aline, Shaun, Sarah, Anja, Linda, Gemma, Melissa, Michelle, Chris, Daniel and Jenny for their proofreading of my thesis and English corrections.

Ein besonderer Dank geht an meine Familie, Mama und Papa ihr habt immer an mich geglaubt und mich bei allen Entscheidungen unterstützt. Danke für Eure Unterstützung und eure Ratschläge. Ein grosser Dank auch an meine Brüder Daniel und Simon und an den Rest der Verwandschaft.

Infine, vorrei ringraziare Stefano. Grazie per il tuo sostegno morale, per aver creduto in me e per 'distratta' dal lavoro ogni tanto.